HERON is jointly edited by:
STEVIN-LABORATORY of the faculty of Civil Engineering, Delft University of Technology, Delft, The Netherlands
and
TNO BUILDING AND CONSTRUCTION RESEARCH. Rijswijk (ZH), The Netherlands
HERON contains contributions based mainly on research work performed in these laboratories on strength of materials, structures and materials science.

ISSN 0046-7316

Secretary:
J. G. M. van Mier
Stevinweg 1
P.O. Box 5048
2600 GA Delft, The Netherlands
Tel. 0031-15-784578
Fax 0031-15-611465
Telex 38151 BUTUD

HERON vol. 37 1992 no. 1

Contents

TENSILE AND TENSILE FATIGUE BEHAVIOUR OF CONCRETE; EXPERIMENTS, MODELLING AND ANALYSES

D. A. Hordijk
TNO Building and Construction Research
Department of Structural Engineering
formerly Delft University of Technology,
Stevin Laboratory

Publication in HERON since 1970

Abstract

A model based on nonlinear fracture mechanics is presented for the fatigue behaviour of plain concrete. Firstly, the tensile behaviour of concrete for a monotonic increasing deformation is treated extensively. The softening relation is described and the way the included fracture mechanics parameters are influenced by several variables is shown. Also a structural behaviour that occurs in a uniaxial tensile test on a softening material is explained. Secondly, based on experimental results, a constitutive model for the crack cyclic behaviour of concrete is proposed. The adequacy of the model is shown by numerical simulation of notched beams under four-point bending. For the analyses, the FE code DIANA and a multi-layer model were applied. The same models have been used to study crack growth in a four-point bending specimen under repeated loading. Qualitatively, the results showed good similarity with those usually found in fatigue experiments. Finally, it is shown by experiments that localization and non-uniform crack opening occurs in tensile fatigue tests just as in monotonically loaded tensile tests.

Tensile and tensile fatigue behaviour of concrete; experiments, modelling and analyses

1 Introduction

In the first half of this century the local treatment of the conditions around a crack tip in a solid body, which discipline is called fracture mechanics, has been applied to several materials, but not to concrete. In the subsequent decades, it was more and more realized that also concrete should be treated in a similar way in order to explain its behaviour under different circumstances. It appeared, however, that the usual fracture mechanics approaches could not be applied to concrete. Therefore, Hillerborg et al. [1] proposed the "fictitious crack model", which still is a major model in fracture mechanics analyses of concrete. Nowadays, the model is being applied in most finite element codes, either in a discrete crack approach or in a smeared crack approach.

After nonlinear fracture mechanics entered the scene of concrete structures, the interest in concrete tensile behaviour, especially its post-peak or "softening" behaviour, increased enormeously. The relation between crack opening and stress is the most important input parameter for the nonlinear fracture mechanics analyses. Direct measurement in a deformation-controlled uniaxial tensile test on concrete looks to be the obvious means to determine this relation. In this study, however, it will be shown that the results of such a test cannot unrestrictedly be used to determine the material property.

As far as the influence of different variables, like mix composition and test conditions, on the tensile behaviour of concrete is concerned, limited information is available in the literature. In this study, it is intended to contribute to the knowledge in this research area.

The main aim of this study is to apply the fracture mechanics approach to model fatigue of concrete. In the last about fifteen years, fatigue of concrete received a considerable amount of attention. So, also an extensive research programme was performed in the Netherlands [2,3,4,5]. This investigation yielded an enormous amount of data like the so-called S-N curves, that serves as input for fatigue analyses based on Miner sums. However, it did not explain the cause and mechanism of fatigue. For the theoretical approach of fatigue of concrete in this study, it will be necessary to determine the cyclic behaviour of concrete in the softening zone. Based on experimental results a constitutive model will be proposed. By numerical analyses of a four-point bending specimen under cyclic loading, the fatigue behaviour of concrete will be studied. Though so far only low cycle, high amplitude fatigue can be studied with the model, the results will be compared with those that are usually found in fatigue experiments.

By now, the fact that concrete tensile fracture is a local phenomenon when loaded monotonically is well known. Yet, it is not clear until what extent fracture under tensile fatigue loading also occurs locally. In order to get an answer to this question, some tensile fatigue tests were performed. The results of these experiments will further be

used to investigate whether the descending branch in a static test is the failure envelop for fatigue tests. In other words, the existence of a failure criterion based on deformations is studied.

2 Behaviour of concrete under tensile and fatigue loading

In this chapter the basic phenomena of concrete loaded uniaxially in tension and fatigue will be reviewed. Concrete will be considered on a macro-level which means that it is treated as a homogeneous, isotropic continuum. In this continuum it is assumed that, after reaching the tensile strength, a crack will arise perpendicular to the direction of the maximum tensile stress.

2.1 *Uniaxial tensile behaviour*

When a tensile bar is loaded uniaxially in tension by means of load-control then fracture occurs when the maximum attainable load is reached (Fig. 1a). If, however, the deformation over a certain measuring length is used as control parameter, then a post-peak behaviour can be found as sketched in Fig. 1b. As a consequence of this material behaviour, there is a zone ahead of a visible crack in concrete in which the transferrable stress depends on the crack opening (Fig. 2a). This model for the nonlinear material behaviour in concrete is the basic principle of the "fictitious crack model", that was proposed in 1976 by Hillerborg and co-workers [1]. In this respect a visible crack is understood to mean a crack that cannot transfer tensile stress, while in the "fictitious" crack (also called the process zone), so-called crack-closing stresses are active. This model resembles the Dugdale-Barenblatt model [6,7] for yielding materials, where a plastic zone with crack-closing stresses is assumed ahead of a crack tip (Fig. 2b). In the Dugdale-Barenblatt model, however, the crack closing stresses are equal to the yield stress of the material.

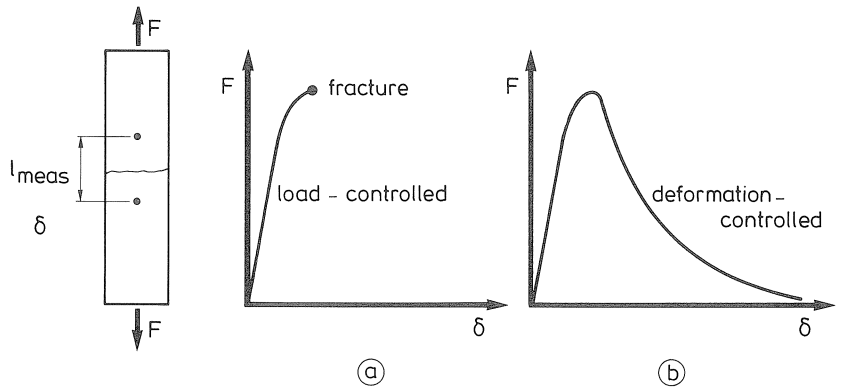

Fig. 1. Schematic representation of the behaviour of concrete in a load-controlled (a) and a deformation-controlled (b) tensile test.

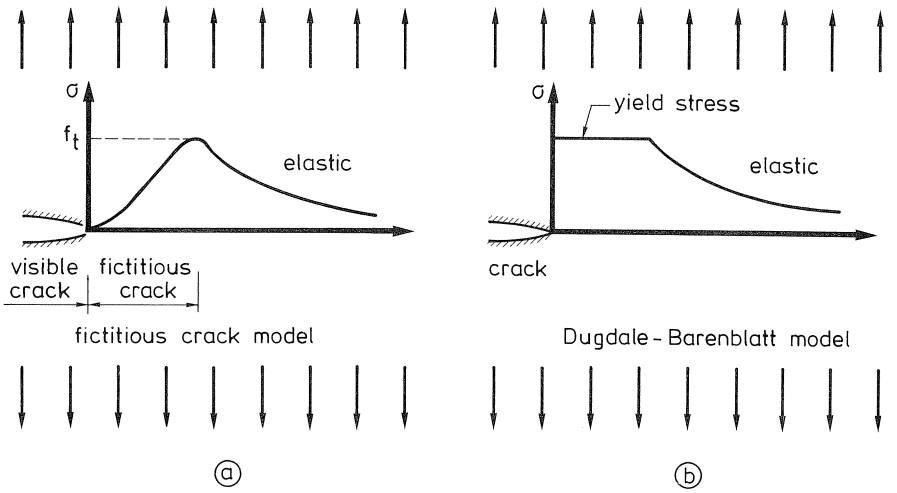

Fig. 2. Assumed stress distribution ahead of a visible crack according to a model for a softening material like concrete (a) and a model for a yielding material (b).

Concrete behaviour in a deformation-controlled uniaxial tensile test

When a concrete bar is strained in uniaxial tension (Fig. 3), it first reacts elastically. A linear load-deformation relation almost up to the peak load will be obtained. At a macro-level the stresses and strains are uniformly distributed over the specimen and the load-deformation relation for the specimen (concrete tensile bar) can therefore be directly replaced by a stress-strain relation for the material (concrete). At peak load, the strains start to localize within a narrow zone of micro-cracks (process zone or softening zone), after which a continuous macro-crack will develop. The process zone will occur

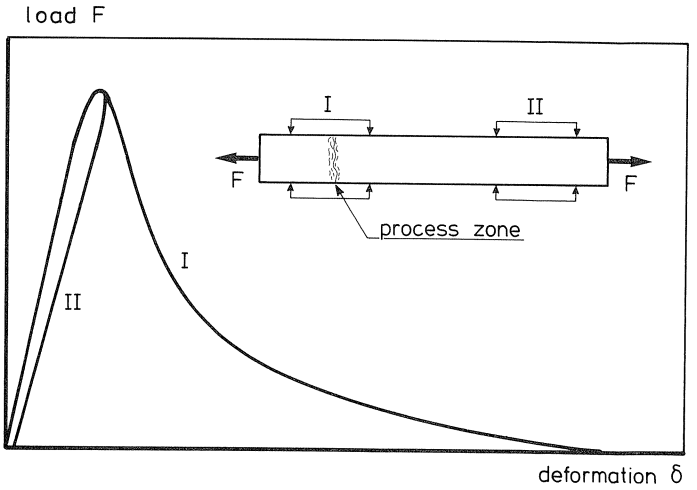

Fig. 3. Load-deformation relations for a concrete bar under uniaxial tensile loading.

at the weakest section of the tensile bar. If the process zone develops within the measuring length whose deformation is used as control parameter, then a load-deformation relation, as indicated by line I in Fig. 3, will be obtained. The load that can be transferred decreases with an increasing deformation of the process zone. As a result of this load reduction, the concrete outside this zone unloads (line II in Fig. 3). Due to the fact that the deformation in the descending branch is built up by strains and crack opening, it is no longer correct to use strain (deformation divided by measuring length) for the horizontal axis instead of deformation. For modelling the tensile behaviour of concrete, deformations must be split up into a stress-strain relation for the bulk material and a stress-crack opening relation for the crack (see Fig. 4).

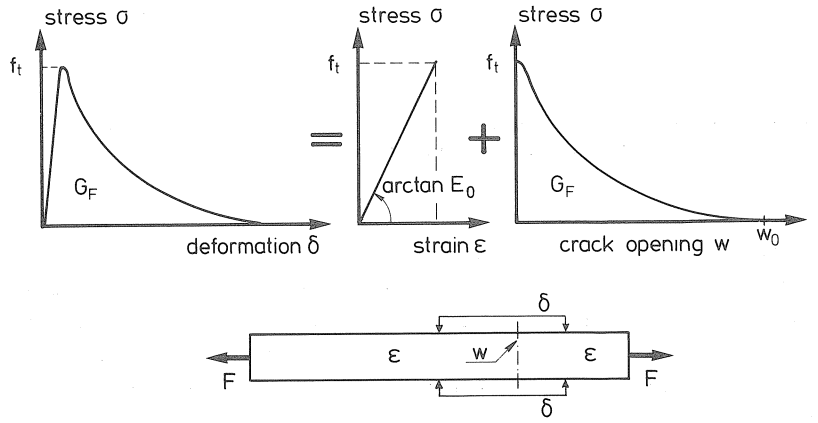

Fig. 4. Separation of the complete tensile stress-deformation relation for concrete into a stress-strain and a stress crack opening relation according to the fictitious crack model.

Stress-deformation relation as influenced by measuring length

Due to the fact that the deformation measurement over the process zone in a uniaxial tensile test on concrete always consists of two contributions, elastic deformation and crack opening, there is an influence of the applied measuring length on the obtained stress-deformation relation. In Fig. 5 this influence is shown for some assumed concrete material properties. It can be seen that the descending branch becomes steeper for an increasing measuring length. In this example, a measuring length of 500 mm yields a σ-δ relation with a so-called "snap-back". If this measuring length is used as control parameter for the deformation, then a sudden jump will occur as indicated by the dashed line. In most experimental set-ups, the equipment will not be fast enough to overcome such a jump, and the result will be unstable fracture. In the past, insufficient stiffness of the test rig has mostly been regarded as the main cause of unstable post-peak tensile behaviour. Although the stiffness of the equipment is still important for performing a stable deformation-controlled tensile test, the measuring length of the feedback signal also appears to play an important role.

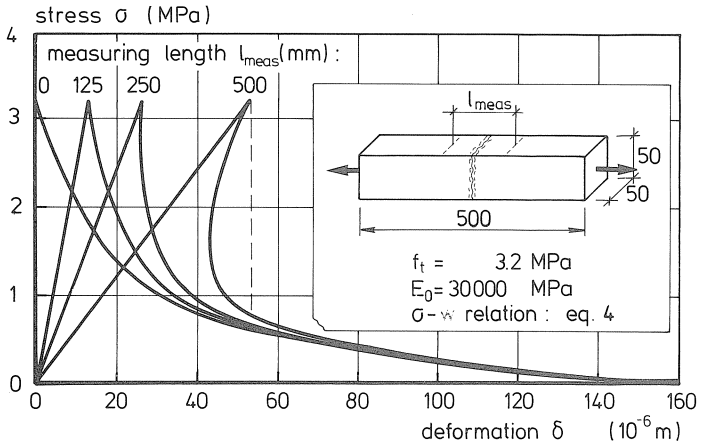

Fig. 5. Stress-deformation relation as influenced by measuring length.

So far, the behaviour of concrete in a deformation-controlled uniaxial tensile test has been discussed for an ideal test performance. There are, however, several effects that may blur the results of such a test. Actually, the ideal situation will never occur in an experiment. A number of these effects are subject of study in several parts of this report.

2.2 *Concrete fatigue behaviour*

For a comprehensive review of the fatigue behaviour of concrete, the reader is referred to [8, 9]. Here, the main findings for concrete fatigue behaviour will be presented, with emphasis being placed on the observed tendencies rather than on quantitative descriptions.

Like in the case of static loading, a distinction can be made between the different loading types, as there are compression, tension, bending and bond between concrete and steel. It appeared, however, that qualitatively more or less the same results were found for these different loading types. See in this respect, for instance, the results for bond behaviour under repeated loading [10].

As far as cyclic loading or fatigue is concerned a distinction is generally made between low cycle high amplitude fatigue and high cycle low amplitude fatigue. The former involves few load cycles of high stress at a lower rate of loading (earthquakes, storms, etc.), while the latter is characterized by a great number of cycles of low stress at a higher rate of loading (traffic loading, wind and wave loading, etc.).

S-N curve or Wöhler curve

The main characteristic of fatigue behaviour of concrete, but also of other materials, is that the number of load cycles, N, that can be performed before failure occurs, increases for a decreasing upper load level. When the relative upper load (or stress) level is plotted against the logarithm of the number of cycles to failure, then a linear relation

will be found (see Fig. 6a). These types of curves are known as Wöhler curves or *S-N* curves. The fatigue strength, which is defined as the fraction of the static strength that can be supported repeatedly for a given number of load cycles, can be taken from the *S-N* curve. As can be seen in Fig. 6b, the fatigue strength depends also on the lower stress level applied in the cycles. A decreasing lower stress level results in a decreasing number of cycles to failure. Furthermore, stress reversals appeared to have a more detrimental effect on tensile fatigue than repeated tensile stresses (see Fig. 6b).

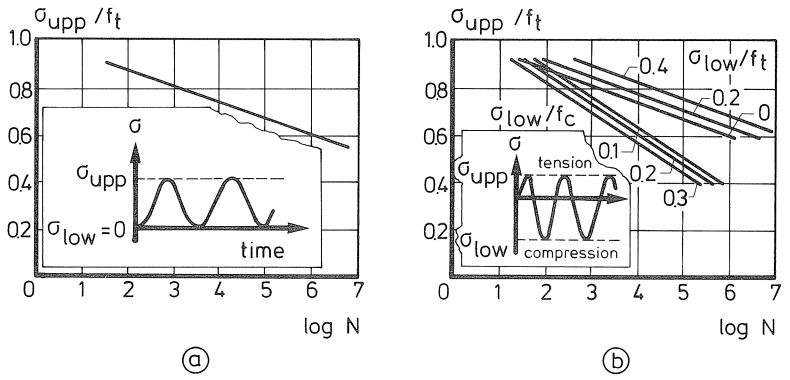

Fig. 6. Relation between relative upper stress level and number of cycles to failure (Wöhler curve or *S-N* curve) (a) and the influence of the lower level (b) [12].

Cyclic creep curve

If the deformations are recorded during a fatigue test on concrete and plotted against the number of cycles performed, then a curve will generally be obtained that is known as a cyclic creep curve (Fig. 7). This curve is characterized by three specific parts. First, the increase of deformation per cycle decreases with increasing number of cycles *n*.

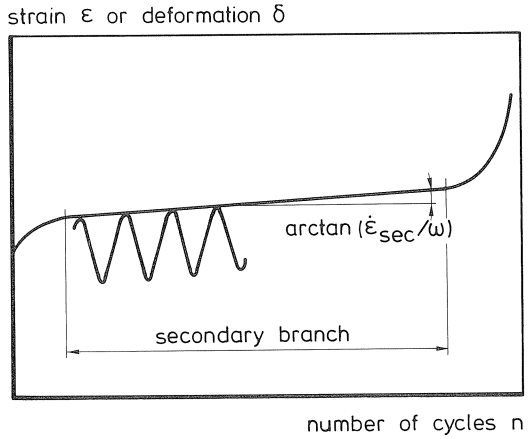

Fig. 7. Schematic representation of a cyclic creep curve.

This first branch of the curve is followed by a secondary branch where this increase is constant. Then, just before failure occurs, the increase of deformation per cycle increases rapidly. Holmen [11] studied the development of the modulus of elasticity in a compressive test during fatigue loading. A typical result showing the reduction of the secant modulus with the number of cycles is plotted in Fig. 8.

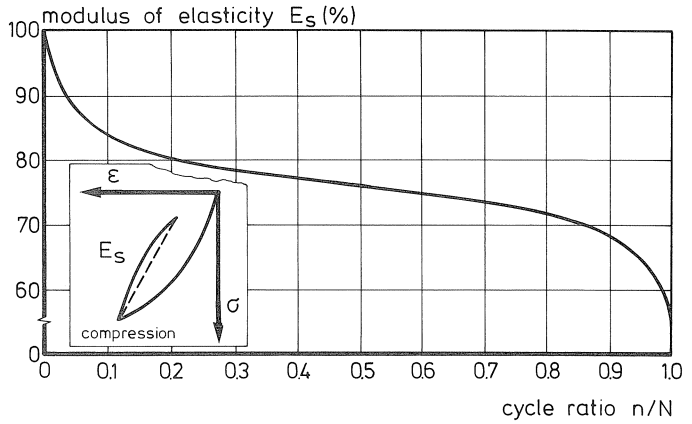

Fig. 8. Development of the secant modulus of elasticity in a compressive fatigue test [11].

Relation between secondary creep rate and number of cycles to failure

There appeared to be a strong relation between the increase of strain per cycle in the secondary branch of the cyclic creep curve and the number of cycles to failure (see Fig. 9). Hence, the remaining life of a cyclically preloaded specimen can be assessed by measuring the total strain variation. This further indicates that the ultimate strain can be used as a fatigue failure criterion for concrete. A formal strain at fracture can be calculated as:

$$\varepsilon = \frac{\mathrm{d}\varepsilon}{\mathrm{d}n} N = \frac{\mathrm{d}\varepsilon}{\mathrm{d}t} \frac{\mathrm{d}t}{\mathrm{d}n} N = \dot{\varepsilon} \frac{N}{\omega} \tag{1}$$

with ω = frequency. For the logarithm of the strain at fracture this results in:

$$\log \varepsilon = \log \dot{\varepsilon} + \log N - \log \omega \tag{2}$$

In Fig. 9 it can be seen that $\log \dot{\varepsilon} + \log N$ is practically constant for ω is constant. For $\omega = 6$ Hz we find that $\log \varepsilon = -4.2 - \log 6 = -5.0$ (corresponding to $\varepsilon = 10^{-5}$). The number of cycles to failure depends not only on the applied stress levels, but also on the testing frequency. The fatigue life in terms of number of cycles to failure appeared to be lower for the lower applied frequency (0.06 Hz) than for the higher one (6 Hz) [12]. This indicates that the damage is not only due to the cyclic loading, but that there is also a time effect. In Fig. 9 it can be seen that for equal secondary creep (per unit time) the number of cycles to failure at 0.06 Hz is approximately 100 times less than at 6 Hz. As a result the strain at fracture for $\omega = 6$ Hz and $\omega = 0.06$ Hz is the same.

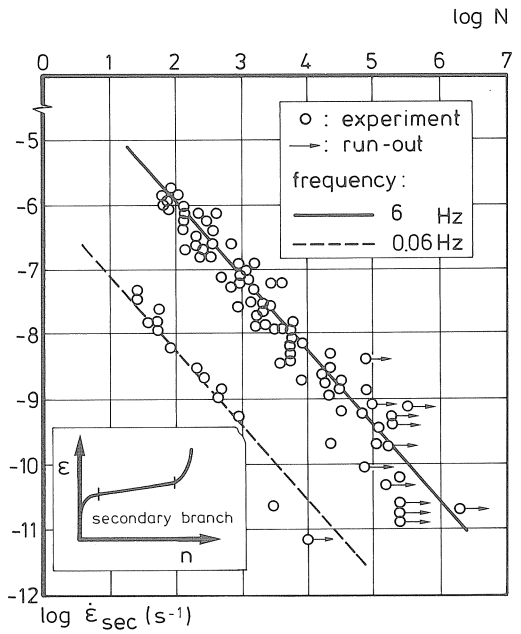

Fig. 9. Relation between secondary cyclic creep rate in tensile fatigue and number of cycles to failure [4].

Sequence effect; strength increase after fatigue preloading

So far, the discussed results of fatigue tests were mainly related to constant amplitude tests. This means that loading cycles were performed with constant values for the lower and upper load levels. When two different stages of constant amplitude loading are applied subsequently, a "sequence effect" can be observed. This means that the fatigue life depends on the order of application of the two stages. When fatigue tests are performed at a rather low upper stress level, it may sometimes occur that no failure is found after a great number of load cycles. Then the experiment is stopped and in the presentation of the fatigue results, this test is denoted with the term "run-out" (see also Fig. 9). In compressive fatigue experiments, Holmen [11] also encountered a number of run-out specimens (stopped after twelve million cycles at a maximum stress level of 60%). He subsequently loaded these specimens statically to failure. When comparing the results of these specimens with similar specimens which had not undergone repeated loading, he observed an increase in strength of about 7%. Besides the increase in strength the stress-strain curve also differed significantly. The specimen that was preloaded with repeated loading displayed a stress-strain curve that was much straighter than that of the "virgin" specimens. Similar results, with a strength increase up to 15%, have also been reported by other investigators.

2.3 *Fatigue modelling*

Two basic approaches are used for the fatigue life assessment of structural elements. One approach is based on fracture mechanics and considers the propagation of a crack. This method is in very common use in fatigue analyses in metals, where linear elastic fracture mechanics (LEFM) can be applied. Generally, the same method cannot be applied for concrete elements, since LEFM is not applicable to normal-sized concrete structures. Nevertheless, if the behaviour of the softening zone in front of a visible crack is modelled properly and if a finite element method (FEM) is used, a fracture mechanics approach is still possible for concrete.
The other method is based on the empirically derived *S-N* curves. This method, which is very simple and is known as the Palmgren-Miner hypothesis, is much more important for engineering practice than the method based on fracture mechanics. Finally, as already mentioned in Section 2.2, it may be possible to define a fatigue failure criterion based on strains or deformations. Below, the basics of the different approaches will be further explained.

Palmgren-Miner hypothesis
From experiments, the number of cycles to failure for loading variations between two fixed stress levels are known. In actual structures, however, the stress cycles vary greatly in magnitude, number and sequence. In the Palmgren-Miner hypothesis [13, 14] the supposition is that damage accumulates linearly with the number of cycles applied at a particular stress level. The failure criterion is written as:

$$\sum_{i=1}^{k} \frac{n_i}{N_i} = 1 \tag{3}$$

where n_i is the number of cycles at stress level i, N_i is the number of cycles to failure at stress level i and k is the number of stress levels.
The hypothesis does not accurately reflect the concrete's properties. One reason for this, for instance, is that sequence effects are not taken into account. Nevertheless, it is applied in design practice, first of all because it is simple, secondly, because no better method is available and, thirdly, because the description of concrete behaviour under random loading is adequate enough for most cases.

Approach based on fracture mechanics
The discipline of fracture mechanics is mainly concerned with the local treatment of the conditions around the crack tip in a body. Since for metals fatigue failure is very clearly associated with the development of a crack, fracture mechanics is a suitable tool for studying fatigue of those materials. The development of a crack can be subdivided into three stages (Fig. 10); crack initiation, crack propagation and unstable crack growth. The similarity to the behaviour observed in fatigue tests on concrete (compare Fig. 7) is evident. The difference between the fatigue behaviour in steel and concrete relates to the visibility and measurability of the crack. For concrete, the approach is

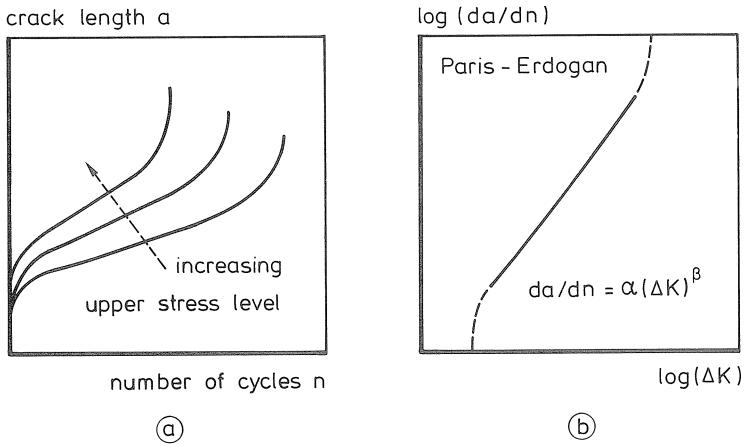

Fig. 10. Typical fatigue results for metals; (a) crack length versus number of cycles and (b) crack propagation law.

more indirect, because it is only possible to measure the elongation of the specimen or the deformation for a certain measuring length.

The initiation of a crack is often associated with points of stress concentrations in the material, which may be due to flaws, surface discontinuities or changes in shape. However, most of the research into the fatigue phenomenon in metals, deals with the crack propagation stage. Crack propagation laws in which the relation between crack growth and the stress-intensity factor is described, have been proposed (Fig. 10b). These laws are empirical and the parameters must be obtained from experimental findings. For a better understanding of the fundamentals of fatigue, the phenomenon of crack propagation has to be studied more theoretically. Such an approach is applied in this report, the basics of which will be explained below.

From deformation-controlled uniaxial tensile tests on concrete, it is known that a loading cycle in the post-peak region of the σ-δ relation displays a behaviour as sketched in Fig. 11. It appears that after an unloading-reloading cycle, the curve will not return to the same point of the envelope curve where it started from, but to a point which belongs to a lower stress. This phenomenon is due to the damage which is caused in such an unloading-reloading loop. Obviously some mismatch of the crack surfaces will occur at unloading, resulting in a propagation of existing micro-cracks. From experiments, it is known that the envelope curve is not significantly affected by the cyclic loading.

In Fig. 12 the stress-state in front of a visible crack after n loading cycles ($n \geq 0$) is plotted (solid line). Suppose that this is part of a total structure which is loaded up to a certain load F. If this structure is subjected to another unloading-reloading cycle, then we know from the post-peak tensile behaviour (Fig. 11) that the various areas in the softening zone cannot attain the same stress as they had at the beginning of this load cycle. This means that for the same maximum external load F, an internal stress-

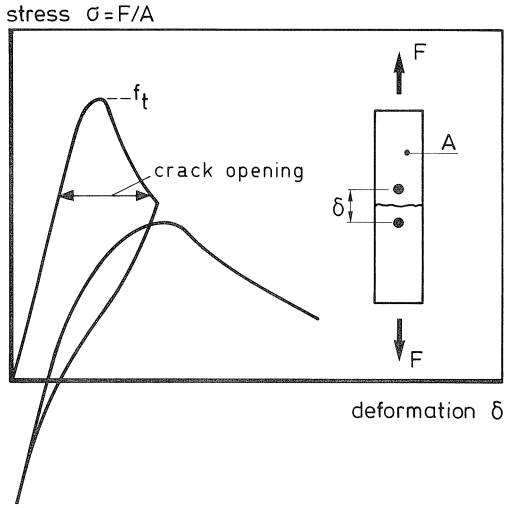

Fig. 11. Post-peak cyclic tensile behaviour of concrete.

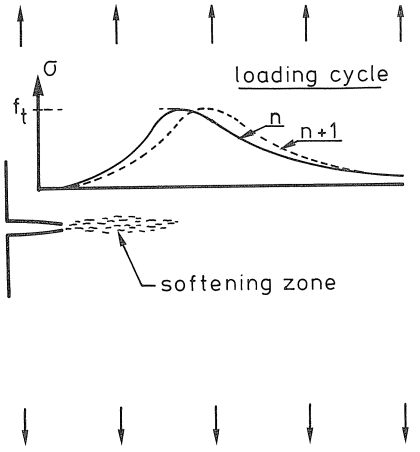

Fig. 12. Assumed stress distribution near a crack; before and after a loading cycle.

redistribution has to take place. The dashed line in Fig. 12, plots a possible stress distribution after the load cycle. The actual new stress distribution depends on the total structure in combination with its load application. Nevertheless, the basic idea is that the softening zone propagates under cyclic or fatigue loading. Furthermore, it can be assumed that deformations increase with the number of load cycles and that this will continue until equilibrium can no longer be found. For the load-deformation relation of the structure, it means that in that case the descending branch is reached. To illustrate this, Fig. 13 shows an assumed load-deformation relation for a certain structure under a continuously increasing deformation. The maximum load bearing capacity is equal to F_{max}. If the same structure is loaded cyclically, loops as sketched in Fig. 13 will

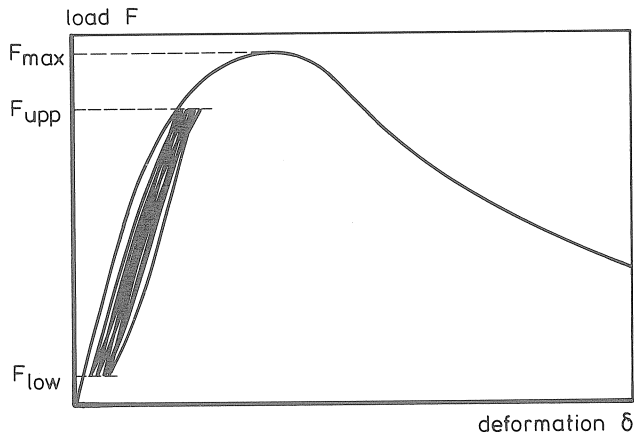

Fig. 13. Schematic representation for the load-deformation relation of a structure loaded under continuous increasing deformation or cyclically loaded between F_{low} and F_{upp}.

probably be found. The loops shift a little to the right, each time a loading cycle is performed. This will proceed until, in a certain cycle, the reloading curve meets the descending branch which forms the boundary for combinations of load and deformation that fulfill the requirement of equilibrium. Then failure of the structure occurs.

Failure criterion based on deformations
In several investigations, the strong relation between the development of strain and the number of cycles to failure was observed. Subsequently, the possibility of a fatigue failure criterion based on ultimate strain was surmised several times. For studying the possible existence of such a failure criterion, a number of tensile fatigue tests were performed. The development of deformations in these experiments have been compared with the deformations in the post-peak part of a deformation-controlled static test (see also Fig. 14).

3 Experimental technique

Experimental results from deformation-controlled uniaxial tensile tests (static and post-peak cyclic), tensile fatigue tests and bending tests are presented in this report. All these results have been obtained on one and the same tensile-compressive loading rig (Fig. 15). Here, the applied test rig and the generally applied procedure for the test performance will briefly be discussed. For a more detailed description, the reader is referred to [15].

3.1 *Deformation-controlled uniaxial tensile tests*
Generally specimens with the dimensions $60 * 50 * 150$ mm^3 were used with two saw cuts reducing the centre cross-sectional area to $50 * 50$ mm^2. The specimens were sawn

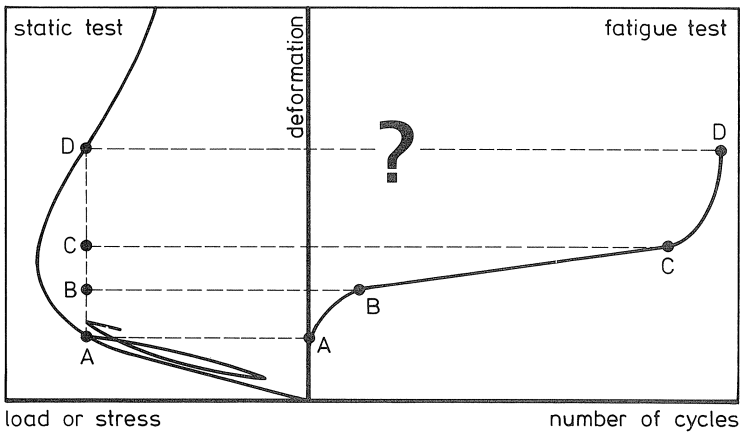

Fig. 14. Schematic representation of a possible relation between deformations in a static test and in a fatigue test.

out of plates with a thickness of 50 mm. These plates were cast vertically in a battery mould. Two days after casting, the slabs were demoulded and subsequently cured under water for two weeks. Then specimens with the desired dimensions were cut out of the slabs. For the generally applied procedure of curing condition, the specimens were stored in the laboratory (20 °C, 60% relative humidity) until testing. For the connection between the specimen and the loading platens a two-component glue was used. In the tensile tests it was intented to prevent rotation of the loading platens. Therefore, a guiding system was designed (see Fig. 15). For the load measurement, four 50 kN load cells placed under the lower loading platen were applied. For the boundary of the specimen a rotational and translational stiffness (upper and lower platen together) of 10^6 Nm/rad and 148 kN/mm respectively, was measured.

For the deformation measurements, two different types of electro-mechanical measuring devices were applied. LVDTs (linear variable differential transducers) and a type of clip gauge (denoted as "extensometers") were used. The arrangement of the measuring devices on the specimen varied in the different test series. Two of them can be seen in Fig. 16. Two different bases (35 mm and 110 mm) were applied for the deformation measurements. As control parameter sometimes the average signal of two additional LVDTs (one on each specimen side) with a 50 mm base and sometimes the average signal of the four 35 mm LVDTs (see Fig. 16b) was used. For the experiments, a loading rate of 0.08 μm/s corresponding to a measuring length of 50 mm was applied. As far as the data-acquisition system is concerned, it can be mentioned that special requirements had to be fulfilled regarding resolution of the measuring devices, amplification of the signal and AD conversion. For the tensile tests, with a peak load at a deformation of about 5 μm (for $l_{meas} = 35$ mm), a resolution of well below 1 μm was required. For the fatigue tests with a difference in deformation of about 1 μm between the ascending and descending branch, the requirements regarding resolution were even more stringent.

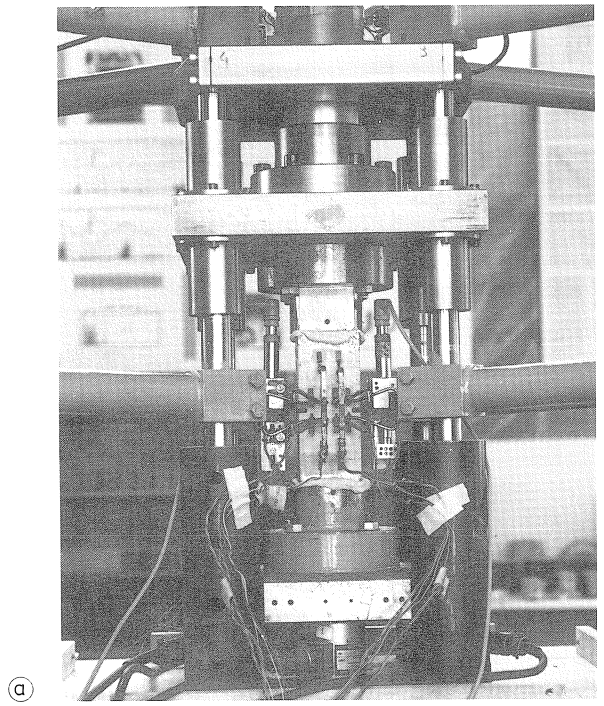

ⓐ

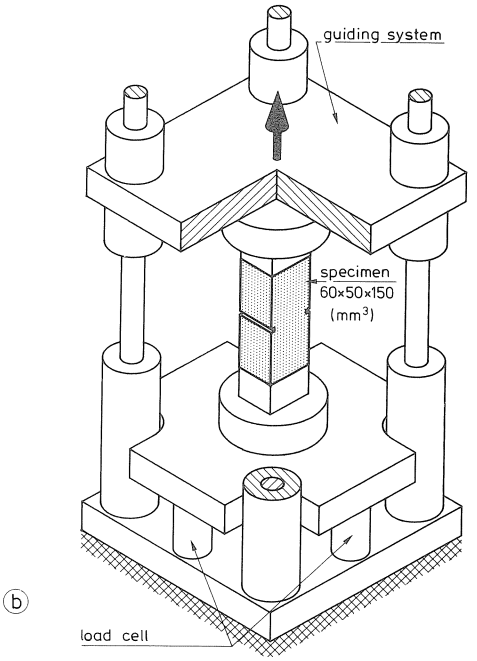

ⓑ

Fig. 15. Photo (a) and schematic representation (b) of a tensile specimen glued in the testing equipment.

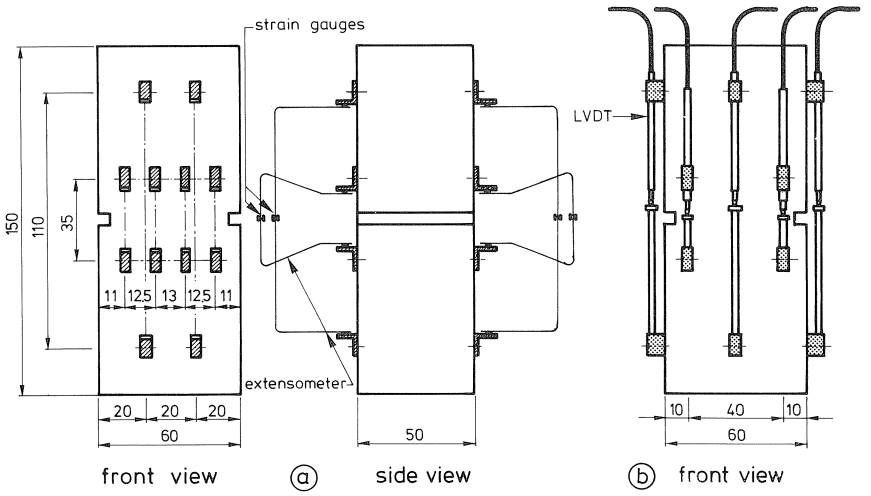

Fig. 16. Two arrangements of measuring devices applied.

3.2 *Bending tests*

A test series was performed in which different types of fracture tests were applied to specimens made from the same type of concrete originating from one and the same batch. Besides the normally applied tensile tests on narrow specimens, the experiments in this test series, denoted as "verification tests", are: bending tests on notched beams and uniaxial tensile tests on single edge notched plates. Fig. 17 shows the different specimens. Three different depths, 10, 30 and 50 mm, were applied for the notches in the bending specimens (total height: 100 mm). In this report, the results of the bending tests will be discussed. For information about the uniaxial tensile tests on the single notched plates, the reader is referred to [15].

In order to perform the bending tests on the same equipment, a specially designed loading arrangement was used which could be directly mounted in the tensile equipment. It was chosen to use a four-point bending test instead of a three-point bending test in order not to have a support in the fracture zone, since this would introduce compressive stresses parallel to the fracture zone. Furthermore, the load and its reactions in the supports are introduced by tensile bars which could easily undergo horizontal movements. Since the total bending equipment (loading arrangement and specimen) had to be placed in the tensile equipment, for which only a certain maximum amount of free space was available, the specimen height was limited to 100 mm. Then a beam with the dimensions $500 * 100 * 50$ mm^3 was chosen (see Fig. 18). The arrangement of the LVDTs (l_{meas}: 35 mm) was equal at the front and rear sides of the specimen and was kept the same for the three notch depths. Two LVDTs, one at the front and one at the rear of the specimen (placed on opposite sides of the notch) were used for measuring the deflection. A steel platen, placed on small steel supports located in the centre of the beam below the outer supports, was used as reference for this measurement.

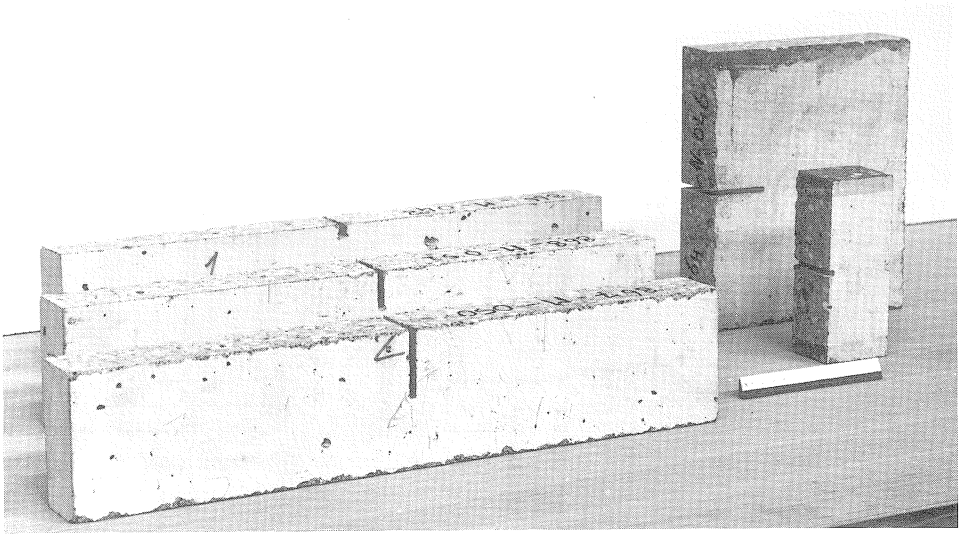

Fig. 17. Specimens applied for the test series "verification tests".

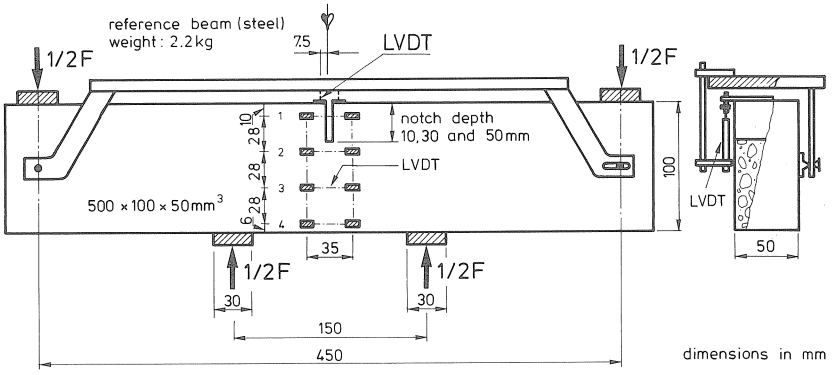

Fig. 18. Schematic view of a bending test.

3.3 *Uniaxial tensile fatigue tests*

In order to investigate several phenomena of the behaviour of a specimen in a tensile fatigue experiment, a limited number of tensile-tensile and tensile-compressive fatigue tests were performed. Initially, it was intended to use unnotched specimens. However, due to the fact that fracture mostly occurred near a glue platen, this proved to be impossible. Nevertheless, two experiments on unnotched specimens, one loaded statically and one loaded dynamically, were successful. For the rest of the experiments, notched specimens were applied. The test ran load-controlled with cycles between an upper and lower load level. These levels could be chosen freely. For generating the load signal, the equipment applied previously in the Stevin Laboratory [12], was used. The loading frequency was 6 Hz.

The difference compared to the fatigue tests previously performed is that load-deformation cycles were measured more precisely, while furthermore deformations were recorded at more locations on the specimen. For measuring the deformations at different loading points in a loop, it is necessary to have a measuring system which is able to measure very accurately. This is understandable if it is realized that for a measuring length of 35 mm, the deformations of the unloading and reloading curves in a loop differ less than 1 μm. On the other hand, the measuring system must be very fast. In order to get some idea about the shape of a loop, the number of measuring points in such a loop should not be too small. It is very hard to meet these two requirements at the same time: a measuring system that is accurate as well as fast. The principles of a data-acquisition system that was specially designed for this purpose, will be shown below.
For the analog-digital conversion a fast A/D-converter was chosen. The resolution and accuracy that could be attained with that converter was not enough. Therefore, for each measurement, eight samples were averaged. The frequency of the fatigue loading was 6 Hz. This means that every second, 6 loops are performed (see Fig. 19). The principle of the data-acquisition system is such that the first half of each second is used to sample and the second half of the second is used to process the data. In the three loops that are recorded, 75 measuring points are available. For each measuring point, the deformation of eight LVDTs (see Fig. 16b) and the load in the four load cells are recorded. Consequently, 900 (= 75 * 12) measurements are taken in 0.5 seconds (sampling frequency: 14400 Hz). The accuracy of the measurements is already rather good. Nevertheless, in order to improve this, the three loops are averaged. It can be expected that the shapes of the loops in three successive cycles will not differ significantly from each other, except for the cycles in the beginning and at the end of the experiment. For averaging the three loops, the measuring points i, $i + 25$ and $i + 50$ ($1 \leq i \leq 25$) were averaged. As an example, an experimental result is shown in Fig. 20. The measurement as described above was taken at regular intervals. The first loop that was measured was loop 144. Thereafter, cycles were recorded after intervals equal to $3 * 2^a$ cycles, in which a has the

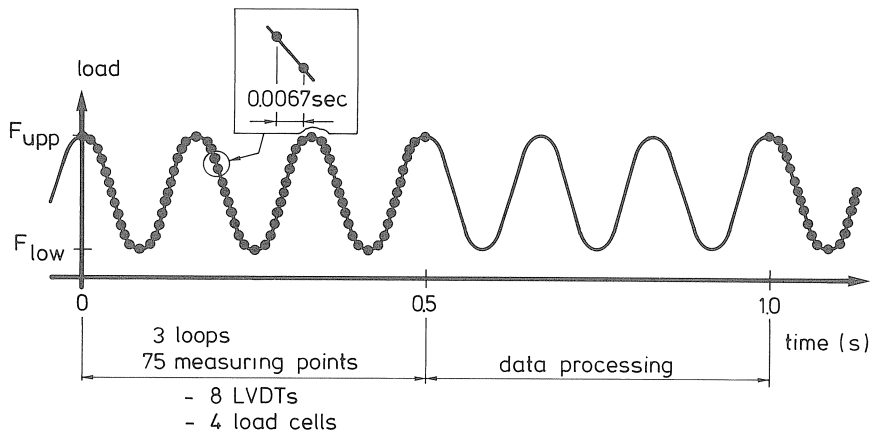

Fig. 19. Principle of the data acquisition for the fatigue tests.

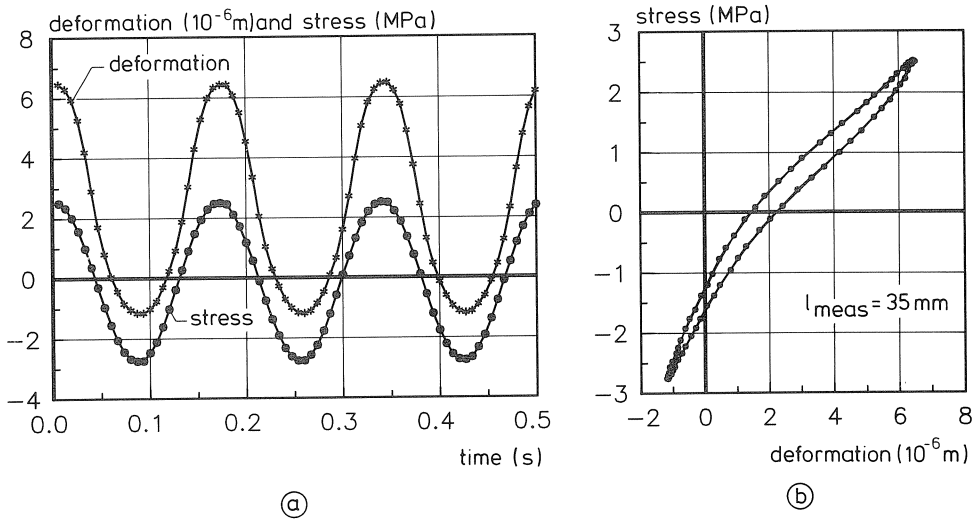

Fig. 20. Experimental result of 3 loops (not averaged) in a fatigue test; stress and deformation versus time (a) and corresponding stress-deformation relation (b).

value 6, 7, 8 and so on, up to a selected maximum. So far, the procedure for measurements at regular intervals is described.

The most interesting part of the experiment is certainly the last part. In that part, the deformations increase strongly. Since it is intended to compare deformations at the envelope curve in a static test and at failure in a fatigue test (see Section 2.3), it is necessary to record data near failure. For that reason a buffer is used, in which the data of the last 20 seconds are stored. This buffer is updated in each second half of a second in which data processing takes place and therefore contains 20 times the data of three loops (not averaged). As soon as the test is stopped, the data in the buffer can be read and stored in a data-file. In order to detect the ending of the experiment, the recorded load at the upper load level is checked. After failure of the specimen, the upper load level will no longer be reached. When this had occurred a preset number of times, the test and measurements were stopped. It was also possible to stop the experiment after a preset number of cycles.

As far as the above described measurements are concerned, the following remarks can be made. It is not claimed that the data-acquisition system is able to measure reproducible deformations of less than 0.1 μm. It was only intended to improve the measurements in such a way that the unloading and reloading curves in a loop do not cross each other. It is realized that some hysteresis may be present in the measurements. Nevertheless, the development of loops can very well be studied. Furthermore, a difference in temperature between day and night, as well as a difference in temperature due to an open door, may influence these measurements significantly. Therefore, an environmental chamber was built around the specimen, in which the temperature could be kept more or less constant during the experiment.

4 Structural behaviour in a uniaxial tensile test

4.1 *Introduction*

The uniaxial tensile test is probably the most fundamental fracture test there is. The former supposition was that this test, when performed under deformation control, directly yields a stress-deformation relation that includes all relevant fracture mechanics parameters. Recently, however, it has been found that this type of test is more complicated than it looks at first sight [16, 17]. It appears that it is often accompanied by a phenomenon that can be regarded as structural behaviour. Since basic material models are derived from this test, it may be obvious that it is very important to know the influence of such a structural behaviour on the obtained test results. This structural behaviour will be elucidated in this chapter by means of tensile experiments with specimens of different length and a simple numerical model. Details of these experiments and analyses have been published before [17, 18].

A precondition for regarding the obtained σ-δ relation as a material property is a uniform deformation distribution over the fracture zone during the entire test. In most of the reported deformation-controlled tensile tests, however, it appeared that this precondition could not be fulfilled. Generally, when the loading platens could freely rotate then at peak load, a crack was initiated on one side of the specimen and with further increasing average deformation, this crack opened while the deformations on the opposite side decreased until, finally, compressive stresses acted in that part [19, 20, 21]. For the test rigs in which rotation of the loading platens was prevented non-uniform crack opening occurred in the first part beyond peak load, whereafter the deformation distribution over the fracture zone was again more or less uniform. A typical result found in these tests was that the descending branch displayed sometimes irregularities of a type as sketched in Fig. 21 [16, 22, 23, 24].

A thorough investigation on tests on a normal-weight concrete (NC) and a lightweight concrete (LC) yielded the following observations:

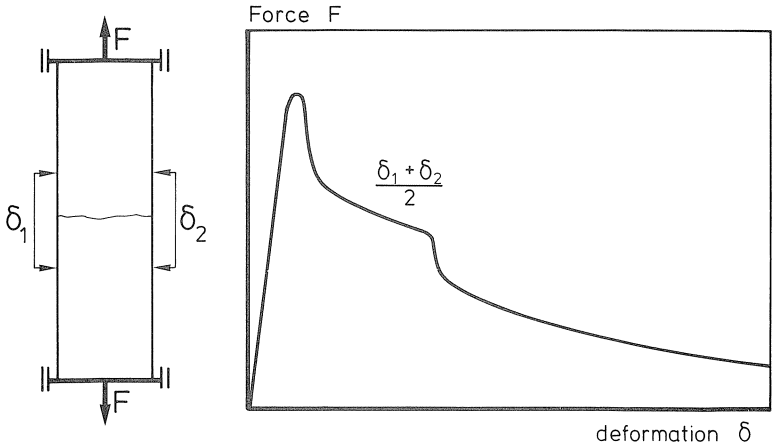

Fig. 21. F-δ relation as can be obtained in a tensile test with non-rotatable loading platens.

- the non-uniform crack opening was a three-dimensional phenomenon;
- dependent on the type of concrete applied, the same maximum non-uniform crack opening was reached in every test and was greater in case of LC than in case of NC;
- the descending branch sometimes displayed irregularities of a type as sketched in Fig. 21, which was most pronounced for LC.

The observations in the tensile tests formed the grounds for thinking that a structural behaviour plays an important role in these tests. Especially the fact that the same maximum non-uniform crack opening was found for different experiments with the same specimen size and boundary condition, led to the belief that it cannot solely be the result of some accidental eccentricity (non-symmetric material property due to heterogeneity or eccentric loading). Much more it was believed that there is a second equilibrium path for a uniaxial tensile test on an elastic-softening material.

Based on the previously obtained experimental results for different boundary conditions, it was expected that a direct relation exists between the degree of non-uniform crack opening and the rotational stiffness of the boundary of the softening zone. In this respect, this boundary condition is determined by the boundary of the specimen (loading equipment), but also by the specimen itself. In order to check this supposition, a test series was performed in which the specimen length was varied and, with it, the rotational stiffness of the boundary of the softening zone (non-rotatable loading platens!). Principal results of this investigation are presented in Section 4.2. Since the observed phenomena are indeed the result of a structural behaviour, FE analyses can be performed in order to study this particular behaviour in a deformation-controlled tensile test on a softening material (see [25]). In Section 4.3 it will be shown that also a very simple numerical model can be used for such a study.

4.2 *Experimental verification*

In order to verify the surmised relation between the boundary rotational stiffness of the softening zone and the degree of non-uniform crack opening, a test series was performed using the specimen length as a variable. Since previous tests on a lightweight concrete (low Young's modulus) had proved that the features which will be investigated, are more pronounced for this material than for normal-weight concrete, the former type of concrete was used in the experiments. Four different specimen sizes were investigated, denoted as types A, B, C and D. Compared to the dimensions of type A ($250 * 60 * 50$ mm^3), the length of the type B and C specimens was reduced to 125 and 50 mm respectively, while for type D a cross-sectional area of $50 * 40$ mm^2 was applied for a length of 250 mm. Further experimental details can be found in [17].

The rotational stiffness of the loading platens was in the order of 10^6 Nm/rad, which was much higher (from about 3 times for specimen C to about 50 times for specimen D) than the rotational stiffness of the specimens (EI/l). This means that the influence of the boundary conditions of the softening zone can very well be studied using the specimen length as a variable.

For each type of specimen, typical deformation distributions for different loading

stages are plotted in Fig. 22. From these diagrams, it can be seen that for shorter specimens, i.e. higher rotational stiffness, the non-uniform crack opening is less pronounced. For type C the crack surfaces remain parallel to each other in almost every loading stage. Furthermore, this figure clearly demonstrates that the deformations must be considered three-dimensionally.

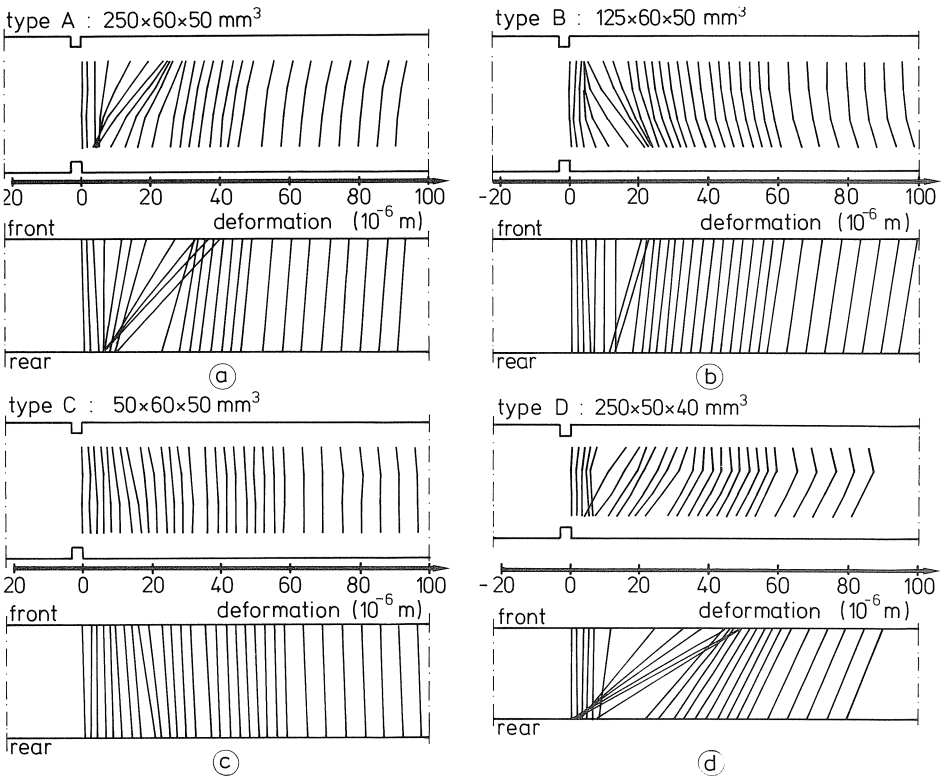

Fig. 22. Typical deformation distributions obtained on specimen types A, B, C and D.

Average stress-deformation curves corresponding to the deformation plots of Fig. 22 are plotted in Fig. 23. Most notable in these diagrams is the smooth descending branch for specimen type C. In the other tests, irregularities of varying degrees of importance can be observed. The results shown in Figs. 22 and 23 pertain to individual tests. The same tendencies were observed in all other tests. In order to compare maximum non-uniform crack openings in the different experiments, two rotations belonging to the principal axes of the critical cross-section are defined (see inset of Fig. 24). It appeared that maximum non-uniform crack openings for specimen types A,B and C were very well positioned on a straight line (Fig. 24), which confirms the relation between rotational stiffness and maximum non-uniform crack opening. The results of the slender type D specimens were somewhat divergent.

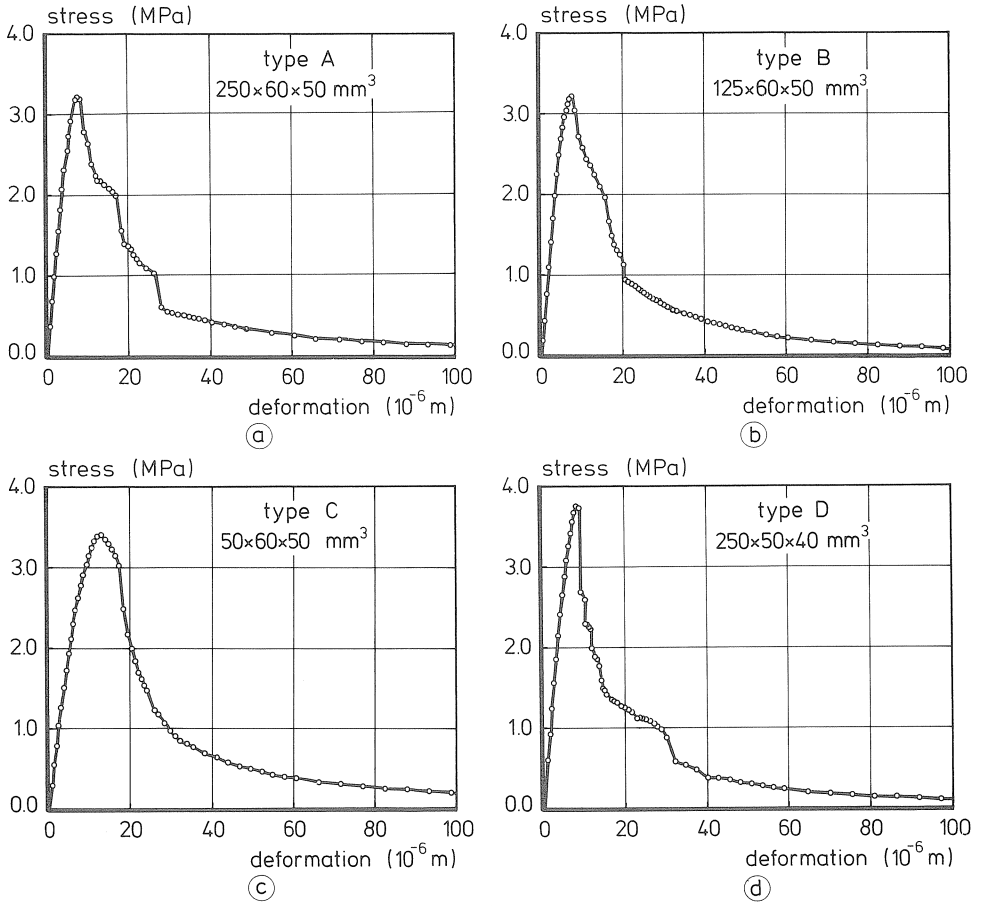

Fig. 23. Average stress-deformation relations corresponding to the results presented in Fig. 22 ($l_{meas}=35$ mm).

From the results shown, the question that immediately arises is whether the shortest specimen (type C) is most suitable for determining the tensile properties. The mean results for the different specimen types (Fig. 25) demonstrate that a quick positive answer to this question cannot be given. The fact that the average results for specimen type C deviate significantly from those for the other specimen types may possibly be explained by an influence of the stiff loading platens that are, for such a small specimen length, located very near to the fracture zone.

Finally, one experiment will be discussed in more detail, because some features can be extracted from it which were also revealed by the numerical analyses of which the results will be presented in the following section. It concerns a post-peak cyclic experiment. It appeared that only out-of-plane non-uniform crack opening occurred in this test, as can be seen in Fig. 26a, where the deformation distributions for loading points

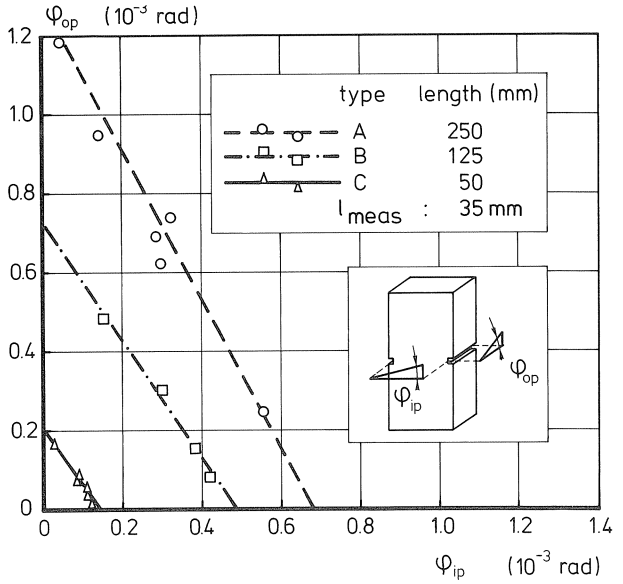

Fig. 24. Maximum non-uniform crack opening for different tests, represented by a combination of in-plane rotation φ_{ip} and out-of-plane rotation φ_{op}.

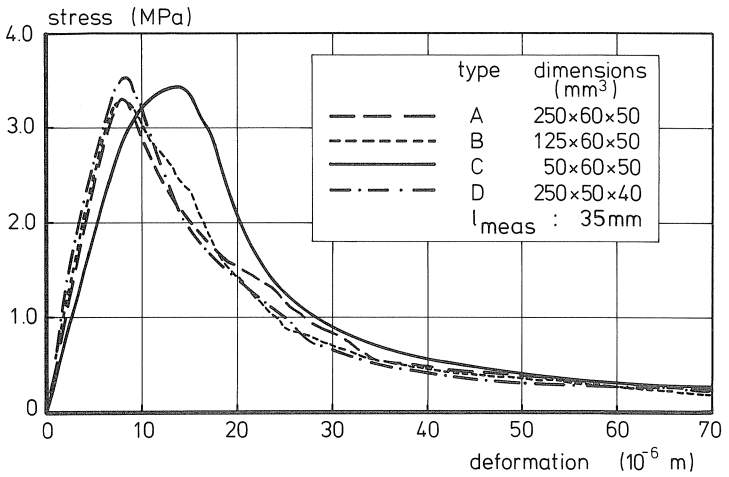

Fig. 25. Mean stress-deformation relations for specimen types A, B, C and D.

at the envelope curve are plotted. In Fig. 26b, the σ-δ envelope curve for the average deformation over the total cross-section is plotted, while Fig. 26c shows the curves for the front and the rear sides of the specimen separately. It appears that in two parts of these curves no measurements were taken despite the regular time intervals for these measurements. This fact points to a snap-back for these parts of the σ-δ relations, because snap-backs in deformation-controlled tests are passed by sudden stress drops.

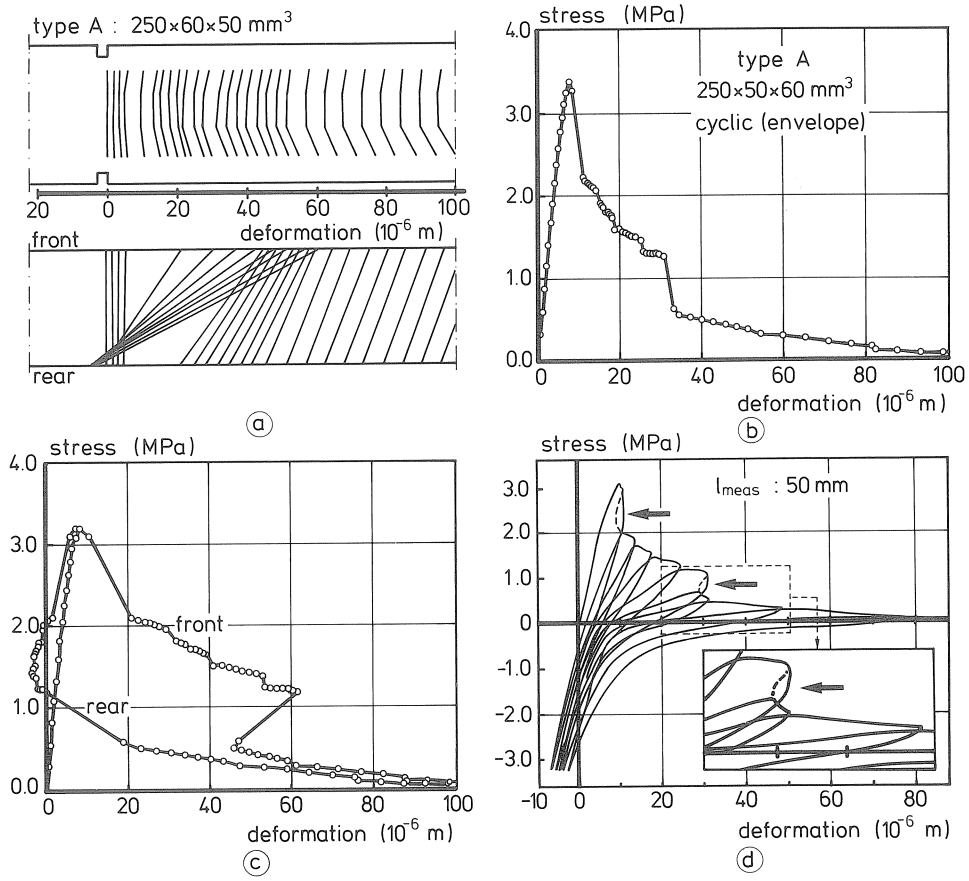

Fig. 26. Typical result for specimen type A; (a) deformation distributions, (b) average σ-δ relation ($l_{meas}=35$ mm), (c) average σ-δ relation for front and rear sides of the specimen and (d) X-Y recorder plot.

Fig. 26d is the X-Y recorder plot for this test. The surmised snap-backs are indicated by dashed lines. By chance, the second snap-back was confirmed by the experiment; at least partly. Probably the loading direction was reversed just at the beginning of the snap-back. In the subsequent loading cycle, the envelope curve was reached at an average deformation which was lower than that at the instant of leaving the envelope curve. The parts of the σ-δ curves besides the dashed lines (indicated by arrows) are created instantaneously and are, according to the above explanation, not genuine.

4.3 *Simple numerical model*

The inferred structural behaviour was also confirmed by a numerical analyses with the FE code DIANA [25]. The FE code can also be used to study the influence of parameters like boundary conditions, specimen dimensions and material input. However, if

one is only interested in the way the different phenomena are influenced by these parameters, then it may be more convenient to reduce the problem to a simple mechanical model. Firstly, the advantage is that a parameter study can be performed easily and quickly and, secondly, such a simple model may bring more transparency in the problem. In this section, such a simple model is proposed, which is based on the theory of bending in combination with a process zone model [18].

For the mechanical model, the tensile specimen is subdivided into two linear elastic parts A and a small zone B, that encompasses the fracture zone (Fig. 27a,b). The material behaviour of parts A and B is shown in Fig. 27c. Now the specimen (parts A) and its boundary can be represented by rotational and translational springs (Fig. 28a). Zone B deforms only in one direction according to a defined tensile softening relation, while the edges of this zone remain plane. Besides Young's modulus, the tensile strength and the stress-crack opening relation (material input), the tensile softening relation for the fracture zone is mainly determined by the depth of this fracture zone (similar to the smeared crack approach). For the sake of clarity, there is no direct relation between the

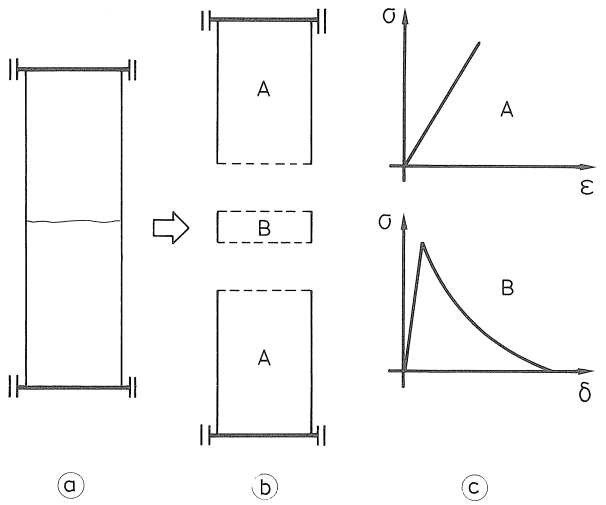

Fig. 27. Subdivision of a tensile experiment (a) into two linear elastic parts and a linear softening zone (b, c).

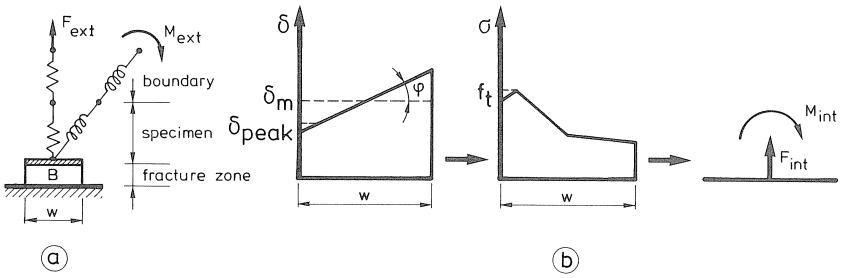

Fig. 28. Model for the tensile test (a) and relation between deformation distribution, stress distribution and internal force and moment (b).

depth of the fracture zone, which will be arbitrarily chosen, and the width of the process zone in an actual experiment. In fact, the depth of the fracture zone links the deformation distribution in that part of the cross-section where a process zone is active, with the strain distribution in that part where the material still shows linear elastic behaviour. The solution procedure for this model is as follows. For an arbitrarily chosen combination of mean deformation δ_m and rotation φ of the fracture zone, the deformation distribution of this zone is defined (Fig. 28b). Using the σ-δ relation (here a bilinear relation is assumed), the corresponding stress distribution can be calculated, which can be replaced by an internal force F_{int} and an internal moment M_{int}. This combination of δ_m and φ will only be a solution for the model where equilibrium and compatibility exist at the boundary of the fracture zone. For the boundary in this tensile experiment, this means that the internal moment M_{int} must be equal to the external moment M_{ext} which is the result of the same imposed rotation φ. Obviously, for every δ_m, there exists at least one solution, which belongs to a rotation equal to zero. These solutions belong to the uniform crack openings and yield the applied σ-δ relation (input) as result. The interesting point, however, is to find solutions for non-zero rotations.

Comparison with FE analysis

For comparison purposes, the FE analysis [25] is simulated. Initially, 35 mm is taken for the depth of the fracture zone, which is equal to the measuring length in the experiments. Furthermore, this 35 mm base will be used as reference length for the σ-δ relations throughout this section. The applied material input can be obtained from Fig. 29.

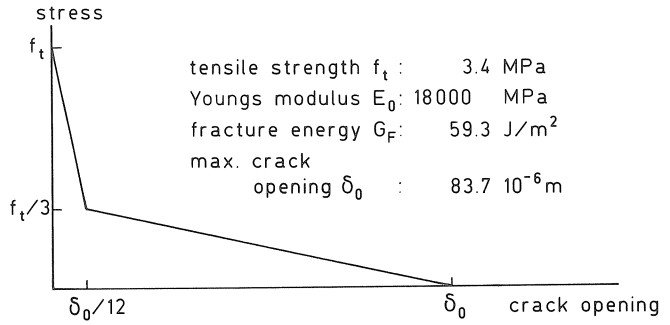

Fig. 29. Input parameters for the material behaviour of the concrete.

For values of the mean deformation δ_m ranging from 5 μm to 15 μm with steps of 0.1 μm and rotation angles varying between 0 and 400 10^{-6} rad with steps of $4 * 10^{-6}$ rad, the corresponding internal moment and internal force were calculated. The relation between M_{int} and φ for a number of δ_m values is given in Fig. 30. The deformation at peak load, δ_{peak} is equal to 6.61 μm. It appears that firstly negative moments are found for rotations starting from zero in case $\delta_m < \delta_{peak}$ and positive moments in case $\delta_m > \delta_{peak}$. In Fig. 30, the linear relation between the external moment at the boundary

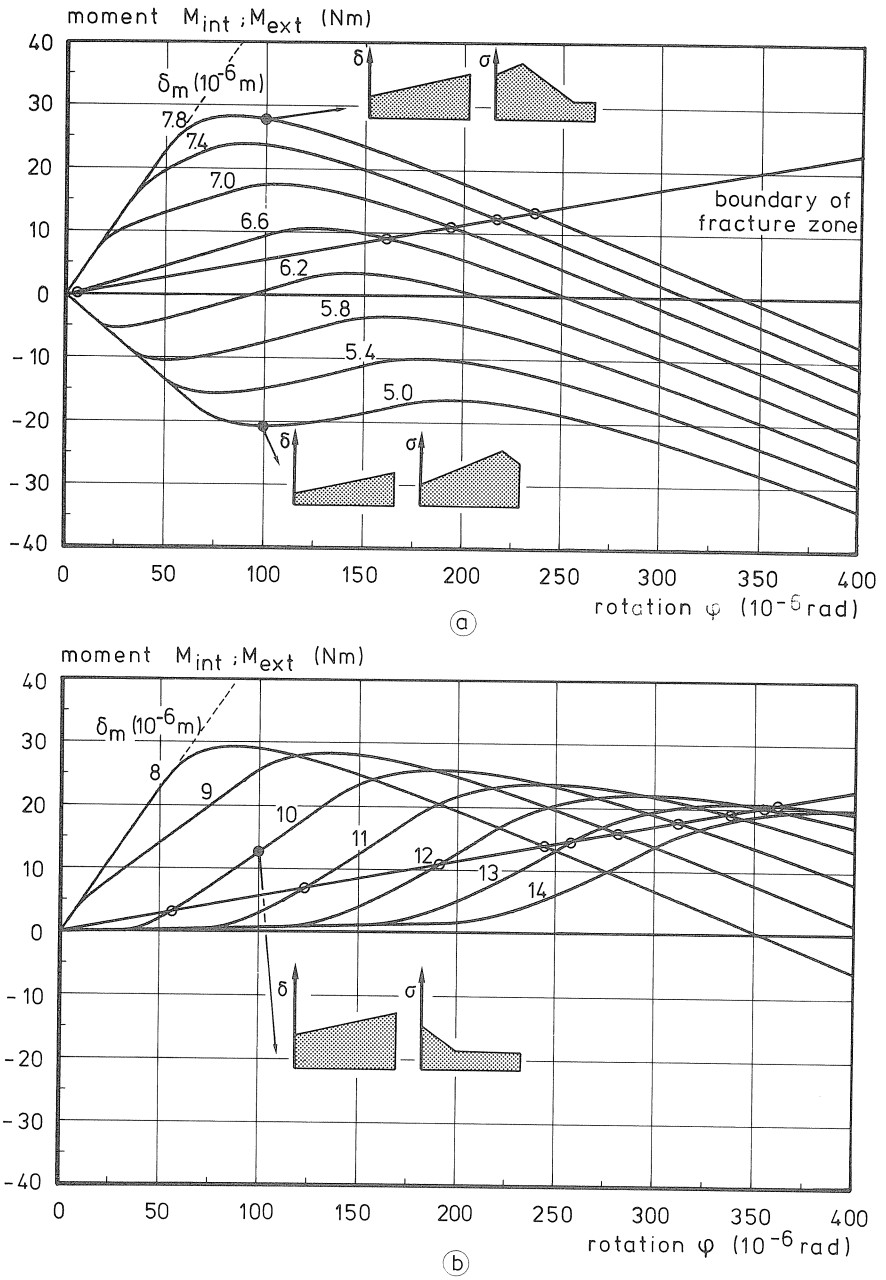

Fig. 30. *M-φ* relations for the fracture zone and average deformations from 5 to 7.8 μm (a) and from 8 to 14 μm (b).

of the fracture zone, M_{ext} and an imposed rotation φ, is included so that solutions can be directly taken from the figure, as being the points of intersection of the straight line and the curved lines. As can be seen, solutions exist for non-zero rotations. For a number of average deformations, there are even two points of intersection besides the origin, which points to the occurrence of a snap-back.
The average stress for the points of equilibrium is determined by the corresponding internal force divided by the critical cross-sectional area. In Fig. 31a the σ-δ relation, which was applied as input, is represented by the straight lines. This relation belongs to the solutions with uniform deformations (origin in Fig. 30). After connecting the solution points found for non-uniform deformations, a second equilibrium path appears to start at peak load and to end in the kink of the descending branch. Thus the point at the peak is a bifurcation point. As far as the existence of snap-backs is concerned, this analysis revealed two snap-backs, as sometimes also seems to occur in experiments (see Fig. 26d).
If the σ-δ relations are being compared with the FE results (Fig. 31b), then it appears that both analyses display the same features. Nevertheless, two differences of minor importance can be observed. The first one concerns the shape of the curves near peak load. The rounded peak for the FE results is due to the stress concentrations at the applied notches which do not play a role in the model discussed above. The second

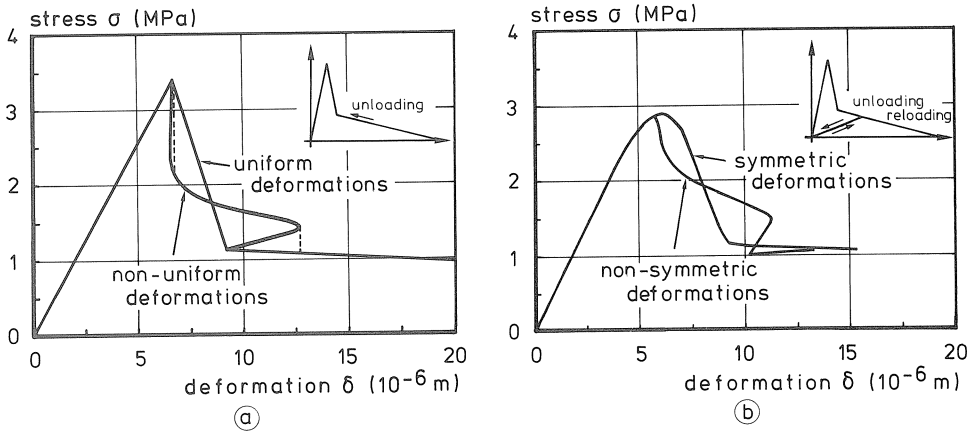

Fig. 31. σ-δ relations predicted by the simple numerical model (a) and the FE analysis [25] (b).

difference can be observed in that part of the σ-δ curve where the path with non-uniform deformations again reaches the path with the uniform deformations. A different modelling for unloading is responsible for this difference. In the FE analysis a secant unloading was applied (see inset in Fig. 31b). In the model as described in this section, possible solutions for an arbitrarily chosen deformation are calculated directly. This solution procedure demands an unambiguous relation between deformation and stress, which means that the loading and unloading path are the same.

The deformation distributions for a number of δ_m-values, whereby the equilibrium path with the non-uniform deformations is followed and δ continuously increases like in a deformation-controlled experiment, are plotted in Fig. 32. The resemblance with results obtained in an actual experiment is good (compare Fig. 22).

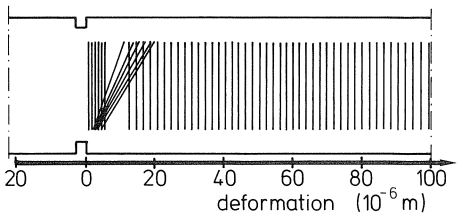

Fig. 32. Deformation distributions predicted by the model.

Influence of fracture zone depth and boundary conditions

The analysis presented clearly demonstrates that the model can be used to study the structural behaviour. However, the model loses its power if the results depend strongly on the chosen depth of the fracture zone. In order to investigate the influence of this parameter, the same calculation has been repeated using 2.5 mm and 50 mm, respectively for this parameter. A comparison of σ-δ relations with that for the 35 mm base is presented in Fig. 33a. It can be concluded that, although there is an influence, the special features of the tensile test are not significantly affected by varying this parameter between 2.5 mm and 50 mm.

The fact that internal and external M-φ relations are determined separately means that a parameter study for the length, stiffness (Young's modulus) and boundary rotational stiffness of the specimen is fairly easy to perform. For a given material input, the M_{int}-φ relations only have to be determined once. For different values of the said parameters,

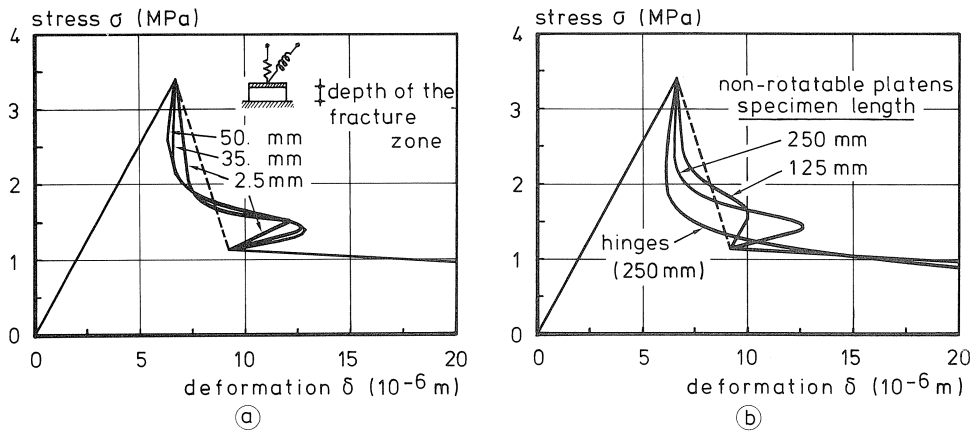

Fig. 33. Predicted σ-δ relations as influenced by the depth of the fracture zone (a) and by specimen size and boundary conditions (b).

the relation M_{ext}-φ can simply be determined and compared with the M_{int}-φ relations. As far as the specimen length is concerned, a shorter length means that the rotational stiffness is higher. In Fig. 30 it can be seen that for a steeper slope of the M_{ext}-φ relation, the maximum attainable rotation decreases. This result, as well as the influence on the σ-δ relation (Fig. 33b) is in agreement with the experimental results (Section 4.2). For rotatable loading platens the boundary condition is given by $M_{ext} = 0$, for which the model predicts a continuously increasing rotation and a smooth descending branch (see Figs. 30 and 33b). This result also seems to be in accordance with experimental results. It must be realized, however, that in this simple model geometrical effects have not been taken into account. For this boundary condition, the effect of bending out may have a significant influence for greater rotations. For a rotation φ in the fracture zone, the eccentricity e is equal to $\frac{1}{4} \cdot l\varphi$ (l = specimen length). Solutions can now be found by using e-φ relations ($e_{int} = M_{int}/F_{int}$) instead of M-φ relations, but otherwise the procedure is the same. This has not been worked out here. Maybe geometrical effects also played a role in the experiments on the slender type D specimens (see Section 4.2).

Imperfection in relation to bifurcation point

Besides the examples that have been given, more phenomena can be studied with the aid of the model. For instance, it is possible to study the influence of imperfections in test performance, like eccentric loading in case of hinges, or the existence of an initial rotation in case of non-rotatable loading-platens. In the latter case, the line for the M_{ext}-φ relation in Fig. 30 is shifted to the right. Then, only one equilibrium path (non-uniform deformations) will be found, because the origin ($\varphi = 0$) no longer leads to a solution. This result is in accordance with the theory that bifurcation points occur only in perfect structures [26]. Since concrete is an inhomogeneous material, the equilibrium path with the non-uniform deformations will always be found in experiments.

4.4 *General remarks*

Previous sections have clarified how a structural behaviour can occur in deformation-controlled uniaxial tensile tests on plain concrete. It was found that the observed phenomena in experimental results can very well be explained with a process zone model in combination with a FE analysis [25] or with a simple mechanical model. If the fracture mechanics parameters are taken directly from the σ-δ relations obtained in such a test, then the descending branch is the most affected parameter. It has been shown that in a uniaxial tensile test on a softening material, a bifurcation phenomenon is encountered. Eccentricities in load application as well as those related to the material property mean that the bifurcation point will not be found in experiments in the same way as it is encountered in the analyses. It should be noted, however, that it is primairily the structural behaviour that causes the non-uniform crack opening and not the eccentricity itself. Very small differences in the eccentricity will hardly affect the results. Only for larger eccentricities will the obtained σ-δ relations and especially the peak stress be significantly influenced. This parameter, however, is not investigated in this chapter.

The structural behaviour as discussed here for the uniaxial tensile test on concrete may also play a significant role in other circumstances. Firstly, it may be obvious that it can occur in uniaxial tensile tests on every softening material. Secondly, this structural behaviour may also influence experiments with other types of uniaxial loading. For instance, it can be expected to be active in impact, fatigue and sustained tensile tests (see also Section 8.4). But a similar structural behaviour can also be encountered in deformation-controlled uniaxial compressive tests (see, for instance, [27]). Thirdly, even other types of test may display a behaviour that parallels the structural behaviour in the uniaxial tests, as demonstrated by Rots et al. [28] in a FE analysis of a double notched shear beam test.
The discussions of the different features of fracture tests on softening materials clearly demonstrate that one must be very careful about making assumptions of symmetry or anti-symmetry [28]. Though such an assumption may seem justified in many cases, it proves to be incorrect in most of them. This affects the interpretation of fracture tests as well as its modelling in calculations.
Finally, it can be remarked that a deformation-controlled uniaxial tensile test is, despite the structural behaviour that occurs, still a suitable test to determine the tensile properties of concrete, especially when the effects of the structural behaviour are minimized.

5 Tensile softening behaviour

5.1 *Introduction*

In this chapter attention will be paid to the tensile softening behaviour of concrete. In Section 5.2 a constitutive relation for the stress-crack opening relation for an ordinary type of normal-weight concrete will be proposed. It can be mentioned that the same relation also proved to predict experimental results for other types of concrete rather well [15]. In Section 5.3 the influence of a number of variables on the fracture mechanics parameters will be discussed. In this section some remarks about the experimental determination of these parameters will be made.
In a uniaxial tensile test on an elastic-softening material like concrete, the recorded maximum tensile load divided by the cross-sectional area of the fracture zone will only represent the *tensile strength* if the deformation distribution and, consequently, the stress distribution in the fracture zone are uniform up to the peak load. It may be obvious that in this respect deformation and stress are considered at a macro-level. Therefore, possible causes of non-uniformity, as sketched in Fig. 34, will be referred to as "macro-structural" effects. The effects in Figs. 34a and 34c may occur in every uniaxial tensile test, while the one in Fig. 34b refers only to notched or necked tensile specimens. Compared to the situation of uniform deformation distributions up to peak load, the effect of these macro-structural effects on the complete tensile load-deformation relation is (see also [29, 30]):
- the maximum load will be lowered and the average stress at peak load does not represent the tensile stress properly;
- pre-peak nonlinearity will increase.

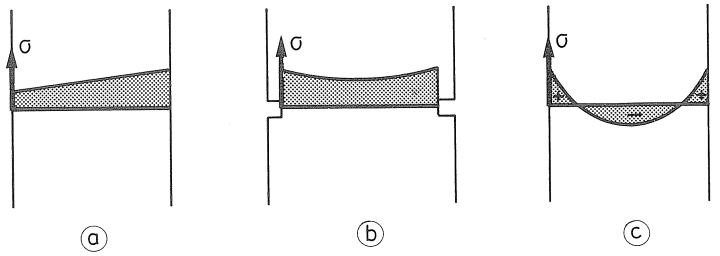

Fig. 34. Non-uniform stress distribution in a uniaxial tensile test due to eccentric loading (a), notches (b) or differential shrinkage or temperature (c).

As an example, a typical result that was found in the investigation into the influence of d_{max} on the softening behaviour is shown in Fig. 35. Since maximum aggregate sizes varying between 2 and 32 mm had to be investigated, it was initially decided to apply two different specimen sizes with an overlap for $d_{max} = 16$ mm. The applied specimen dimensions can be obtained from the inset in Fig. 35. For the large specimen a σ-δ relation was found that deviates significantly from the average relation that was found for the small specimens. The peak load is lowered and the pre-peak nonlinearity is more pronounced in the curve for the larger specimen. In this case, initial stresses due to differential shrinkage were probably the main cause for the observed behaviour. Besides for a larger critical cross-sectional area it is generally more difficult to see that each area of this cross-section reaches its maximum tensile force at the same instant.

The *fracture energy* is defined as the energy that is required to create one unit area of crack surface and is represented by the area under the stress-crack opening relation. In the different fracture mechanics experiments that are being performed, the fracture energy is determined as the total energy that is supplied to fracture a specimen (area

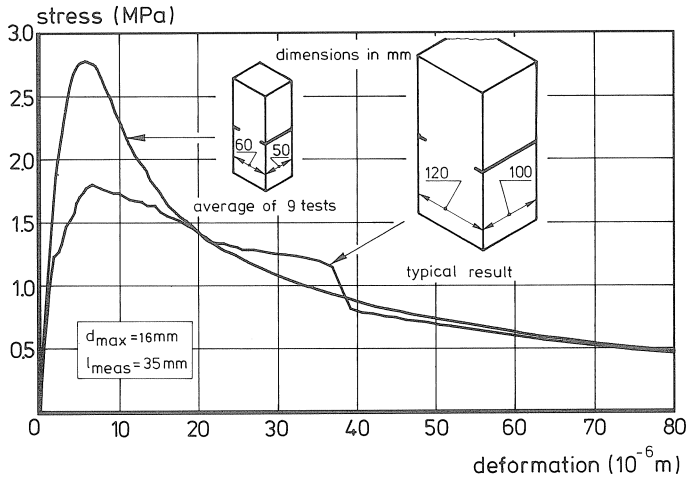

Fig. 35. σ-δ relations for $d_{max} = 16$ mm obtained on a large and a small specimen.

under the load-deformation relation) divided by the fractured cross-sectional area. In deformation-controlled uniaxial tensile tests, as well as in a lot of other fracture tests, the load-deformation relation displays a long tail in which stress gradually approaches a zero value. Mostly tests have to be stopped at a crack opening where still a small stress can be transferred. Consequently for the determination of G_F an assumption has to be made for the last part of the σ-δ relation. In Fig. 36 it can be seen that the energy in the last part of the σ-δ relation significantly influences the G_F-value. This is one of the reasons why absolute values for G_F from different investigations cannot directly be compared.

The tensile experiments with the applied specimen dimensions and notches are not very suitable for the determination of *Young's modulus*. Nevertheless, values for E_o have been determined because it is still possible to obtain qualitative information about the way the investigated variables influence this parameter.

For characterizing the material by means of a single parameter, the *characteristic length* $l_{ch}(l_{ch} = E_o G_F / f_t^2)$ is used [31]. The value is smaller for more "brittle" materials. It should be obvious that possible influences on the determination of the separate values of f_t, G_F and E_o will also affect the calculated value for l_{ch}.

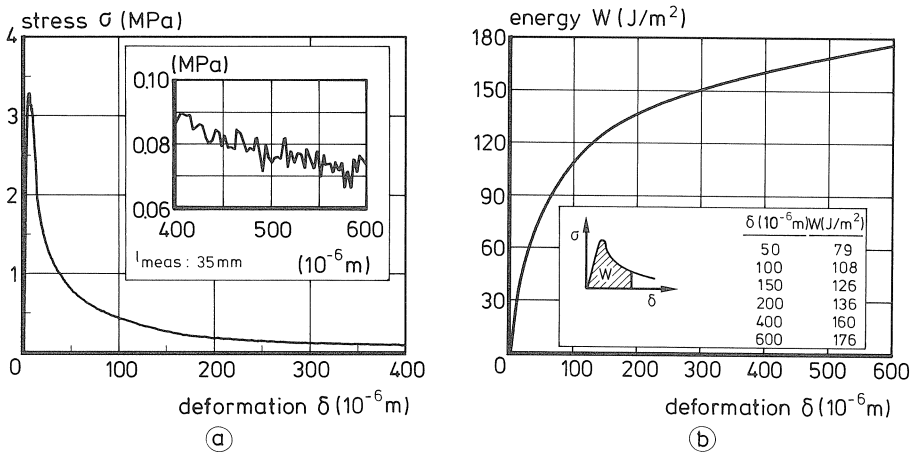

Fig. 36. Stress-deformation relation (a) and the corresponding energy-deformation relation (b).

5.2 *Stress-crack opening relation*

The most important input parameter for nonlinear fracture mechanics calculations of concrete is undoubtedly the stress-crack opening relation. Its importance has been demonstrated by several investigators [31, 32, 33]. The most direct way to obtain the σ-δ relation for concrete is still the determination by means of a deformation-controlled uniaxial tensile test.

A test series on a normal-weight concrete was used to determine a σ-w relation. Experimental details can be found in [34]. Data points of individual experiments, representing

the relation between relative stress σ/f_t and crack opening w, are plotted in Fig. 37. The mean value for f_t was 3.2 MPa. The chosen expression for the stress-crack opening relation is:

$$\frac{\sigma}{f_t} = \left\{1 + \left(c_1 \frac{w}{w_c}\right)^3\right\} \exp\left(-c_2 \frac{w}{w_c}\right) - \frac{w}{w_c}(1 + c_1^3) \exp(-c_2) \tag{4}$$

The best fit was obtained for $c_1 = 3$, $c_2 = 6.93$ and $w_c = 160$ μm. As far as w_c is concerned, the following remark can be made. The function (equation 4) was chosen in such a way that there is an intersection point w_c (critical crack opening) with the horizontal axis ($\sigma/f_t = 0$), which corresponds with the real material behaviour where the crack surfaces are completely separated at a certain crack opening, w_o. However, the experimental determination of w_o is very difficult due to the long tail of the descending branch. In equation 4, w_c is more or less used as a fitting parameter.
With the tensile strength f_t, the critical crack opening w_c and the shape of the σ-w line, the fracture energy can be calculated. The integration $G_F = \int \sigma \, dw$ gives for equation 4:

$$G_F = f_t w_c \left[\frac{1}{c_2}\left\{1 + 6\left(\frac{c_1}{c_2}\right)^3\right\} - \left\{\frac{1}{c_2} + c_1^3\left(\frac{1}{c_2} + \frac{3}{c_2^2} + \frac{6}{c_2^3} + \frac{6}{c_2^4}\right) + \tfrac{1}{2}(1 + c_1^3)\right\} \exp(-c_2)\right] \tag{5}$$

For the values of c_1, c_2 and w_c as given above and $f_t = 3.2$ MPa, G_F has a value of 99.7 J/m^2. Now, the fracture energy can be used in order to normalize the crack opening w. Therefore the critical crack opening w_c is chosen in accordance with the results of Fig. 37 ($f_t = 3.2$ MPa, $w_c = 160$ μm and $G_F = 99.7$ J/m^2). For the critical crack opening this gives the relation:

$$w_c = 5.14 G_F / f_t \tag{6}$$

Results from a number of deformation-controlled uniaxial tensile tests known from the

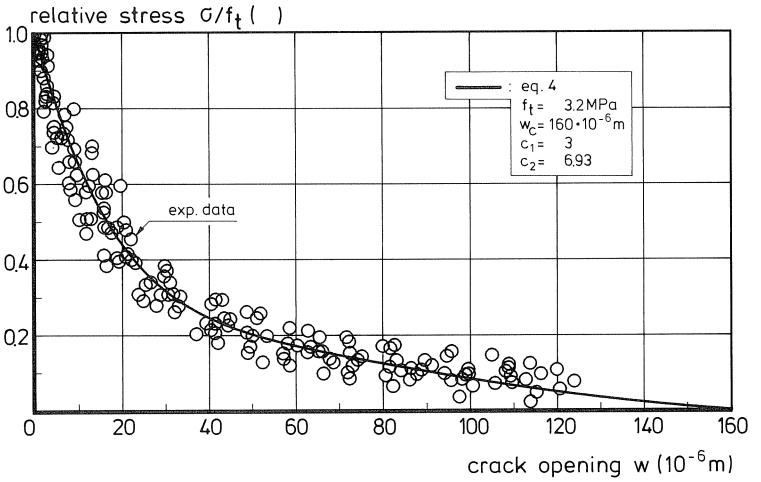

Fig. 37. Regression analysis for the σ-w relation; data points and fitted relation (equation 4).

literature have been compared with predictions by equations 4 and 6 [15]. Even though different concrete mixes were investigated, the shape of the stress-crack opening relation was very well described by the proposed constitutive relation.

5.3 *Tensile properties as influenced by different variables*

Besides the knowledge about the softening behaviour for an ordinary type of concrete, it is important to know how this behaviour can be influenced by different variables. In this respect one may think of variables related to the mix composition, like type of aggregate, maximum aggregate size and water-cement ratio, but also of variables concerning environmental and loading conditions. In an extensive research programme [15] the influence of the variables: type of concrete (normal-weight versus lightweight concrete), maximum aggregate size, compressive strength, curing condition and compressive preloading were investigated. Here the results will be summarized and comparisons with results known from the literature will be shown. For more detailed information, the reader is referred to [15].
As far as the mechanism for the softening behaviour of concrete is concerned, there is still no consensus among investigators. Possible explanations deal with cracking in matrix and aggregate, debonding, interlocking (sliding friction when aggregates are being pulled out of the matrix) and overlapping cracks. In fact, for the macro-structural approach in this study, it is not very important to know exactly the real explanation for the observed behaviour. However, in order to explain differences that can be observed when certain variables are investigated, the mechanism has to be taken into account. In that respect, it is assumed that stresses in the descending branch will increase when the crack path becomes more tortuous [15].

Type of concrete
A type of structural lightweight concrete (LC) with sintered clay for the bigger aggregates was investigated. For the lightweight concrete, the value for the facture energy was approximately 30 to 40% lower than for the normal-weight concrete (NC). This difference in G_F was mainly caused by the fact that the transferable stresses at larger crack openings in the descending branch were significantly smaller for LC than for NC, which supports the assumption regarding the crack path tortuosity. In LC the crack path will be more smooth due to the fact that cracks run through the aggregates, whereas for NC cracks go around the aggregates. As far as the tensile strength is concerned, mostly a smaller value for LC than for NC is reported in the literature. However, it should be remarked that for lightweight concrete initial stresses due to differential shrinkage can be very important, because the porous aggregates act as a buffer for the water in the inner part of the specimen. Probably, this phenomenon, that can affect the obtained tensile strength significantly, has not always been accounted for in the different investigations. For the investigated type of LC the tensile strength differed not significantly from the value for NC, which was approximately 3.0 MPa. Young's modulus was much smaller for LC than for NC, which is generally found. With representative values for f_t,

E_o and G_F, as presented in Table 1, a characteristic length for LC (140 mm) can be calculated that is about 60% smaller than for NC. This indicates that lightweight concrete behaves more brittle than normal-weight concrete.

Table 1. Values for the characteristic length l_{ch} of the types of concrete investigated and representative values of f_t, E_o and G_F

type of concrete investigated	f_{cc} (MPa)	f_t (MPa)	E_o (MPa)	G_F (J/m^2)	l_{ch} (mm)
normal-weight concrete	50	3.0	30000	105	350
lightweight concrete	50	3.0	18000	70	140

Maximum aggregate size

Five different mixes with maximum aggregate sizes 2, 4, 8, 16 and 32 mm respectively, were investigated. Average stress-deformation relations are plotted in Fig. 38. The observed difference in σ-δ relations for $d_{max} = 16$ mm and two different specimen sizes (see Fig. 35) were the reason to apply the small specimen size for all the mixes. Especially for the mixes with the bigger aggregates ($d_{max} = 32$ mm), the significance of the results may be doubted since the dimension of the critical cross-sectional area ($50 * 50$ mm^2) is of the same order as d_{max}. As far as tensile strength and fracture energy is concerned a tendency to increase for increasing d_{max} can be observed. Though it should be remarked that rather low values for f_t were found as compared to other investigations for the mix with $d_{max} = 8$ mm.

As far as the influence of mix parameters like d_{max} is concerned, one should bear in mind that it is not possible to vary one parameter without changing the other mix parameters. Furthermore, it is probably not only the maximum aggregate size but, even more so the concentration of the coarse aggregates which influences the fracture behav-

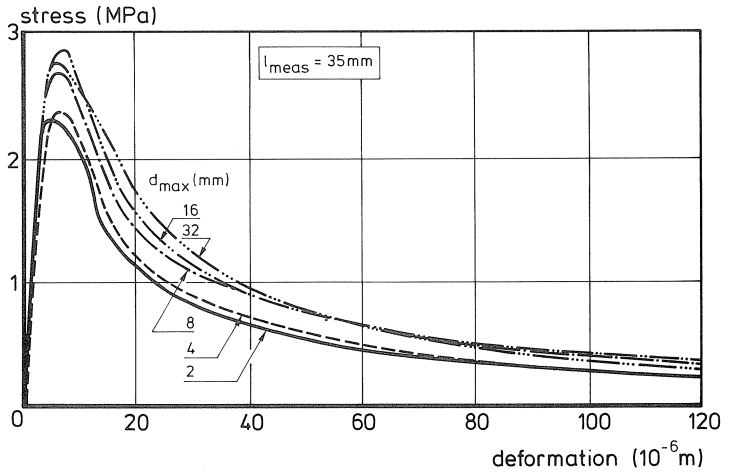

Fig. 38. Average stress-deformation relations for the concrete mixes with different maximum aggregate size.

iour. These factors mean that a simple comparison of experimental results by different investigators may lead to divergent results. Nevertheless a comparison is given in Fig. 39 for the fracture energy. As can be seen, there is a general tendency for G_F to increase with d_{max}.

In the first draft of the CEB-FIP Model Code 1990 [39], a relation between compressive strength and fracture energy is given which contains a coefficient that depends on the maximum aggregate size. There it is proposed that, "in the absence of experimental data" G_F in (J/m^2) should be estimated by

$$G_F = \alpha \cdot f_{ck}^{0.7} \tag{7}$$

in which f_{ck} (MPa) is the characteristic strength. For some comparisons with experimental data in this chapter, f_{ck} will arbitrarily be taken as equal to the cube compressive strength, f_{cc} in (MPa). The coefficient α is equal to 4, 6 and 10 for d_{max} values of 8, 16 and 32 mm respectively. In Fig. 39, G_F values calculated with equation 4 for an assumed f_{cc} of 50 MPa are connected by the dashed lines. The tendency of G_F to increase with increasing d_{max} coincides well with experimental results.

As can be seen in Fig 39, the results obtained in this investigation deviate from other results for d_{max} varying between 8 mm and 32 mm. The fact that there were minor differences in G_F values between the mixes with $d_{max} = 8$, 16 and 32 mm was probably caused by too small a cross-sectional area. The chance of a large aggregate being positioned between the saw cuts and thus affecting the fracture zone is rather small. For $d_{max} = 16$ mm, the aggregates with $d_{max} > 8$ mm occupy about 17% of the total volume, while it is 27% for $d_{max} = 32$ mm. So, firstly the fracture behaviour between the saw cuts for the mixes with larger aggregates will probably not differ much from the mix with

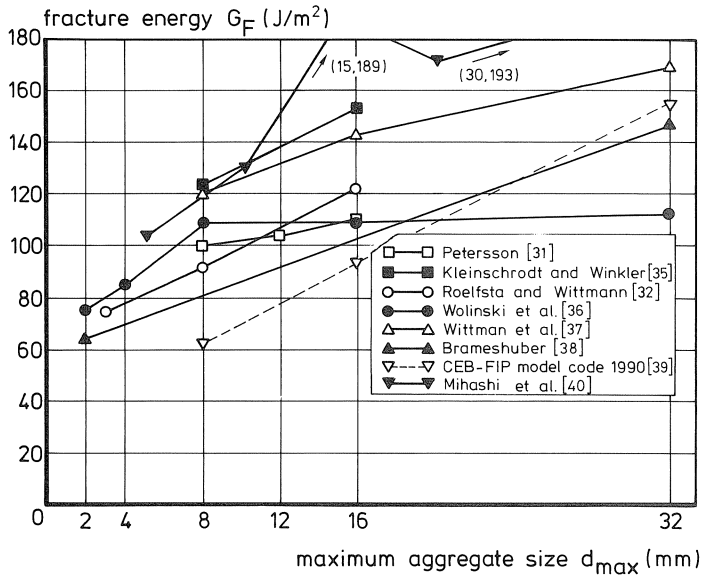

Fig. 39. Fracture energy as a function of d_{max} for a number of investigations.

d_{max} is 8 mm. Secondly, since it can be assumed that in a number of specimens larger aggregates will still have affected this fracture behaviour, a larger scatter can be expected for the mixes with larger aggregates, which indeed was observed in the tests.
The Young's modulus and the characteristic length varied not significantly between the different mixes.

Compressive strength
In order to investigate a possible relation between the concrete compressive strength and the fracture energy, three mixes ($d_{max} = 8$ mm) have been investigated. The average cube compressive strength of the concretes was 36, 47 and 77 MPa respectively, while for the latter type of concrete, silica fume was added to the mix. Average stress-deformation curves are plotted in Fig. 40. Mainly the tensile strength and the fracture energy were influenced.

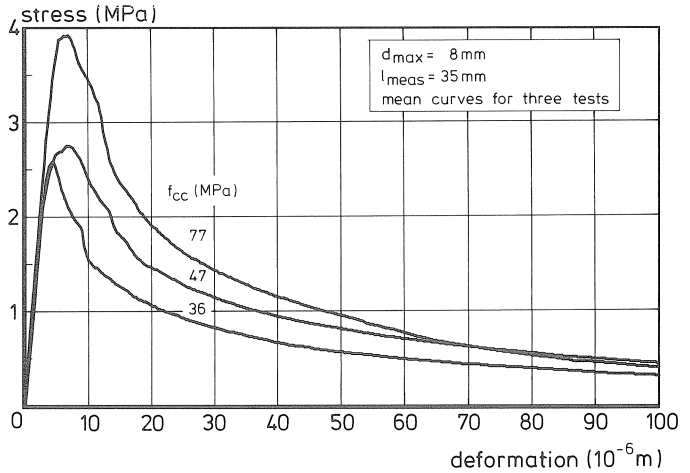

Fig. 40. Average σ-δ relations for three different concrete qualities.

Again, for G_F the results are compared with a number of results known from the literature (see Fig. 41). For the sake of clarity, G_F has been measured and evaluated in different ways by different researchers, which explains some of the differences. As can be seen, all presented investigations, including the relation presented in the draft of the CEB-FIP Model-Code 1990 [39] (equation 7), show more or less the same tendency for G_F; increasing with compressive strength f_c. If it is realized that the difference in strength is mainly caused by a difference in water-cement ratio, then the results of Fig. 41 can also show a relation between G_F and water-cement ratio (see Fig. 42). As can be seen, the decrease in G_F with increasing water-cement ratio shows good resemblance between the different investigations.

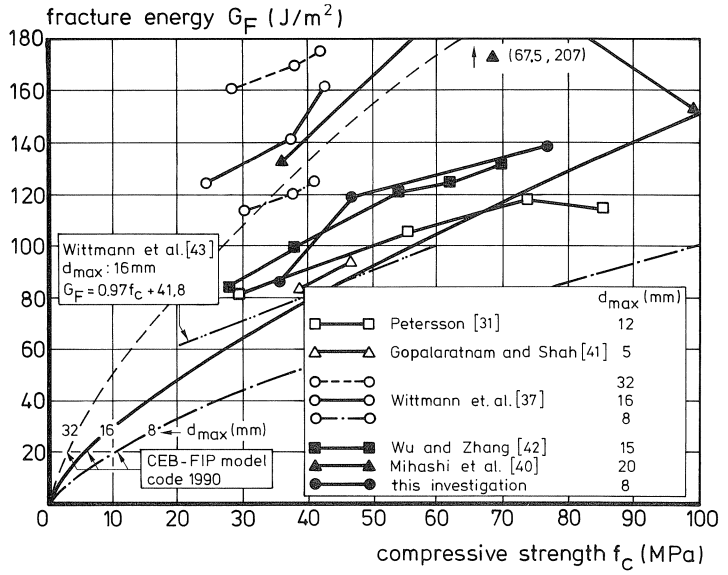

Fig. 41. Fracture energy as a function of compressive strength for a number of investigations.

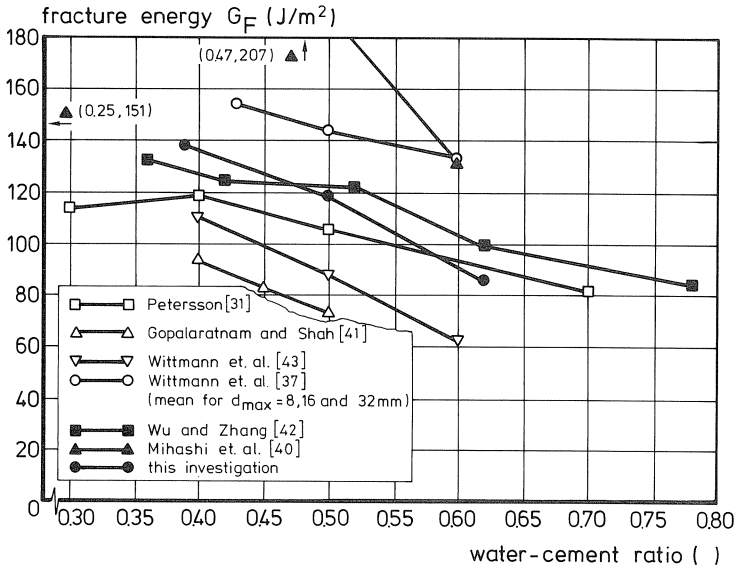

Fig. 42. Fracture energy as a function of water-cement ratio for the results of Fig. 41.

Curing condition; water content

With respect to the influence of curing conditions on the fracture mechanics parameters, two different test series were performed. In the first series, a normal-weight concrete (NC) and a lightweight concrete (LC) were tested for three different curing procedures. Besides the procedure previously applied (denoted as LAB), two extreme

conditions with respect to moisture content (WET and OVEN-DRY) were applied. In the second test series, the influence of drying time (under laboratory conditions) was investigated for NC.

Average stress deformation curves for lightweight concrete and normal-weight concrete are plotted in Figs. 43 and 44 respectively. The following main tendencies could be observed in the results (see also [15]):

- For NC and for LC, Young's modulus was significantly lower for the OVEN-DRY specimens compared with the specimens for LAB and WET. A possible explanation is that drying in the oven has caused small cracks in the hardened cement paste and at the interface of grains.
- Based on a significant lower maximum peak load and an important pre-peak non-linearity, it could be assumed that initial stresses due to differential shrinkage were active in the LAB-specimens for the lightweight concrete and the WET-specimens for the normal-weight concrete. Possibly, the procedure of wrapping the specimens in foil was not sufficient to prevent the NC specimens from drying out, resulting in eigenstresses.

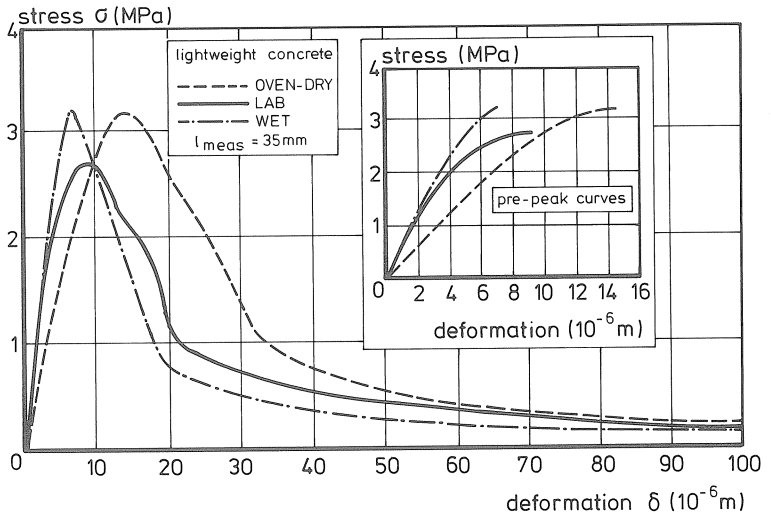

Fig. 43. Average stress-deformation curves for the lightweight concrete investigated.

- Except for some deviating results, a tendency for G_F to increase with drying of the concrete could be observed. Maybe the increase of G_F can be explained by the phenomenon that also causes the concrete strength for dry concrete to be higher than for wet concrete, as it is generally observed. Mills [44] suggested that the strength reduction for wet concrete is due to dilation of the cement gel by absorbed water, causing a reduction in the cohesion forces of the solid particles. Another phenomenon that may be responsible for a lower G_F value deals with the stress transfer at larger crack openings. For these crack openings, the main contribution to the stress-transferring

capacity is expected to be the interlocking effect, due to the tortuosity of the crack path. The sliding friction can be expected to be lower in the case where water is available between the two crack surfaces. Furthermore, shrinkage of the cement paste may embed the aggregates more strongly in the matrix, resulting in higher sliding friction for dry specimens. Indeed, Figs. 43 and 44 show the descending branch to be the lowest for WET-specimens.

- Despite the fact that the influence of experimental conditions on the separate fracture mechanics parameters also affect the calculated characteristic length, a tendency for concrete to be more brittle for dry concrete than for wet concrete could be observed.

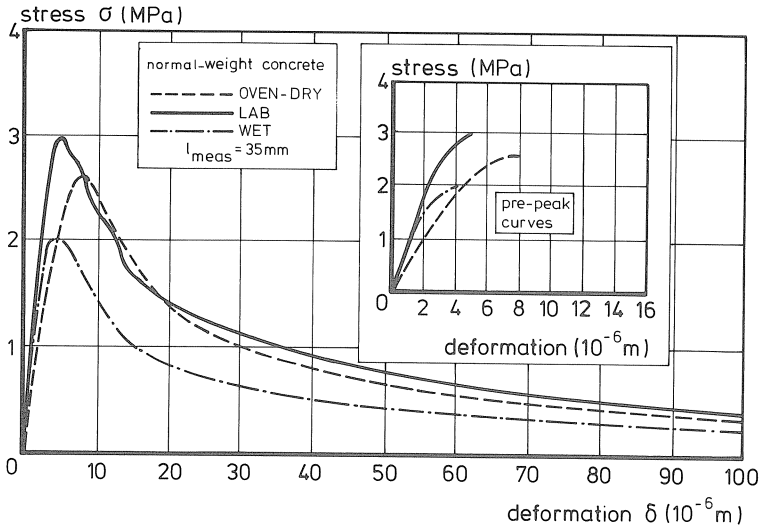

Fig. 44. Average stress-deformation curves for the normal-weight concrete investigated.

Compressive preloading

The experiments in which the tensile specimens were preloaded in compression before they were fractured in a deformation-controlled way in tension, showed two main influences of a compressive preloading. Firstly, Young's modulus appeared to decrease with increasing compressive preload level. This result can be explained by the occurrence of micro-cracks in the direction of the load application (see also [45]). Secondly, the preloaded specimens displayed a kind of horizontal plateau at or just after peak load in the σ-δ relation, while in case of non-preloaded specimens the stress drops almost directly after peak load. As a result, G_F was a little higher for the preloaded specimens than for the non-preloaded specimens. The compressive preloading stress level appeared not to have an influence. So far it is not clear whether this result is due to an altered fracture process after compressive preloading or if it is caused by the notches that were applied.

6 Crack cyclic modelling

6.1 *Constitutive model*

In the literature only a few investigations in which the post-peak cyclic tensile behaviour is determined, have been reported. Also the number of constitutive models for this material behaviour is limited. Yet, in most FE codes, there is either no option for unloading in the softening zone or only a simple secant unloading (linear through the origin) is available. For the fatigue approach of plain concrete, as proposed in this report (see Section 2.3), the cyclic behaviour in the fracture zone is an essential parameter. From the existing constitutive models for the crack cyclic behaviour (see [15]), the "focal-point model" (FPM) proposed by Yankelevsky and Reinhardt [46,47] probably gives the best approximation of the real material behaviour. The model uses a set of geometrical loci (so-called "focal points") to compute the piecewise linear branches of the unloading-reloading cycles (see Fig 45). Formulae for the keypoints in the loops can be found in [15]. In their model, the damage that occurs in a loading cycle (represented by a stress-drop at the envelope curve) is independent of the lower stress level in the loop. This is not in accordance with the experimental results that have been found and

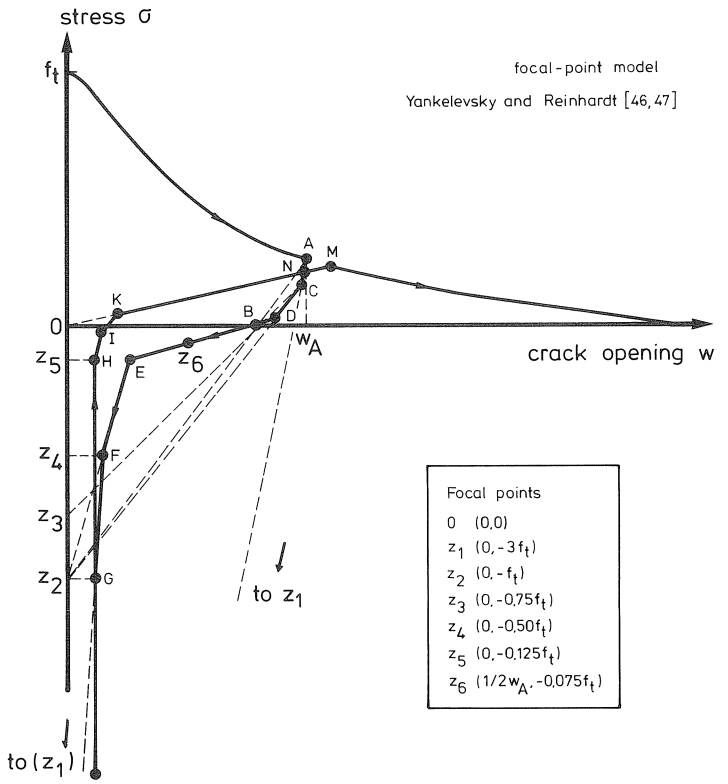

Fig. 45. Geometrical loci and procedure of the focal-point model by Yankelevsky and Reinhardt [46, 47].

makes that the lower stress level cannot be taken into account in the fatigue study. This was one reason for proposing a new constitutive model. Another reason has to do with the simplicity of numerical modelling and the number of operations that have to be executed in a FE analysis. An analytical description for the unloading curve and the reloading curve would, in this respect be preferable to the focal-point model which demands many more operations. So, it was felt worthwhile to search for such analytical expressions, in addition to which the complexity of the expressions themselves is not very important.

Based on experimental results from deformation-contolled uniaxial tensile tests with post-peak cyclic loading and five different lower stress levels (σ_L is approximately 1 MPa, 0 MPa, −1 MPa, −3 MPa and −15 MPa), a new constitutive model was proposed. Besides the expression for the envelope curve, the new model basically consists of three expressions (Fig. 46). These are respectively: expressions for the unloading curve (I), the gap in the envelope curve (II) and the reloading curve (III). It has been chosen to use only characteristic points in the σ-w relation (f_t, w_c, w_{eu}, σ_{eu}, σ_L) as variables in the expressions. Before the expressions are presented, it should be made clear that the aim was to tackle the whole problem (unloading starting between crack openings 0 and w_c and lower stress levels σ_L, between f_t and f_c) by using only these three expressions and, of course, the expression for the envelope curve, while furthermore continuous functions were preferred. Therefore, the name "Continuous-function model" (CFM) was chosen for the model.

The expressions that were chosen are based on a close inspection of the experimental results. Starting from point (w_{eu}, σ_{eu}) at the envelope curve, the unloading curve is

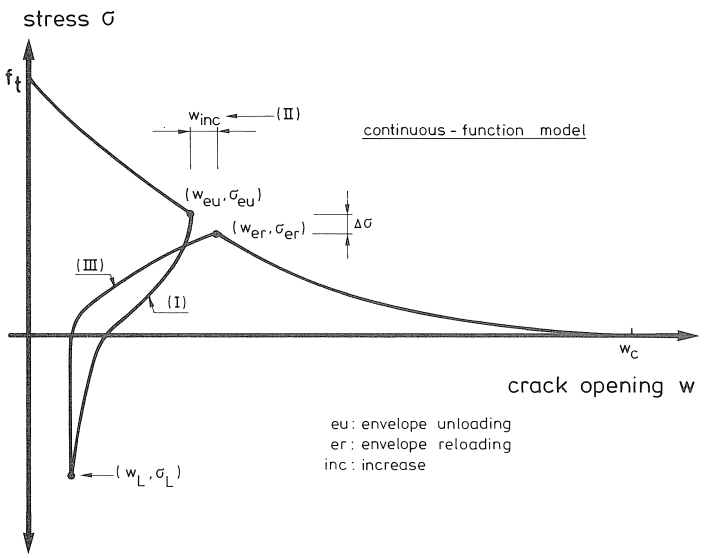

Fig. 46. Set-up for the description of crack cyclic behaviour with the continuous-function model.

determined by:

$$\frac{\sigma}{f_t} = \frac{\sigma_{eu}}{f_t} + \left\{\frac{1}{3(w_{eu}/w_c) + 0.4}\right\} \cdot \left[0.014\{\ln(w/w_{eu})\}^5 - 0.57\sqrt{\left(1 - \frac{w}{w_{eu}}\right)}\right] \tag{8}$$

For the description of the gap in the envelope curve the increase in crack opening $w_{inc}(w_{er} - w_{eu})$ is used. The expression for w_{inc} as a function of the coordinates at the point of leaving the envelope curve and of the lower stress level is:

$$\frac{w_{inc}}{w_c} = 0.1 \cdot \frac{w_{eu}}{w_c} \cdot \left\{\ln\left(1 + 3 \cdot \frac{\sigma_{eu} - \sigma_L}{f_t}\right)\right\} \tag{9}$$

The coordinates of the returning point on the envelope curve (w_{er}, σ_{er}) can be found with

$$w_{er} = w_{eu} + w_{inc} \tag{10}$$

and equation 4. Starting from the point at the lower stress level (w_L, σ_L) up to point (w_{er}, σ_{er}) at the envelope curve, the reloading curve is determined by

$$\frac{\sigma}{\sigma_L} = 1 + \left[\frac{1}{c_3} \cdot \left\{\frac{(w - w_L)}{(w_{er} - w_L)}\right\}^{0.2c_3} + \left\{1 - \left(1 - \frac{(w - w_L)}{(w_{er} - w_L)}\right)^2\right\}^{c_4}\right] \cdot \left(\frac{c_3}{c_3 + 1}\right) \cdot \left(\frac{\sigma_{er}}{\sigma_L} - 1\right) \tag{11a}$$

with for the coefficients c_3 and c_4:

$$c_3 = 3 \cdot \left(3 \cdot \frac{f_t - \sigma_L}{f_t}\right)^{\left(-1 - 0.5\frac{w_{eu}}{w_c}\right)} \cdot \left\{1 - \left(\frac{w_{eu}}{w_c}\right)^{\left(\frac{0.71 f_t}{f_t - \sigma_L}\right)}\right\} \tag{11b}$$

$$c_4 = \left[2 \cdot \left(3 \cdot \frac{f_t - \sigma_L}{f_t}\right)^{-3} + 0.5\right]^{-1} \tag{11c}$$

Inner loops

So far, constitutive relations have been given for post-peak cyclic loading with loops that start from and return to the envelope curve with only one reversal in the crack opening direction at the lower stress level σ_L. Obviously, in reality, reversals from an opening crack into a closing crack, or vice versa, may occur at any place in the loading history. Therefore, for the sake of completeness, FE codes also require a description for these so-called "inner" loops.

For the description of the inner loops, a counter i is used, which is taken equal to zero for the envelope curve and increases by 1 each time there is a reversal in crack opening direction before the crack opening at the previous reversal has been reached (see Fig. 47). The principle that is used for inner loops is that they return to the same point they started from. This means that a damaging effect due to cycling within a loop is not taken into account. As far as notation is concerned, A_i is used for a point where the direction changes from an opening crack into a closing crack and L_i is used for the opposite reversal in crack opening direction. Furthermore, there are the variables $\Delta\sigma_{A_i}$ and $\Delta\sigma_{L_i}$, while $\sigma_{u_i}(w)$ and $\sigma_{r_i}(w)$ denote the stresses as a function of crack opening for

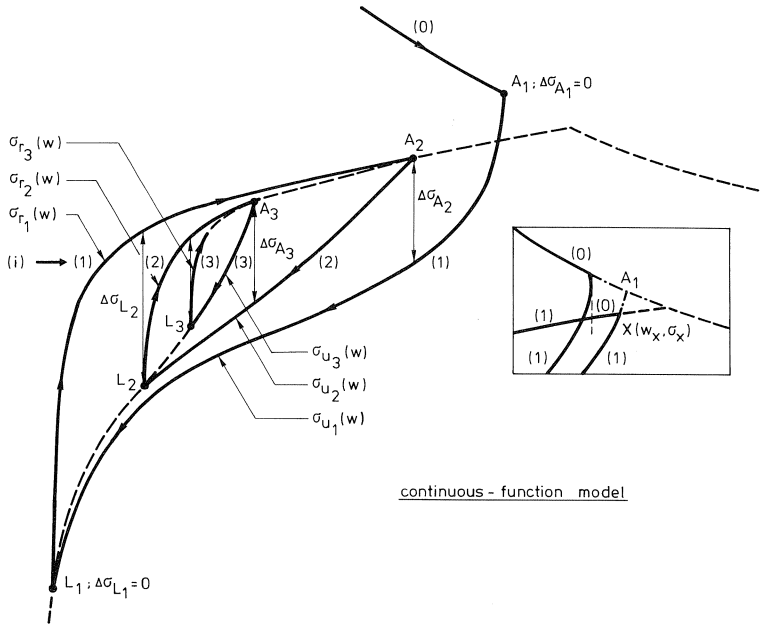

Fig. 47. Procedure for inner loops in the CFM.

unloading and reloading curves respectively. The unloading curves are now determined by:

$$\Delta\sigma_{A_i} = \sigma_{A_i} - \sigma_{u_1}(w_{A_i}) - \sum_{n=3}^{i} \left(\frac{w_{A_i} - w_{L_{n-2}}}{w_{A_{n-1}} - w_{L_{n-2}}} \right)^2 \cdot \Delta\sigma_{A_{n-1}} \tag{12}$$

$$\sigma_{u_i}(w) = \sigma_{u_1}(w) + \sum_{n=2}^{i} \left(\frac{w - w_{L_{n-1}}}{w_{A_n} - w_{L_{n-1}}} \right)^2 \cdot \Delta\sigma_{A_n} \tag{13}$$

and the reloading curves can be found with

$$\Delta\sigma_{L_i} = \sigma_{r_1}(w_{L_i}) - \sigma_{L_i} - \sum_{n=3}^{i} \left(\frac{w_{L_i} - w_{A_{n-1}}}{w_{L_{n-1}} - w_{A_{n-1}}} \right)^8 \cdot \Delta\sigma_{L_{n-1}} \tag{14}$$

$$\sigma_{r_i}(w) = \sigma_{r_1}(w) - \sum_{n=2}^{i} \left(\frac{w - w_{A_n}}{w_{L_n} - w_{A_n}} \right)^8 \cdot \Delta\sigma_{L_n} \tag{15}$$

After completion of an inner loop, the counter i decreases with 1, which can be expressed by:

$$\begin{aligned} &\text{if } w \geq w_{A_i} \quad \text{then } i = i - 1 \\ &\text{if } w \leq w_{L_{i-1}} \text{ then } i = i - 1 \end{aligned} \tag{16}$$

In the formulations presented above, only crack opening reversals at crack openings corresponding to the gap in the envelope curve have not yet been described. For the case where unloading starts at point X, it is proposed to determine point A_1 as sketched

in the inset of Fig. 47. This point is the intersection point of the envelope curve (eq. 4) and an unloading curve (equation 8), while $X(w_X, \sigma_X)$ is part of this latter curve. This intersection point can be obtained by an iterative procedure.
With the equations 4, 6 and 8 to 16 a complete description for post-peak tensile behaviour is given. As an example, a σ-w relation with different cyclic loading regimes, as obtained with the proposed model, is given in Fig. 48. A flow chart for the model is given in [15].

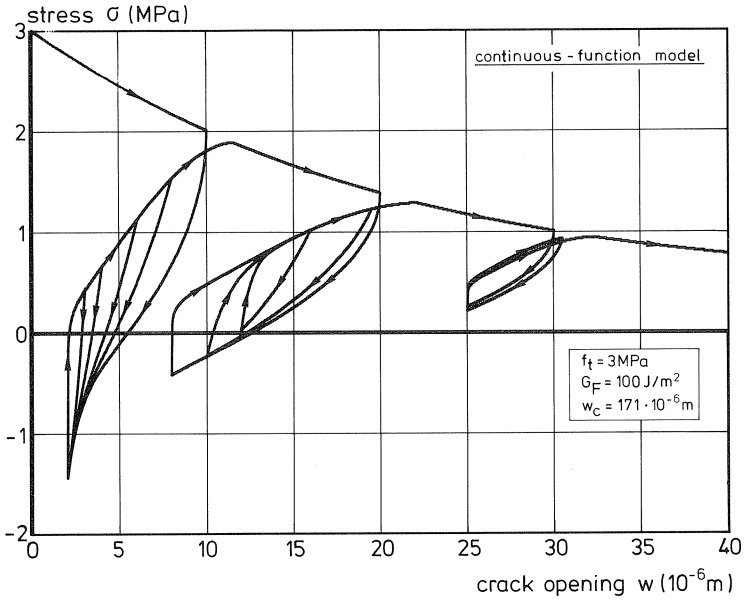

Fig. 48. σ-w relation for an arbitrarily chosen loading path as predicted with the continuous-function model.

6.2 *Comparison between experimental results and constitutive models*

The focal-point model and the continuous-function model have been compared with the experimental loops as found in the experiments. The results for a number of cycles can found in Fig. 49. For the prediction of the loops the following procedure was applied. For f_t and G_F in equations 8 to 11, the average value for the total test series was used. In order to find a point where the reloading curve meets the envelope curve again (w_{er}, σ_{er}), an assumption had to be made for the relation of the envelope curve. Here equation 4 has been used, with w_c equal to the value that was obtained with the average values for f_t and G_F $(5.14G_F/f_t)$ and for f_t a fictive value which is taken so that point (w_{eu}, σ_{eu}) is part of the envelope curve. Finally, the predictions were done using w_{eu}, σ_{eu} and σ_L as input. Though both models appear to predict the cyclic behaviour very well, it looks as if the continuous-function model approaches the experimental results a little better than the focal-point model does. In [15] it is shown that the CFM also predicts experimental results known from literature rather well.

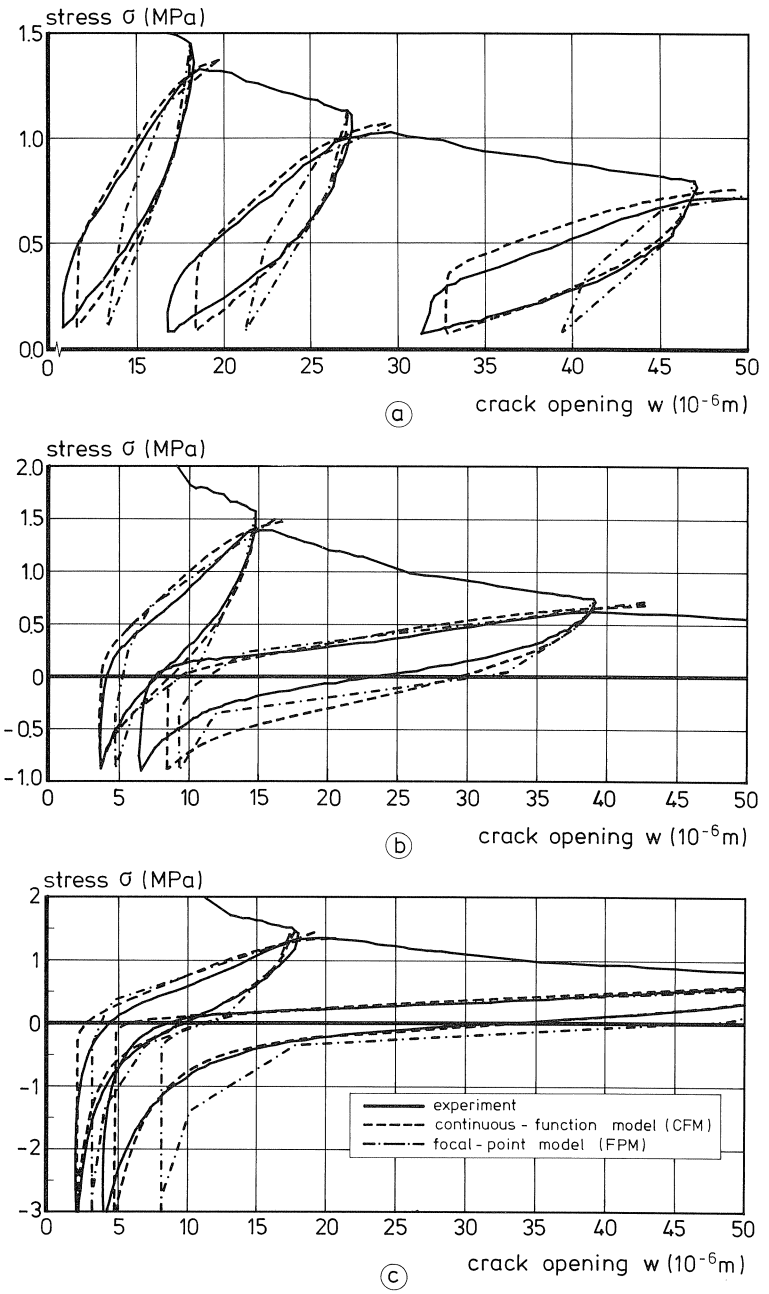

Fig. 49. Experimental results for crack cyclic loops and the predictions with CFM and FPM.

In Fig. 50 experimental results for the relative stress drop ($\Delta\sigma/\sigma_{eu}$) at the envelope curve and model predictions are compared. This figure clearly demonstrates that in the focal-point model the stress drop is independent of the lower stress level, whereas in the continuous-function model the stress drop increases for a decreasing lower stress level in the loops. A close inspection of the experimental results shows that there is a significant difference in $\Delta\sigma/\sigma_{eu}$ values between a tensile or zero lower stress level on the one hand and a compressive lower stress level on the other. Between the values of $\sigma_L = -1$, -3 and -15 MPa, however, there is no longer much difference. This phenomenon of an especially damaging effect of stress reversals was also observed in fatigue experiments (see Fig. 6b) and is not explicitly modelled in the continuous-function model.

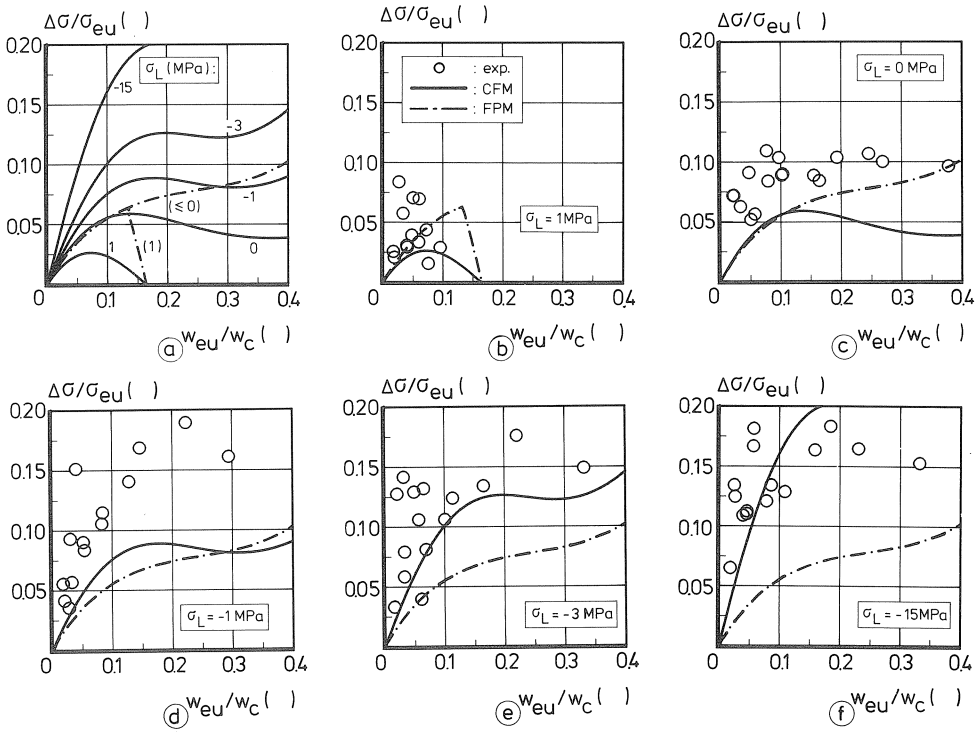

Fig. 50. Model predictions and experimental results for the relation between $\Delta\sigma/\sigma_{eu}$ and w_{eu}/w_c.

7 Model verification

7.1 *General*

The material behaviour of plain concrete under tensile loading has been discussed in previous chapters and described by a constitutive model. In order to verify the validity of the proposed model a number of mode I fracture tests were performed on specimens made of concrete originating from one and the same batch. Besides deformation-controlled uniaxial tensile tests, which were used to determine the material properties,

f_t, E_o and G_F, four-point bending tests and tensile tests on single notched plates were performed. Details about the experiments can be found in [15]. Here, attention will be paid to some results of the bending tests (see also Fig. 18) and a number of numerical simulations with the FE code DIANA[1] and a multi-layer model.
Results form the deformation-controlled uniaxial tests yielded the following fracture mechanics parameters: tensile strength is 3.3 MPa, fracture energy is 115 J/m^2 and Young's modulus is about 40000 MPa. When special attention was paid to the assumption for the last part in the F-δ_{fl} curve, then approximately the same G_F value could be obtained from the bending tests.

7.2 *FE simulations of the four-point bending tests*

The continuous-function model was implemented in the finite element code DIANA. This code was used to simulate the four-point bending tests. Details about the analyses can be found in [48].

FE idealization
Symmetry was used for the applied FE idealization as can be seen in Fig. 51, where the FE idealization for the specimen with a 50 mm deep notch is shown. For the concrete, eight-node and six-node quadratic elements were used, while six-node interface

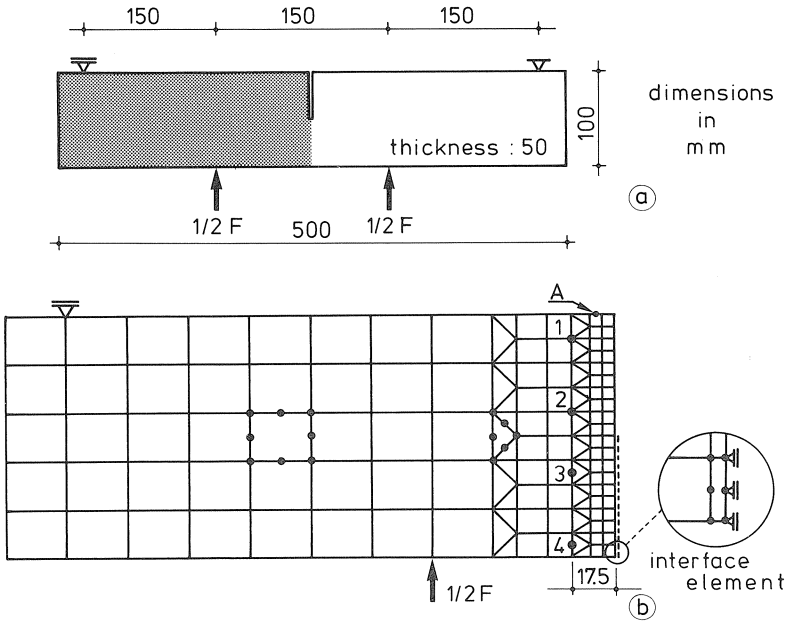

Fig. 51. FE idealization for the beam with a 50 mm notch depth.

[1] DIANA is the finite element code being developed at TNO Building and Construction Research in combination with other institutes and universities in the Netherlands.

elements were applied to model the crack. For the interface elements, the vertical displacements of each two nodes positioned beside each other were assigned to be equal. In the horizontal direction, the interface elements use a finite initial stiffness. In order to represent the uncracked beam properly, a large value was chosen for this initial stiffness. The continuous-function model becomes active as soon as the tensile strength is reached. To enable comparison with the experiments, the vertical displacement of point A (see Fig. 51) was used for the deflection of the beam, while the horizontal displacements of points 1 to 4 were used to compare crack openings (see also Fig. 18).

Simulations

Initially, for the material parameters the values presented in Section 7.1 were taken. Then already a rather good approximation of the F-δ_{fl} curves was obtained for the three different beams (notch depth 10, 30 and 50 mm respectively). Nevertheless, in order the improve the results, the input parameters were slightly adjusted after which they were kept the same for the analyses of the three beams. The chosen material parameters were: tensile strength $f_t = 3.0$ MPa, Young's modulus $E_o = 38000$ MPa and fracture energy $G_F = 125$ J/m^2. Results for the beams with a 30 mm deep notch are presented in Fig. 52. Two experimental F-δ_{fl} curves are plotted, of which one pertains to a static test, while the other represents the envelope curve in a post-peak cyclic test. As can be seen in Fig. 52a, the prediction of the F-δ_{fl} curve up to a deflection of about 0.25 mm is very good. For larger deflections the predicted value underestimates the measured one. This result can be explained by the long tail in the stress-crack opening relation, that was not modelled in the continuous-function model. It has been demonstrated [15] that with a proper description of the long tail in the constitutive model, also the predictions for larger deflections improve. Fig. 52b and c show that also the deformation distributions are predicted very well by the FE code. Finally, the same can be said for the loops in the post-peak region (Fig. 52d).

Similar results as presented for the beam with a notch depth of 30 mm were found for the beams with a 10 and a 50 mm notch depth respectively.

7.3 *Simulation by a multi-layer model*

In the bending tests, fracture only occurs in a narrow zone, while the rest of the specimen behaves linear elastically. Similarly to the tensile tests (see Section 4.3), the bending tests will be simulated with a simple model (multi-layer model). For the sake of clarity, it is only intended to show that, with some assumptions, the behaviour of plain concrete in bending tests can rather easily be studied. For more accurate simulations, an FE analysis has to be performed. In Chapter 8, the same model will be used to predict the behaviour of a beam under fatigue loading.

The principle of the model, which is shown schematically in Fig. 53, is the same as used for the tensile test model (Section 4.3). A fictive part of the beam, encompassing the fracture zone, is replaced by springs, representing the behaviour of small layers. For simplicity, "fracture zone" will also be used in this section to describe this part of the

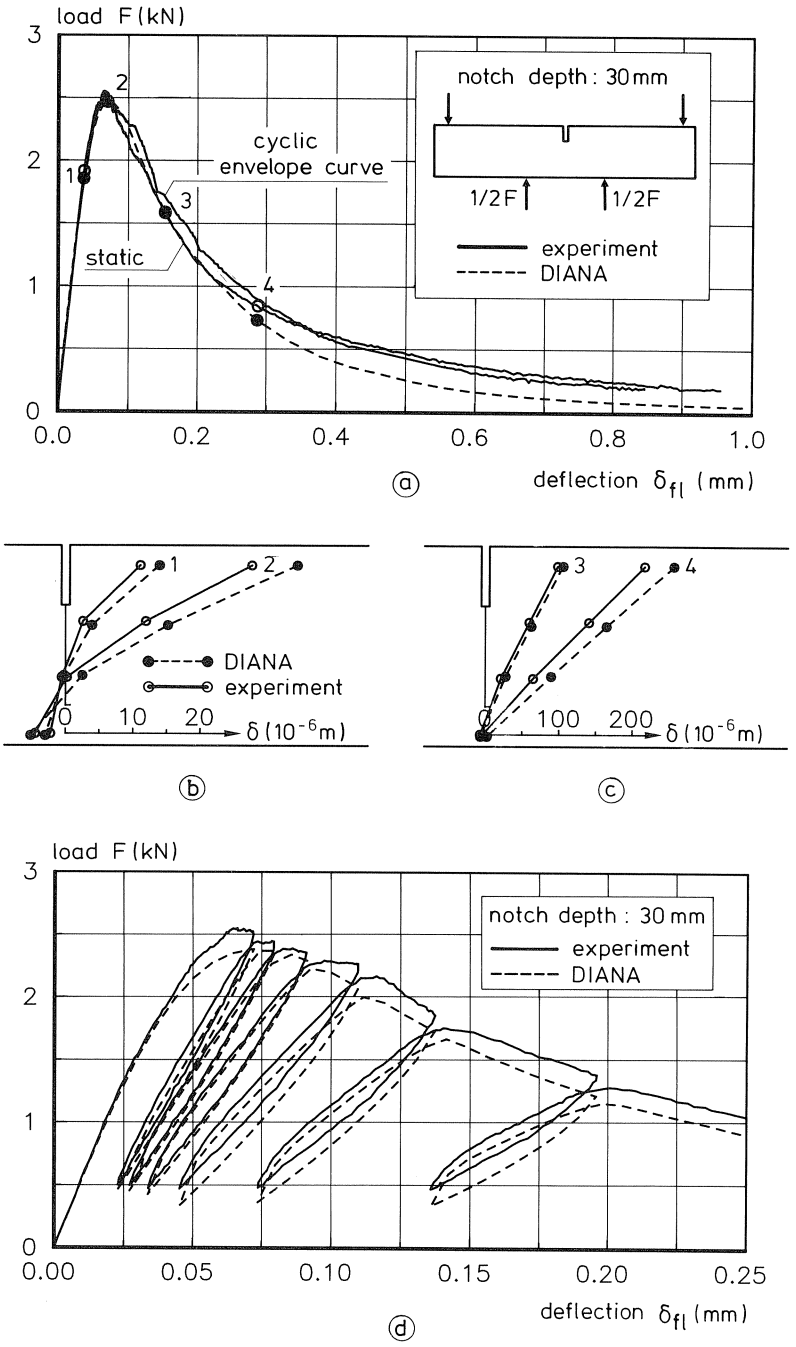

Fig. 52. Results for the beams with a 30 mm deep notch.

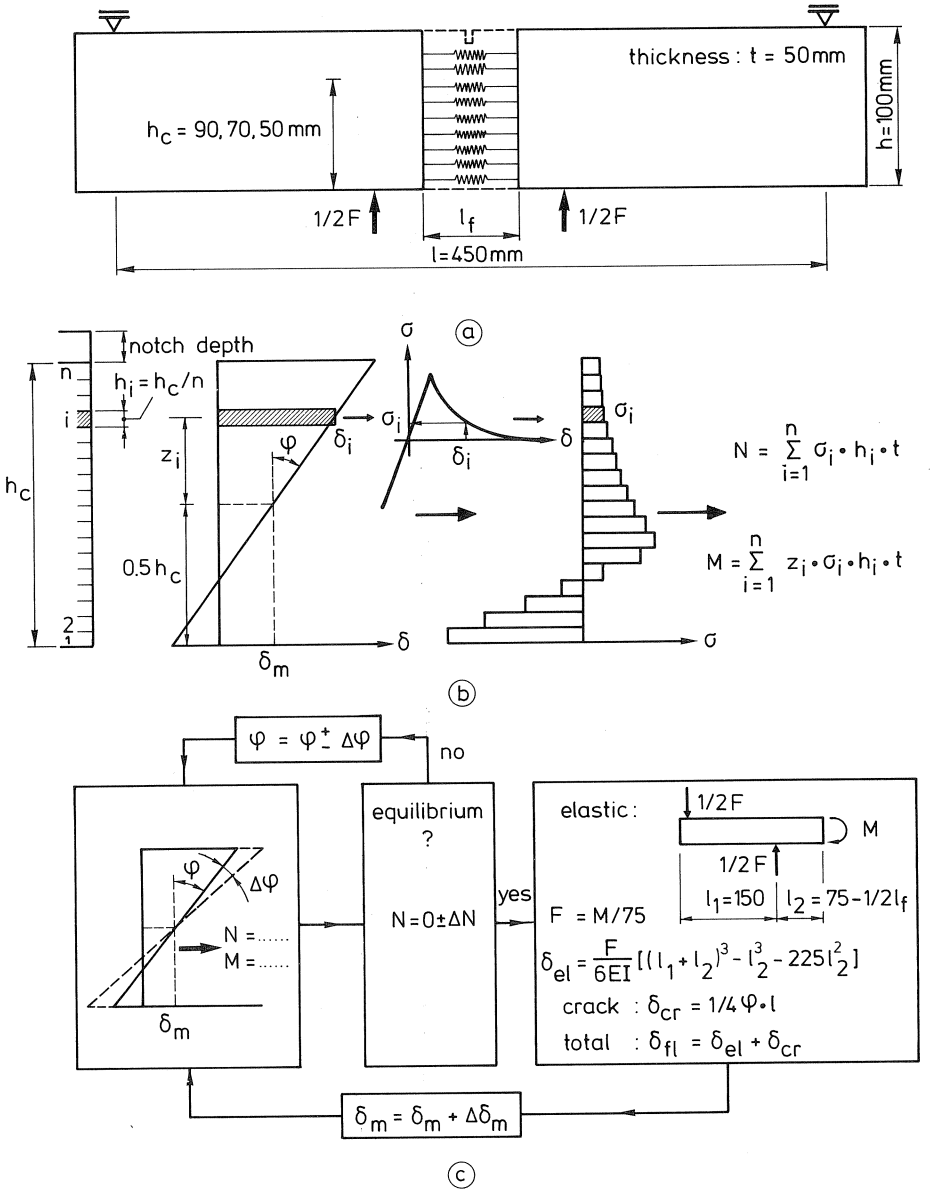

Fig. 53. Principles of the multi-layer model.

beam. The load-deformation (or stress-deformation) characteristic of the springs is determined by the combination of the stress-crack opening relation (CFM) and the elastic deformation over the arbitrarily chosen length of the fracture zone l_f (see Fig. 53a). In fact, the smeared crack approach is used. The remaining parts of the beam are assumed to behave elastically. The main characteristic of the model is that for a

deformation distribution of the fracture zone, the corresponding resulting force N and moment M are calculated (Fig. 53b). Therefore, the net cross-sectional area is subdivided over its height into n elements or layers. For each element, the deformation is determined by an average deformation δ_m and a rotation φ of the fracture zone. Then, with the aid of an iterative procedure, the corresponding stress can be determined, after which summing up over all elements yields the internal force N and moment M. Equilibrium is found when N is equal to zero. Unlike in Section 4.3, an incremental procedure is applied (see Fig. 53c). For an average deformation δ_m, the rotation φ is adjusted until N is equal to zero within a certain range ($\pm \Delta N$). Then, with the corresponding internal moment M, the external load F and the deflection δ_{fl} are calculated. In the subsequent step, the average deformation is increased by $\Delta\delta_m$, while in the first iteration of this step, the rotation as found for equilibrium in the previous step, is used. In the analyses whose results will be presented, the element height was chosen as equal to 1 mm, resulting in 90, 70 and 50 elements for the three different types of beam.
Just as for the tensile tests, the length of the fracture zone l_f must be chosen arbitrarily and this affects the solution. The influence of this length on the F-δ_{fl} relation for the beam with a 10 mm notch depth is shown in Fig. 54. It can be seen that the value of l_f primarily affects the peak load, while the initial slope and the curve beyond 0.1 mm is only slightly affected. For the simulation of the three different beams, a constant value of l_f, which is 50 mm, was chosen. A comparison with the DIANA FE analyses is shown in Fig. 55. Despite the simplicity of the layer model, there appears to be a good resemblance. The limitation of the layer model, especially for peak load, also becomes clear from Fig. 56, where the ratio between a calculated bending strength and the tensile strength are plotted for the three different beams. For a constant value of l_f, no size

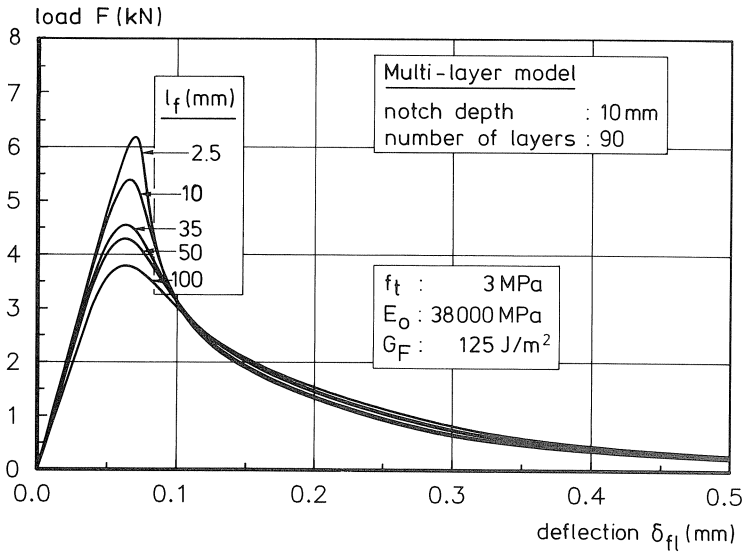

Fig. 54. The influence of l_f on the F-δ_{fl} relation.

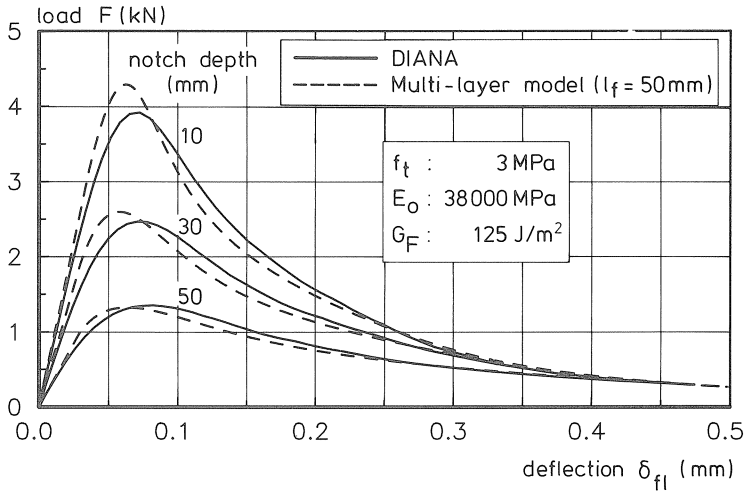

Fig. 55. F-δ_{fl} relations predicted with DIANA and the multi-layer model with l_f=50 mm.

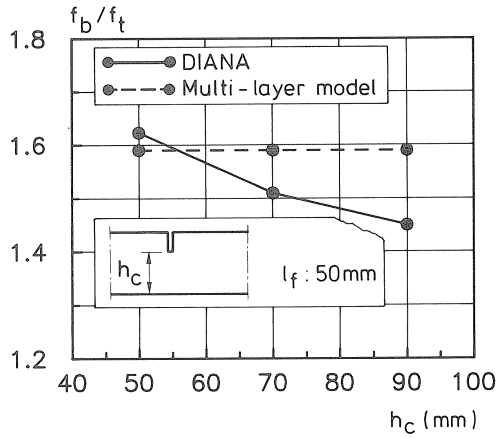

Fig. 56. Relative bending strength as a function of h_c.

effect will be found with the multi-layer model. If, however, the length of the fracture zone is adjusted to the beam depth, then also with the multi-layer model a size effect will be found (see also [49]).

7.4 *Concluding remarks*

In general, it can be concluded that the experimentally determined results could be predicted very well with the material model and the two simulation techniques. In the FE analyses, the best fit was found with input parameters that deviated slightly from those determined in deformation-controlled uniaxial tensile tests on narrow speci-

mens. In this respect it should be realized that there is always a scatter in the experimental results and that only a limited number of experiments were performed. Furthermore, the process of making a notch as well as the drying procedure used for the specimens, may have caused initial cracking in front of the notch, or elsewhere in the fracture zone.
The results of the bending tests confirm the existence of a long tail in the stress-crack opening relation. Therefore, for those analyses, where it is expected that large crack openings occur, it is recommended to extend the σ-w relation in the continuous-function model (see also [15]).

8 Fatigue analyses and experiments

8.1 *Introduction*

In this chapter the results of numerical fatigue analyses will be presented. First, in Section 8.2 the results of a few analyses with the FE code DIANA will be discussed. These analyses were found to be quite time-consuming. Analyses with the multi-layer model can be performed in a much shorter time period thanks to the simple way of modelling. Therefore, the multi-layer model is a very suitable tool for studying fatigue phenomena (Section 8.3). For the sake of clarity, only low cycle high amplitude fatigue analyses were performed. For most analyses, the number of cycles to failure is so small that it would in fact be better to use the term repeated loading rather than fatigue. Nevertheless, the term fatigue will in general be used in the remainder of this chapter. A limited number of tensile fatigue experiments were performed in order to study the relation between deformations in a quasi-static tensile test and in a tensile fatigue test. Results from these experiments are presented and discussed in Section 8.4.

8.2 *Fatigue analyses with DIANA*

The DIANA finite element code has been used to investigate the fatigue behaviour of a notched beam [48]. Here, only some principal results will be presented. For the analyses, the beam with the 50 mm notch depth was taken. The same FE idealization as used in Chapter 7 (see Fig. 51) was applied, while the material parameters were also the same ($\nu = 0.2$, $f_t = 3.0$ MPa, $E_o = 38000$ MPa and $G_F = 125$ J/m^2).

Load-deflection relations
The load-deflection relation for a continuously increasing deformation is plotted in Fig. 57 by the dashed line. For the force at peak load F_{max}, a value of 1292 N was found. For the purpose of the fatigue analysis, the load was applied by load steps (load-controlled). First, load steps up to a maximum of 95% of the peak load were performed. Subsequently, the beam was unloaded until zero load again, followed by a reloading up to the same upper value of $0.95F_{max}$. This procedure was repeated until it was no longer possible to find a new equilibrium. The result of this analysis, as far as the load-deflection relation is concerned, can be seen in Fig. 57. It was found that 35 unloading-

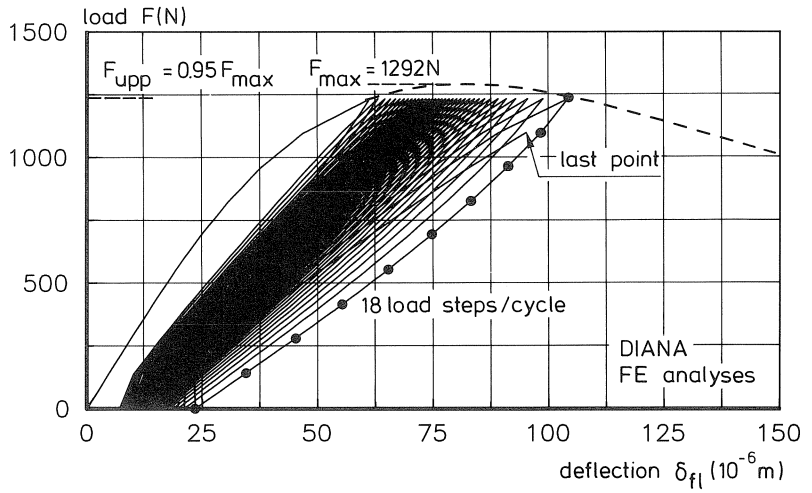

Fig. 57. Load-deflection relations predicted by FE analyses.

reloading loops could be performed, while in the subsequent reloading part it was not possible to find a solution at the upper load level. It can be assumed that for smaller loading steps the descending branch as found in the quasi-static analysis would have been reached at a load level smaller than F_{upp}. The conclusion from this is that the descending branch of a quasi-static analysis was an envelope curve and also formed the failure criterion for the fatigue loading.

Stress distributions

For a number of loops the stress distributions at the upper ($F = F_{upp}$) and lower ($F = 0$) load level are plotted in Fig. 58. First of all, it can be seen that the length of the softening zone increases with the number of load cycles. Furthermore, the stress distributions at zero load show that major residual stresses are active after a preloading up to 95% of the

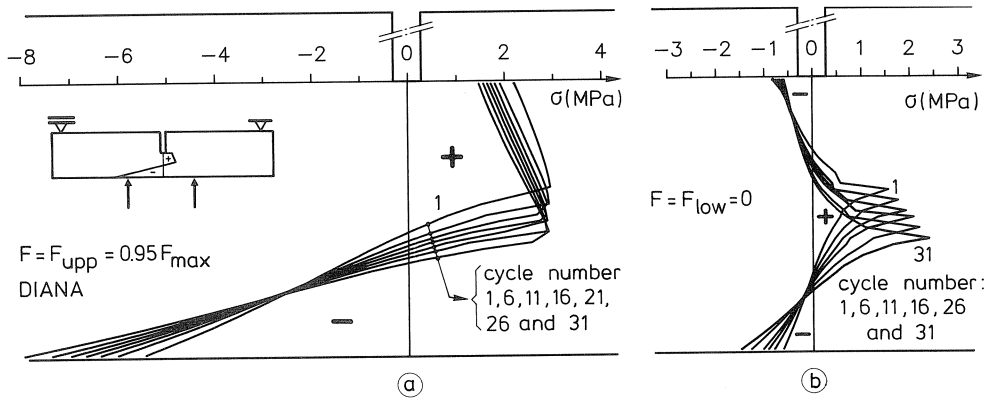

Fig. 58. Stress distributions at the upper and lower load level for a number of load cycles.

maximum load. It appears that the tensile residual stresses in the centre part of the cross-section increase with the number of cycles performed.

8.3 *Fatigue analyses with the multi-layer model*

The analyses made with the DIANA FE code and described in the previous section had already shown some promising results as far as the fatigue approach in this report is concerned. Though the analyses are quite time-consuming, the FE code can now be used to make further investigations of the fatigue behaviour of concrete. However, since the only intention is to study phenomena, the use of the multi-layer model for such a study is much more suitable, because the analyses are much less time-consuming. Therefore, a number of analyses were performed with that model. The results of these will be presented in this section. In Fig. 54 it was shown that the parameter l_f (length of the fracture zone) in the multi-layer model specifically affects the load-deflection relation around peak load. Since the upper load level in fatigue experiments is generally represented by a percentage of the peak load in static tests, it should be obvious that a quantitative comparison with experimental results is in fact not possible. Despite this limitation the multi-layer model can very well be used, as will shortly be shown. First, some details are given about the analyses. After that, the results of one particular analysis will be discussed in detail. Then, results of a number of analyses with different upper and lower load levels are presented.

For all the analyses in this section, the chosen specimen type and material properties were the same as for the finite element analyses, i.e. four-point bending specimen with a 50 mm notch depth, $E_o = 38000$ MPa, $f_t = 3$ MPa and $G_F = 125$ J/m^2. The value for the length of the fracture zone l_f was chosen as equal to 35 mm, which was kept the same for all the analyses. The analyses were performed with 100 layers. In other words: the critical cross-section (height = 50 mm) is subdivided into layers with a height h_i of 0.5 mm each.

Results of a specific analysis

For the structure under investigation a value of 1403.6 N was found for the peak load, F_{max}. For the fatigue analysis that is to be discussed, an upper load level of $0.94F_{max}$ and a lower load level equal to zero were chosen. It appeared that 146 loops could be performed before the descending branch of the static test was reached. Three loops (1, 100 and 146 respectively) are plotted in Fig. 59. Due to the fact that in this analysis the average crack opening is used as control parameter (deformation-controlled), the last loop continues directly with the descending branch of the static test.

The development of four different parameters in relation to the number of cycles is plotted in Fig. 60. The deflection versus the number of cycles displays a typical cyclic creep curve (compare Fig. 7). The growth of the softening zone with the number of cycles can be seen in Fig. 60b. If this parameter is regarded as a crack length, then the resemblance with crack growth curves for metals (see Fig. 10a) is clear. In fatigue compression tests, Holmen [11] observed that the secant modulus of elasticity decreases

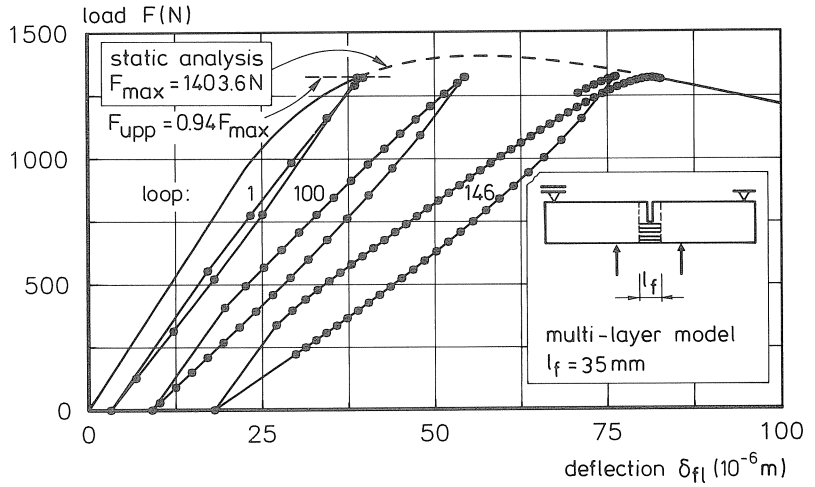

Fig. 59. Load-deflection relations obtained with the multi-layer model.

with the number of cycles (Fig. 8). A similar relation as noted in the compression tests is found for the development of the secant stiffness k_{sec} with the number of cycles (Fig. 60c). Finally, the area enclosed by a loop is sometimes also used as a parameter to show the development of damage in fatigue tests. The development of the energy W with the number of cycles is plotted in Fig. 60d, with the energy being defined according to the schematic representation given in the inset of that figure. All four curves in Fig. 60 display three different stages, the second one of which is a linear relation like in cyclic creep curves.

Fatigue analyses with different load levels

A number of analyses were performed with different upper and lower load levels. For the upper load level, the values applied were equal to 99, 98, 97, 96, 95 and 94% of the maximum load in a static test respectively, while for the lower load level – 50, 0 and 50% of F_{max} were used. The results of these analyses, plotted in S-N curves, can be seen in Fig. 61. Before discussing this result, a remark first has to be made about inner loops. For most of the analyses inner loops were not active. This means that in those analyses the crack opening increased in every loop for every layer in the softening zone. For the smaller upper load levels, especially for $F_{upp} = 0.94F_{max}$, inner loops were encountered. The occurrence of inner loops and the fact that damage in inner loops is not taken into account in the continuous-function model is probably the reason why analyses with smaller upper load levels could not be performed. In fact, after a number of cycles in such analyses, all the layers in the softening zone are in inner loops, which means that the deflection no longer increases with the number of cycles.

As already mentioned above, the results of the analyses with the multi-layer model cannot be directly used for a quantitative comparison with experimental results. Nevertheless, see the inset in Fig. 61 for an illustration of the relation between the obtained

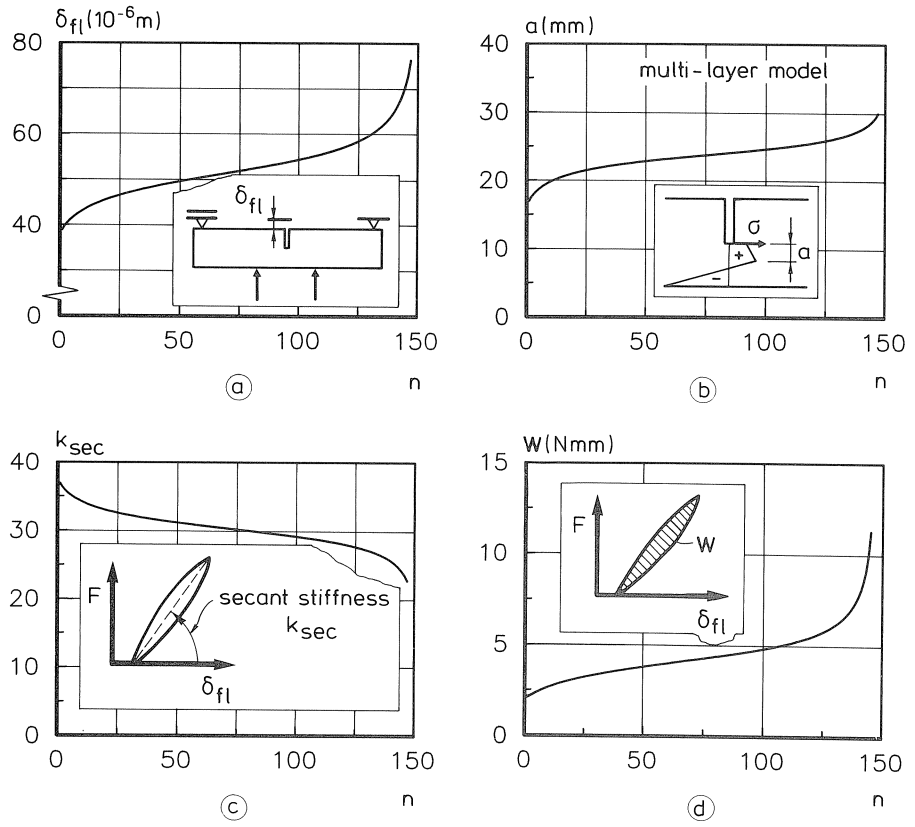

Fig. 60. The variation of four different parameters: deflection (a), length of fracture zone (b), secant stiffness (c) and a parameter to represent the energy within a loop (d); in relation to the number of cycles.

results and experimental results. The straight line represents a regression equation of the S-N curve for flexural tension in the case of a zero lower load level [12]. Experimental results are not available for load levels as applied in the analyses. Nor, as a matter of fact, is this possible, since in experiments the maximum load is not known exactly due to scatter in the results. Notwithstanding this, the results of the analyses will now be looked upon as fatigue results. The first noteworthy aspect is that the number of cycles plotted on a semi-logarithmic scale is almost linear, as is usually observed in fatigue tests. As far as the influence of the lower load level on the number of cycles to failure is concerned, a number of remarks can also be made. If the results for the lower load levels equal to 0 and $-0.5F_{max}$ are compared, then a decrease in the lower load level indeed results in a smaller number of cycles to failure, as could be expected from the principle of the model. None the less, the two curves in Fig. 61 are almost parallel to each other, while in fatigue experiments the transition from a positive or zero lower load (or stress) level to a negative one is accompanied by a change in the slope of the

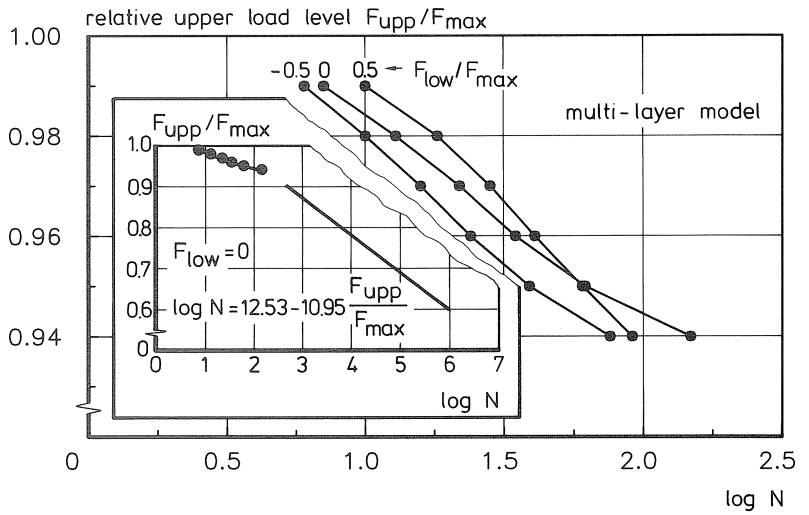

Fig. 61. Results from the multi-layer model plotted as S-N curves.

S-N curve (see Fig. 6b). This result can be directly explained on the basis of the continuous-function model and the experimental results of post-peak cyclic tensile tests (Section 6.2 and Fig. 50). For the increase of crack opening as a function of the lower stress level in the loop the experimental results show a discontinuity at a zero lower stress level. This discontinuity (a suddenly stronger increase in crack opening for negative lower stress levels) is not taken into account in the CFM. It can be expected that, once this part of the CFM has been improved so that it gives an even closer description of the experimental results, the results of fatigue analyses will also provide a better approximation of the experimental fatigue results. As regards the S-N curve for the lower load level equal to $0.5F_{max}$, a rather peculiar result is encountered. For the upper load levels equal to $0.95F_{max}$ and $0.94F_{max}$, N is smaller for the lower load level equal to $0.5F_{max}$ than for the zero lower load level. For a constitutive model that is based on a decrease in damaging effect with an increasing lower stress level, this result does not seem to be possible. However, a close inspection of the CFM learns that this result is indeed possible (for more information see [15]). Also on this point the continuous-function model can be improved.

Concluding remarks

From the analyses with the multi-layer model the following conclusions can be drawn. In general, the results of the fatigue analyses show qualitatively rather good similarity with results of fatigue experiments. For two aspects, both concerning the increase in crack opening w_{inc}, or stress drop $\Delta\sigma$, it was demonstrated that the CFM can be improved. With the CFM, only the fatigue behaviour for very high upper load levels could be investigated so far. For a further study of fatigue along the lines of the approach used in this report, it will be necessary also to incorporate damage effects in inner loops.

Finally, it can be remarked that damage, so far only is considered to be the result of a loading cycle, while time effects are totally ignored. In reality, of course, time effects will always play a role. For sustained loading tests, time effects are even the only contribution to crack growth. To the author's opinion a similar approach can be applied to study crack growth under sustained loading. In this respect it can be mentioned that the load (or average sress) also decreases, when the deformation in the post-peak part of a deformation-controlled tensile test is kept constant. If then, after some time, the deformation is increased again, the envelope curve is also reached at a lower stress level.

8.4 *Fatigue experiments*

In order to investigate more thoroughly the development of deformations in a uniaxial tensile fatigue test, a limited number of these experiments were performed. With these experiments, it was mainly intended to compare deformations in a static test with those in a fatigue test and to get an answer to the question of whether the descending branch in a static test is also the failure envelope in a fatigue test (see also Fig. 14). Besides, the non-uniformity in crack opening in a fatigue test will also be demonstrated and some attention will be paid to the topics of sequence effect and remnant strength after cyclic preloading.

Details of the specially designed data-acquisition system are given in Section 3.3. The normal type of concrete was used. For more information about mix proportions and 28-day mechanical properties, see [15]. Initially, it was intended to use unnotched specimens. The reason for that was that the process of localization in a fatigue test was also to be investigated. Notches in the specimens cause such a local increase in stress that one may not draw conclusions on the phenomenon of localization when notched specimens are used. Tests on unnotched specimens, however, are very difficult to perform. In most of the experiments, fracture occurred near a glue platen. Nevertheless, one fatigue experiment and one static experiment were successful. Furthermore, a number of fatigue experiments were performed on notched specimens. The applied upper and lower stress levels and the number of cycles to failure, N, can be obtained from Table 2. Additionally, four specimens were loaded under a continuous increasing deformation (denoted as static tests). The results of these tests will be used as reference for the fatigue tests.

Table 2. Upper and lower stress levels in the fatigue tests and number of cycles to failure

experiment No.	notched/unnotched	σ_{upp} (MPa)	σ_{low} (MPa)	N
1	unnotched	2.51	-2.75	12812
2	notched	3.18	-5.30	86
3	notched	3.00	0.67	13026
4	notched	3.00	0.05	1951
5	notched	2.75	-5.20	2378
6	notched	2.69	-5.14	10784
7	notched	2.50	-4.82	50720

Localization; results of a particular experiment

For static tensile experiments it is now well-known that localization occurs. Fracture takes place in a small zone, the process zone, while the rest of the specimen behaves elastically. Now it is interesting to see how the same specimen behaves when it is loaded dynamically. Or in other words, we are interested in the question: "To what extent does fracture occur in the total specimen?" In order to obtain some answer to this question, the results of the experiment on the unnotched specimen (No. 1) will now be shown. In the experiment on the unnotched specimen, fracture fortunately occurred within the base of the 35 mm LVDTs. The number of cycles to failure was 12812. In Fig 62a, the stress-deformation relation for a number of loops is plotted, while deformation is the average of the four 35 mm LVDTs. In the same figure the stress-deformation relation for the static test on the unnotched specimen is plotted. As can be seen, the deformation at the upper stress level for the last loop that was recorded more or less coincided with the descending branch of the static test. However, two remarks need to be made. First of all, it is not known whether the last recorded loop is also the last loop that was performed. There is a possibility that three more loops were performed. Since the increase in deformation is the greatest in the last loops, this may have a significant effect on the measured deformation at failure. In actual fact the real value for the deformation at failure is equal to or larger than the last one recorded. The second remark concerns the result of the static test. Here, only the result of one experiment is shown. It should be borne in mind, however, that due to scatter, the position of the descending branch may vary significantly, especially in this part of the stress-deformation relation where non-uniform crack opening occurs. This will become also clear from the results obtained on the notched specimens.

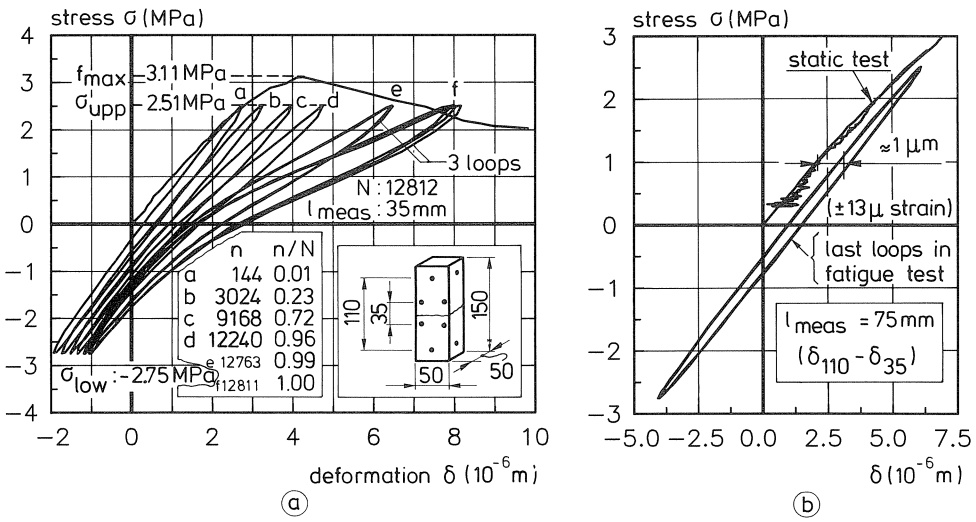

Fig. 62. Stress-deformation relation from a static and a fatigue tensile experiment on an unnotched specimen.

In order to quantify the damage that occurred outside the final fracture zone, the deformations obtained with the 35 mm LVDTs were subtracted from the deformations obtained with the 110 mm LVDTs. This results in a deformation pertaining to a measuring length of 75 mm (two parts of 37.5 mm each), which does not encompass the final fracture zone. It appeared that the shape of the stress-deformation curve of a loop varied only a little in the beginning of the test, while it remained more or less the same during the subsequent cycles to failure. The shape of the last cycles is shown in Fig. 62b. The irreversible deformation is about 1 μm, which is equal to about 13 μstrain. This result shows that also in a tensile fatigue test, fracture mainly occurs in a small zone. This can also be seen when the deformations at the upper stress level in a cycle are plotted versus the cycle ratio n/N (see Fig. 63). This figure also clearly shows that the largest part of increase in deformations in the fracture zone occurs during the last cycles before failure.

The observed irreversible deformation outside the final fracture zone may be the result of distributed tensile cracking (Fig. 64a). In the author's opinion, however, it might also be possible that the loading in compression ($\sigma_{low} = -2.75$ MPa) contributed to this increase in deformation. The compressive loading in fact causes small micro-cracks in the vertical direction (Fig. 64b), reducing the stiffness of the concrete. This phenomenon may also play an important role in the case where the deformation at the descending branch of a static test is compared with the deformation at failure in a fatigue test.

The result of the experiment on the unnotched specimen has also been used to calculate the development of the secant stiffness and the energy within a cycle respectively, with the cycle ratio. In Fig. 65, it can be seen that the obtained relations show good similarity with those found in the fatigue analyses (Figs. 60c and 60d) and, as far as the secant modulus is concerned, with results from compressive fatigue tests (Fig. 8).

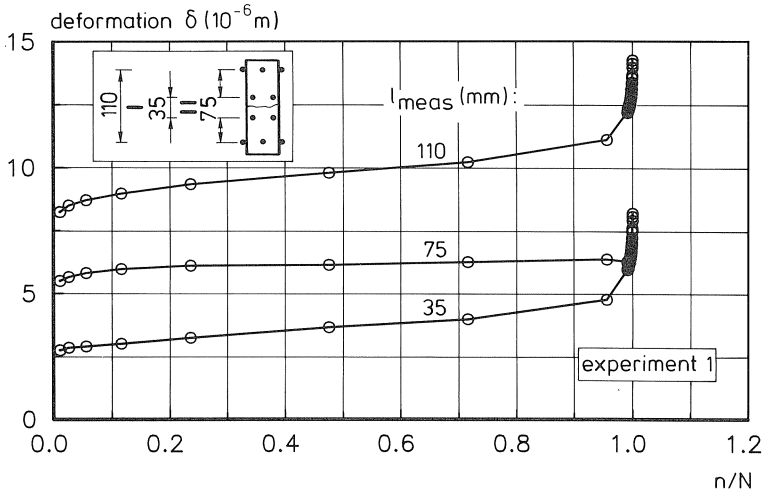

Fig. 63. Deformations at the upper stress levels versus the cycle ratio.

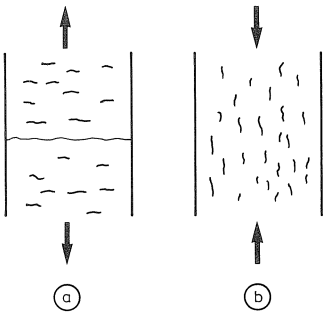

Fig. 64. Possible micro-cracking due to tensile fatigue (a) and compressive (b) loading.

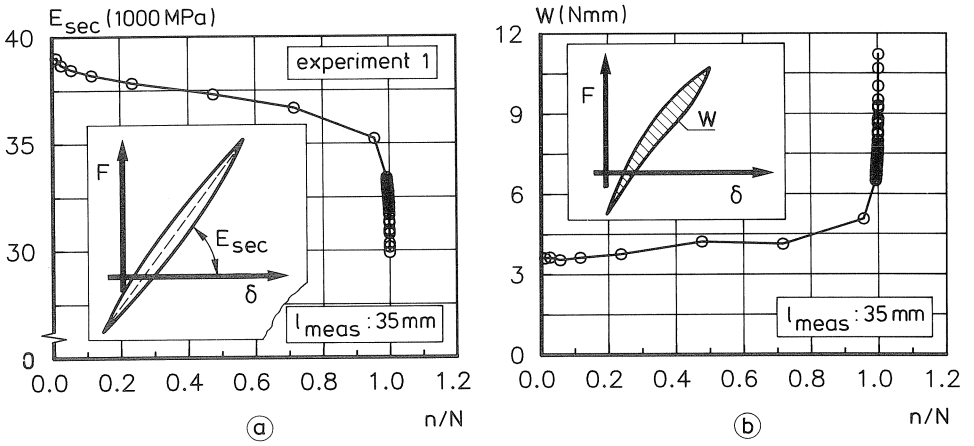

Fig. 65. Secant stiffness (a) and energy within a cycle (b) versus cycle ratio.

Non-uniform crack opening

In Chapter 4 the non-uniform crack opening in tensile experiments was investigated. There, the phenomenon was explained by a structural behaviour and it was surmised that it plays a role in many more tests on a softening material like concrete. One of these tests in which it can also be expected to occur, is the tensile fatigue test. Therefore, the non-uniformity in crack opening in the fatigue experiments was also investigated. First, in Fig. 66, the deformation of the four 35 mm LVDTs is plotted separately for the experiment on the unnotched specimen. This figure already clearly confirms the existence of the phenomenon in tensile fatigue tests. While the deformation of LVDT 3 (for the position on the specimen, see the schematic representation in the inset) increases with the cycle ratio, that of LVDT 1 decreases. The figure in the inset shows how the fracture zone opens with an increasing number of cycles. Similar to Fig. 24, the non-uniform crack opening can be shown by the combination of the in-plane rotation (φ_{ip}) and the out-of-plane rotation (φ_{op}). This relation is plotted in Fig. 67. Also the combinations of φ_{ip} and φ_{op} pertaining to the last recorded upper stress levels in the

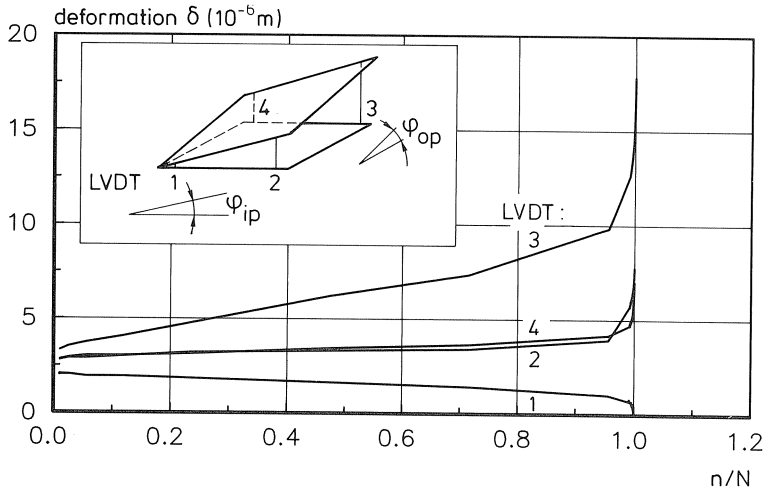

Fig. 66. Development of the deformation of the four 35 mm LVDTs with the number of cycles.

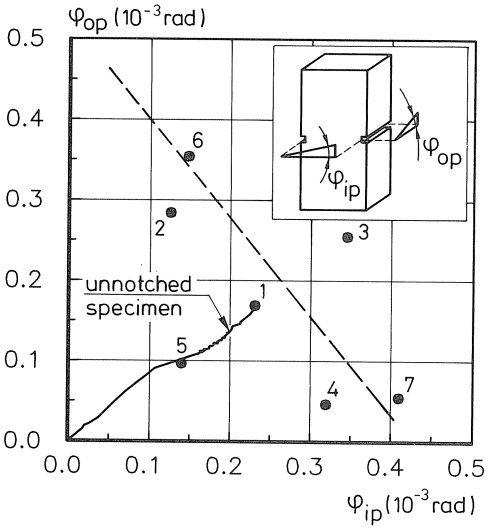

Fig. 67. Combinations of maximum in-plane and out-of-plane rotations in the tensile fatigue tests.

tests with notched specimens are plotted in this figure. The similarity with results from static tests (Fig. 24) is rather good. The fact that the dots are much less well situated on one line than in the static experiments is again related to the fact that it is not clear whether the last recorded cycle is also actually the last cycle. In the static test, the crack opening will always reach its maximum non-uniformity, while for the described reason, this is not necessarily true in the fatigue tests. Nevertheless, if the result of test 5 is omitted, a more or less linear relation between the maximum values of φ_{ip} and φ_{op} can again be seen.

Deformations in a static test versus deformations in a fatigue test

For the experiment on the unnotched specimen, it was found that the descending branch of the static test coincided more or less with the failure point in the fatigue test. Now the same comparison of deformations will be made for the notched specimens, while the relation between characteristic points in the cyclic creep curve and the stress-deformation relation will also be investigated. First, however, the results of the static tests which serve as a reference will be presented.

The stress-deformation relations for the four static experiments are plotted by the thin lines in Fig. 68. As can be seen, a rather significant scatter can be observed in the descending branches. However, this scatter is no larger than that found in previous experiments (compare Fig. 37). The thick solid line represents the average of the four separate tests and will be used for comparisons with fatigue results in the remainder of this section. The thick dashed line relates to the test on the unnotched specimen. No significant difference from the average curve for the notched specimens can be seen.

Now the relation between deformations in a fatigue experiment and in a static test will be shown. In the upper part of Fig. 69, the average σ-δ relation for the static experiments is plotted, while in the lower part of the same figure, the cyclic creep curve for fatigue test 7 is plotted in such a way that the axes for the deformation correspond. Characteristic points in the cyclic creep curve denoted as B, C and D are projected in the σ-δ diagram. Similarly, the points B, C and D for all the fatigue experiments are plotted in Fig. 70. No distinct relation can be obtained from the results. Nevertheless, the following remarks can be made. Except for the result of the unnotched specimen, the deformation at failure in the fatigue experiments is larger than the deformation for σ_{upp} at the descending branch in the static experiments, even if the scatter in the static experiments is taken into account. This result may suggest that the notches play an important role. Further research should clarify to what extent the notches are responsible for the observed results. Furthermore, the remark made previously about deforma-

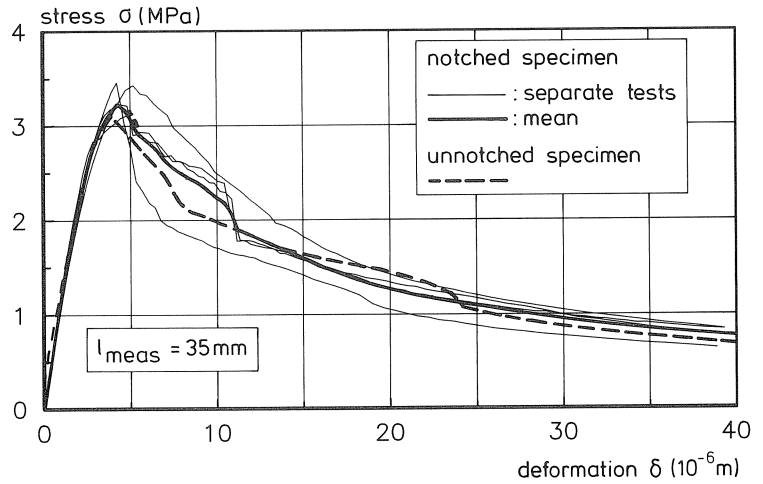

Fig. 68. Stress-deformation relations obtained in the static tests.

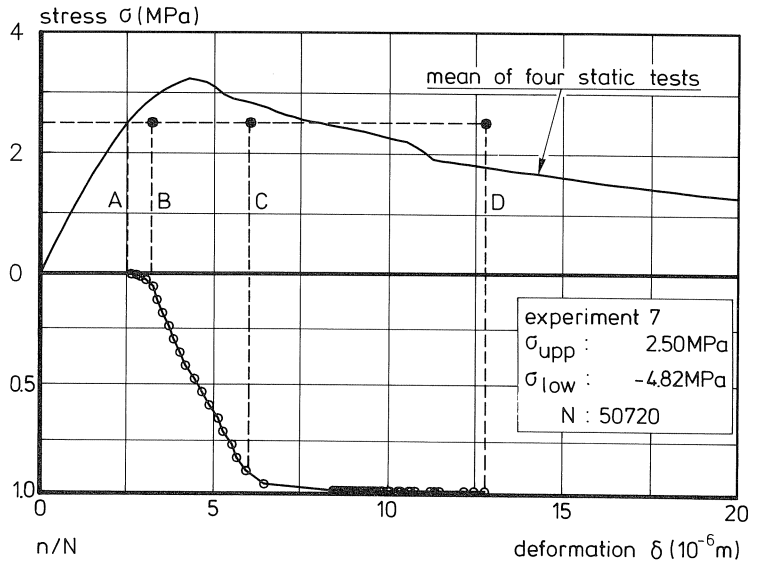

Fig. 69. Average stress-deformation relation of the static tests and the cycle ratio versus deformation of fatigue test 7.

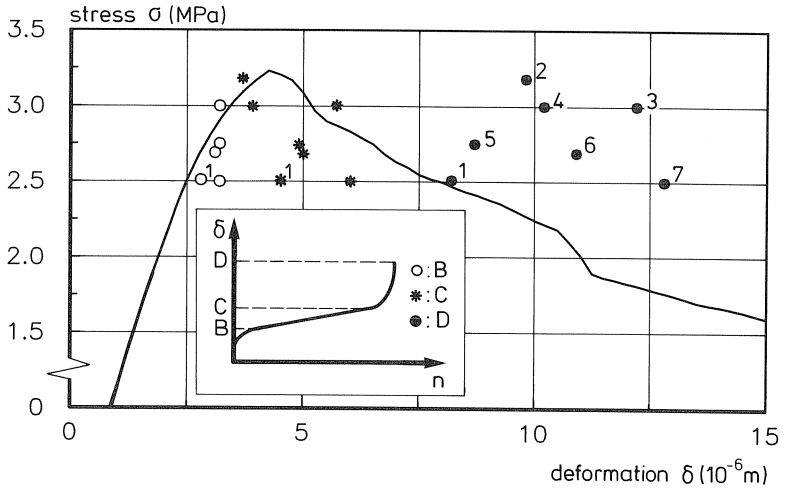

Fig. 70. Characteristic points in the cyclic creep curves of fatigue tests, compared with the average σ-δ relation of the static test.

tions in the bulk of the specimen due to compressive loading should be kept in mind when interpreting these results. The points C indicating the ending of the secondary branch in the cyclic creep curve do not give a decisive answer to the question of whether this point coincides with the deformation at peak load in static tests, as was assumed by Balázs [10] for the stress-slip behaviour of a bar pulled out of the concrete. In the author's opinion, however, there are several reasons why such a relation is not possible

in these experiments. The main reason is that the deformation at peak load depends on the measuring length; elastic deformation (see Fig. 5), while the deformation at point B is partly due to elastic deformation and partly due to the opening of the crack or process zone, which is independent of the measuring length. Therefore, if there is a criterion based on a deformation marking the end of the secondary branch in the cyclic creep curve, it will be related to a crack opening.

Sequence effect and remnant strength

Via two other experiments, which are not included in Table 2, it was intended to investigate the phenomenon of sequence effect. For that purpose a two-stage fatigue loading was performed. In the first stage of experiment A (see Fig. 71), the stress levels were chosen as equal to those of experiment 3. In this respect it should be mentioned that it was not possible to install the actual average stress levels exactly. Therefore, the stress levels deviated a little, as can be seen in the inset of Fig. 71. In the first stage, 5000 cycles were performed, after which the test was stopped and restarted with an upper stress level equal to 2.68 MPa and a lower stress level equal to 0.00 MPa. Unfortunately, fracture occurred near one of the glue platens after about another 20000 cycles had been performed. In experiment B, the reversed order of load application was applied. The relation between strain and the number of cycles can be seen in Fig. 71. Despite the fact that the upper stress level in the first 5000 cycles was lower than in experiment A, the increase in deformation is greater. So far it is not clear whether this result is due to σ_{low}, which is lower than for experiment A, or due to scatter in the results. It may be clear that this single test result with a relatively low number of cycles and involving stress levels which do not differ too much between the two stages of loading, cannot be used to draw strong conclusions. Nevertheless, the development of deformation with the number of cycles gives the impression that, for the applied stress ranges, a high σ_{upp} followed by a

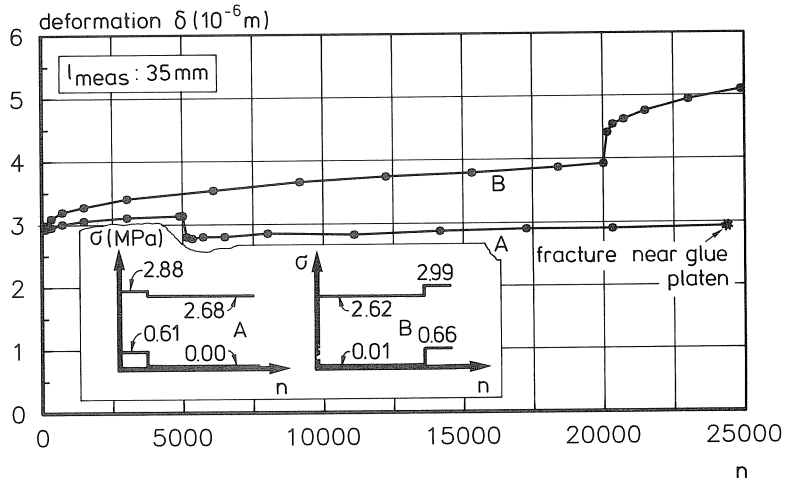

Fig. 71. Deformation versus number of cycles for two two-stage loading experiments.

lower σ_{upp} leads to a longer fatigue life than the reversed order of load application. In the author's opinion, more research is required in order to gain a better insight into the sequence effect in fatigue behaviour. The fatigue model presented in this report is a good tool for such a study, in which the influence of the lower stress level should also be taken into account.

Experiment B in Fig. 71 was unloaded after 25000 load cycles. Subsequently, the same specimen was loaded statically. The total result of this test in a stress-deformation diagram is plotted in Fig. 72. Compared to the average curve for the non-preloaded specimens (dashed line), a small increase in maximum stress can be observed. However, this increase still lies within the scatter band of the separate results. A comparison of the two pre-peak parts of the curves further shows that the nonlinearity just before peak load is much less for the specimen that was cyclically preloaded. The observed phenomena are in agreement with what was also found in compressive fatigue experiments (see Section 2.2). Though no clear evidence is available yet, the author has the following explanation for these phenomena. In Section 5.1, the influence of non-uniform stress distributions on the σ-δ relation in a uniaxial tensile test was discussed. These non-uniform stress distributions, for which several causes may exist (see, for instance Fig. 34), result in a lower maximum load and an increased pre-peak non-linearity. These are exactly the two phenomena that can be observed in the non-preloaded specimen as compared with the preloaded specimen. Or, put in another way, non-uniform stresses, like eigenstresses due to differential shrinkage in a virgin specimen cause the different areas in the fracture zone to reach their peak load one after another. Due to the cyclic preloading, some micro-cracking may have occurred in the most stressed regions, resulting in stress redistribution. These micro-cracks may have very locally decreased the strength of the concrete slightly. That, however, is outweighed by the increase in maximum load that is attained by the more uniform stress

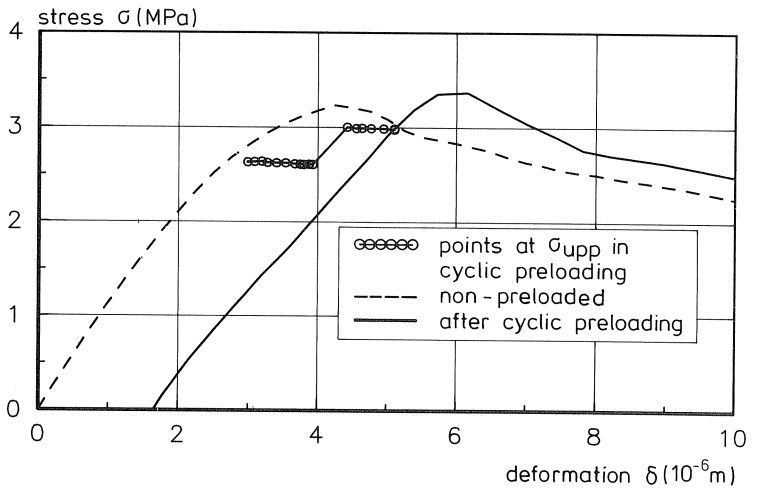

Fig. 72. Stress-deformation history for the cyclic preloaded specimen compared to the average σ-δ relation of non-preloaded specimens.

distribution that was reached after stress redistribution. In this respect, one need not only think of initial stresses at the macro-level, as discussed in Section 5.1, but also of such stresses at the micro-level.
The fact that the descending branch of the preloaded specimen is positioned more to the right than that of the non-preloaded specimens is in agreement with the results of the fatigue tests. As last notable point in the σ-δ curve of the preloaded specimen in Fig. 72 concerns the small nonlinearity in the first part of the solid curve. This is in agreement with the reloading curves in the post-peak cyclic region (compare Fig. 49).

Concluding remarks
Summarizing the results of the fatigue experiments in this section, the following main conclusions can be drawn:
- The specially developed data-acquisition system is suitable for studying the tensile fatigue behaviour more thoroughly.
- Tensile fatigue failure is a local phenomenon like tensile failure in a static experiment.
- The non-uniform crack opening that is the result of a structural behaviour, has also been demonstrated for tensile fatigue experiments.
- As regards a failure criterion based on deformations, sequence effect and remnant strength, more research is required before conclusions can be drawn about the mechanisms which occur.

9 Concluding remarks

The importance of fracture mechanics for concrete building practice is more and more recognized nowadays. As a result, many investigations deal with this topic at the moment. In this report, a fracture mechanics approach is applied to study the fatigue behaviour of plain concrete. Results that were obtained with the model, like cyclic creep curves and S-N curves, showed qualitatively good similarity with those usually found in fatigue experiments. So far, only low cycle high amplitude fatigue could be investigated. In order to enable high cycle low amplitude fatigue to be studied as well, it is necessary also to include damaging effects in inner loops. Furthermore, for a better approximation for the real fatigue behaviour of concrete time effects should also be taken into account.
The fatigue model is presented on a macro-level and becomes active as soon as a softening zone exists in the structure. Generally, cracks or softening zones occur in concrete structures, so that the process of stress-redistribution will take place in most structures when the loading varies in time. In the author's opinion, a similar model can be applied on a meso-level, where stress concentrations and micro-cracks or softening zones occur in the vicinity of aggregates.
The approach to fatigue of plain concrete as a local phenomenon was supported by experimental results of a fatigue test on an unnotched specimen, where fracture also occurred mainly locally.

In this report also the tensile behaviour of plain concrete has been discussed extensively. The occurrence of a "structural behaviour" in a deformation-controlled uniaxial tensile test on a softening material has been demonstrated. The continuous-function model was proposed for the stress-crack opening relation. With the two input material parameters, tensile strength and fracture energy, the complete unloading-reloading behaviour in the tensile and the tensile-compressive region is determined.

Acknowledgements

The publication reports on a doctoral study at Delft University of Technology carried out under the supervision of Prof. dr.-Ing. H. W. Reinhardt. The experimental part of this study was performed in the Stevin Laboratory of the Delft University of Technology and the FE analyses were performed at TNO Building and Construction Research. The study was financially supported by the Netherlands Technology Foundation (STW grant DCT 38.0552), the Netherlands Centre for Civil Engineering, Research, Codes and Specifications (CUR) and the "Stichting Professor Bakkerfonds". The author is indebted to Mr. A. S. Elgersma and to ir. J. G. Janssen for their support in the experimental and numerical part of this study respectively.

Notation

The following symbols are used in this report:

A	cross-sectional area
a	crack length, length of process zone
c	coefficient
CFM	continuous-function model
E	Young's modulus
e	eccentricity
exp	experiments
F	force, load
f	strength
FE	finite element
FPM	focal-point model
G	energy
h	height
I	moment of inertia
K	stress intensity factor
k	stiffness
l	length
LAB	laboratory
LC	lightweight concrete
LVDT	linear variable differential transducer
M	moment
N	number of cycles to failure, normal force

n	number of cycles, number of elements
NC	normal-weight concrete
S	relative stress level
t	thickness
W	energy
w	crack opening, width
z	distance
α	coefficient
β	coefficient
σ	stress
δ	deformation, displacement
ε	strain
$\dot{\varepsilon}$	strain rate
φ	rotation
ω	frequency

subscripts

b	bending
c	compressive, critical
cc	cube compressive
ch	characteristic
ck	cube characteristic
er	envelope reloading
eu	envelope unloading
ext	external
inc	increase
int	internal
ip	in-plane
F	fracture
f	fracture zone
fl	flexural
L, low	lower
m	mean
max	maximum
meas	measuring
o	initial, stress free
op	out-of-plane
peak	peak
r	reloading
s, sec	secant
t	tensile
u	unloading
upp	upper

References

1. Hillerborg, A., Modeer, M. and Petersson, P. E., Analysis of crack formation and crack growth in concrete by means of fracture mechanics and finite elements. Cement and Concrete Res., 6, 1976, pp. 773–782.
2. CUR, Fatigue of concrete, part 1: Compressive stresses. CUR-VB report 112 in co-operation with MaTS-IRO, 1983, 80 pp. (in Dutch).
3. CUR, Fatigue of concrete, part 2: Tensile and tensile-compressive stresses. CUR-VB report 116 in co-operation with MaTS-IRO, 1984, 83 pp. (in Dutch).
4. CUR, Fatigue of concrete, part 3: Tensile and tensile-compressive stresses (2). CUR report 137 in co-operation with MaTS-IRO, 1988, 90 pp. (in Dutch).
5. CUR, Fatigue of concrete, part 4: Random compressive stresses. CUR report 150, in co-operation with MaTS-IRO, 1989 (in Dutch).
6. Dugdale, D. S., Yielding of steel sheets containing slits. Journal of Mechanics and Physics of Solids, 8, 1960, pp. 100–104.
7. Barenblatt, G. I., The mathematical theory of equilibrium cracks in brittle fracture. Advances in Applied Mechanics, 7, 1962, pp. 55–129.
8. RILEM, Long term random dynamic loading of concrete structures. Report by RILEM committee 36-RDL, RILEM Materials and Structures, 17(97), 1984, pp. 1–28.
9. Cornelissen, H. A. W., State of the art report on fatigue of plain concrete. Stevin report 5-86-3, Delft University of Technology, 1986, 62 pp. and Chapter 3 "Fatigue of concrete structures", CEB Bulletin No. 188.
10. Balázs, G. L., Bond behaviour under repeated loads. Studi e Ricerche, 8, 1986, pp. 395–430.
11. Holmen, J. O., Fatigue of concrete by constant and variable amplitude loading. Doctoral Thesis, NTH Trondheim, 1979, 218 pp.
12. Cornelissen, H. A. W., Fatigue failure of concrete in tension. Heron, 29(4), 1984, 68 pp.
13. Palmgren, A., Die Lebensdauer von Kugellagern. Zeitschrift Verein Deutscher Ingenieur, 68(14), 1924, pp. 339–341.
14. Miner, M. A., Cumulative damage in fatigue. J. of Applied Mechanics, Trans. ASME, 12(1), 1945, pp. A159–A164.
15. Hordijk, D. A., Local approach to fatigue of concrete. Doctoral Thesis, Delft University of Technology, Delft, 1991, 210 pp.
16. Van Mier, J. G. M., Fracture of concrete under complex stress. HERON, 31(3), 1986, 90 pp.
17. Hordijk, D. A., Reinhardt, H. W. and Cornelissen, H. A. W., Fracture mechanics parameters of concrete from uniaxial tensile tests as influenced by specimen length. In Fracture of Concrete and Rock (Eds. S. P. Shah and S. E. Swartz), preprint SEM-RILEM Int. Conf., Bethel, 1987, pp. 138–149.
18. Hordijk, D. A. and Reinhardt, H. W., Macro-structural effects in a uniaxial tensile test on concrete. In Brittle Matrix Composites – 2 (Eds. A. M. Brandt and I. H. Marshall), Elsevier Applied Science, 1989, pp. 486–495.
19. Rüsch, H. and Hilsdorf, H., Verformungseigenschaften von Beton unter zentrischen Zugspannungen. Bericht Nr. 44, Materialprüfungsamt für das Bauwesen der Technischen Hochschule München, 1963.
20. Notter, R., Schallemissionsanalyse für Beton im dehnungsgesteuerten Zugversuch. Doctoral Thesis, Zürich, 1982.
21. Scheidler, D., Experimentelle und analytische Untersuchungen zur wirklichkeitsnahen Bestimmung der Bruchschnittgrössen unbewehrter Betonbauteile unter Zugbeanspruchung. DAfStb, Heft 379, 1987, 94 pp.
22. Budnik, J., Bruch- und Verformungsverhalten harzmodifizierter und faserverstärkter Betone bei einachsiger Zugbeanspruchung. Doctoral Thesis, Ruhr-University, Bochum, 1985, 180 pp.
23. Willam, K., Hurlbut, B. and Sture, S., Experimental and constitutive aspects of concrete failure. In Finite Element analysis of Reinforced Concrete Structures (Eds. C. Meyer and H. Okamura), 1985, pp. 226–254.
24. Van Mier J. G. M. and Nooru-Mohamed, M. B., Geometrical and structural aspects of concrete fracture. Engineering Fracture Mechanics 35(4/5), 1990, pp. 617–628.

25. Rots, J. G., Hordijk, D. A. and De Borst, R., Numerical simulation of concrete fracture in "direct" tension. In Numerical methods in Fracture Mechanics (Eds. A. R. Luxmoore et al.), Pineridge Press, Swansea, 1987, pp. 457–471.
26. De Borst, R., Non-linear analysis of frictional materials. Doctoral Thesis, Delft University of Technology, Delft, 140 pp.
27. Vonk, R., Rutten, H., Van Mier, J. G. M. and Fijneman, H., Influence of boundary conditions on softening of concrete loaded in compression. In Fracture of Concrete and Rock; Recent Developments (Eds. S. P. Shah et al.), Elsevier Applied Science, 1989, pp. 711–720.
28. Rots, J. G., Kusters, G. M. A. and Blaauwendraad, J., Strain-softening simulations of mixed-mode concrete fracture. In Fracture of Concrete and Rock (Eds. S. P. Shah and S. E. Swartz), Springer-Verlag, 1989, pp. 175–188.
29. Gustafsson, P. J., Fracture mechanics studies of non-yielding materials like concrete. Report TVBM-1007, Lund Inst. of Technology, Sweden, 1985.
30. Hordijk, D. A., Deformation-controlled uniaxial tensile tests on concrete, A survey of the literature up to 1981. Report 25.5-89-15/VFA (SR-84), Stevin Laboratory, Delft University of Technology, 1989, 119 pp.
31. Petersson, P. E., Crack growth and development of fracture zones in plain concrete and similar materials. Report TVBM-1006, Lund Inst. of Technology, Sweden, 1981, 174 pp.
32. Roelfstra, P. E. and Wittmann, F. H., Numerical method to link strain softening with failure of concrete. In Fracture Toughness and Fracture Energy (Ed. F. H. Wittmann), Elsevier, 1986, pp. 163–175.
33. Rots, J. G., Strain-softening analysis of concrete fracture specimens. In Fracture Toughness and Fracture Energy (Ed. F. H. Wittmann), Elsevier, 1986, pp. 137–148.
34. Cornelissen, H. A. W., Hordijk, D. A. and Reinhardt, H. W., Experiments and theory for the application of fracture mechanics to normal and lightweight concrete. In Fracture Toughness and Fracture Energy (Ed. F. H. Wittmann), Elsevier, 1986, pp. 565–575.
35. Kleinschrodt, H. D. and Winkler, H., The influence of the maximum aggregate size and the size of specimen on fracture mechanics parameters. In Fracture Toughness and Fracture Energy (Ed. F. H. Wittmann), Elsevier, 1986, pp. 391–402.
36. Wolinski, S., Hordijk, D. A., Reinhardt, H. W. and Cornelissen, H. A. W., Influence of aggregate size on fracture mechanics parameters of concrete. Int. J. Cement Composites and Lightweight Concrete, 9 (2), 1987, pp. 95–103.
37. Wittmann, F. H., Rokugo, K., Brühwiler, E., Mihashi, H. and Simonin, P., Fracture energy and strain softening of concrete as determined by means of compact tension specimens. RILEM Materials and Structures, 21(121), 1988, pp. 21–32.
38. Brameshuber, W., Bruchmechanische Eigenschaften von jungem Beton. Doctoral Thesis, University of Karlsruhe, report 5, 1988, 233 pp. (in German).
39. CEB-FIP Model Code 1990, First Draft; Chapters 1-5. CEB Bulletin No. 195, 1990.
40. Mihashi, H., Nomura, N. and Izumi, M., Influence of matrix strength and gravel grain size on fracture properties of concrete. In Fracture of Concrete and Rock; Recent Developments (Eds. S. P. Shah et al.), Elsevier Applied Science, 1989, pp. 503–512.
41. Gopalaratnam, V. S. and Shah, S. P., Softening response of plain concrete in direct tension. ACI-Journal, 82(3), 1985, pp. 310–323.
42. Wu, K. and Zhang, B., Fracture energy of lightweight concrete. In Fracture Toughness and Fracture Energy; Test Methods for Concrete and Rock (Eds. H. Mihashi et al.), Balkema, 1989, pp. 117–124.
43. Wittmann, F. H., Roelfstra, P. E., Mihashi, H., Huang, Y.-Y., Zhang, X.-H. and Nomura, N., Influence of age of loading, water-cement ratio and rate of loading on fracture energy of concrete. RILEM Materials and Structures, 20(116), 1987, pp. 103–110.
44. Mills, R. H., Strength-maturity relationship for concrete which is allowed to dry. In Studies in concreting in hot countries (Eds. R. Shalon and D. Ravina), pp. 1–28.
45. Cornelissen, H. A. W. and Reinhardt, H. W., Effect of static and fatigue preloading on the residual strength and stiffness of plain concrete. In Fracture Control of Engineering Structures (Eds. H. C. van der Elst and A. Bakker), Vol III, 1986, pp. 2087–2103.

46. YANKELEVSKY, D. Z. AND REINHARDT, H. W., Focal points model for uniaxial cyclic behaviour of concrete. In Computational Mechanics of Concrete Structures; Advances and Applications, IABSE Colloquium, Delft, 1987, pp. 99–106.
47. YANKELEVSKY, D. Z. and REINHARDT, H. W., Uniaxial behaviour of concrete in cyclic tension. ASCE J. of Structural Eng., 115(1), 1989, pp. 166–182.
48. JANSSEN J. G., Mode-I fracture of plain concrete under monotonic and cyclic loading. Graduate Thesis, Delft University of Technology, IBBC-TNO report BI-90-110, 1990.
49. BRAAM, C. R., Control of crack width in deep reinforced concrete beams. Heron, 35(4), 1990, 106 pp.